

STEREOVISION IN UNDERWATER ENVIRONMENTS

JAMES ANDERSON

Stereovision in Underwater Environments

by

© James Anderson

A thesis submitted to the

School of Graduate Studies

in partial fulfillment of the requirements for the degree of

Master of Engineering

Faculty of Engineering & Applied Science

Memorial University of Newfoundland

October 2013

St. John's

Newfoundland

Abstract

Stereoscopic vision is the modern field of using multiple cameras to extract three dimensional information about a scene. This technology is used in a wide variety of applications from motion capture used in the movie industry to the industrial monitoring and validation of production lines. This technology however has seen limited use in the challenging environment of underwater photography. This thesis attempts to implement and adapt this technology for use in the Marine Institute flume tank. The flume tank is used for scientific modeling and validation of fishing gear and other objects in ocean environments. This work focuses on the challenges involved in doing this, as well as experimental validation of modern camera calibration and triangulation and adding several novel improvements on these processes.

This work shows that a modern system using a properly calibrated system functions faster, more accurately and more precisely than any human driven monitoring system. The testing of the various modern calibration techniques reveals several weaknesses when exposed to the challenging underwater environment. The comparison of several methods for stereo location showed the accuracy of these methods is greatly reduced in challenging environments. Both these results open the way for several novel improvements on the methods which increase accuracy and improve performance over the original methods.

Acknowledgements

I would like to acknowledge my supervising professor, Nick Krouglicof, for his help and guidance on this project. Without his expertise and encouragement this project would not have been possible.

I would like to acknowledge Taufiqur Rahman for his help and expertise with camera calibration. His guidance helped make this project not only successful but also accurate.

I acknowledge the help of David Keating and the other students who helped with the construction of the camera calibration cube and the camera housing and support.

I would like to thank the entire staff at the Center for Sustainable Aquatic Resources. I would like to especially thank George Legg and Craig Hollett for their expertise with the flume tank and as well as the installation and testing of this project. I would also like to thank Paul Winger and Kelly Moret for their help with the organization of this project and as well as securing the funding required for this work.

I would like to thank my family and my girlfriend for their help and support of me on this project. Without their encouragement and pushing me to excel, this project would never have been completed.

Financial support for this thesis was provided by the Atlantic Canada Opportunities Agency (ACOA), Fisheries and Marine Institute of Memorial University of Newfoundland, the

Department of Fisheries and Aquaculture of Newfoundland and Labrador, Research and Development Corporation (RDC), Vónin Canada Ltd., and Vónin Ltd.

Table of Contents

Stereovision in Underwater Environments	1
Abstract.....	2
Acknowledgements.....	3
List of Figures	12
List of Tables	15
List of Equations.....	17
Chapter 1.....	18
1.1 Introduction.....	18
1.2 Project Definition	18
1.3 Challenges	19
1.4 Flume Tank	20
1.5 Organization	22
Chapter 2.....	24
2.1 Camera Model.....	24
2.2 Pinhole Camera Model.....	24
2.3 Mathematical Model.....	25
2.4 Image Distortion.....	28
2.4.1 Radial Distortion	28

2.4.2	Tangential Distortion	29
2.4.3	Complete Distortion Model	30
Chapter 3.....		31
3.1	Camera Calibration.....	31
3.2	Data Collection	31
3.2.1	Photogrammetric Calibration	31
3.2.2	Self-Calibration.....	32
3.2.3	Calibration through Motion	33
3.3	Calibration Methods.....	33
3.3.1	Tsai	33
3.3.2	Zhang.....	34
3.3.3	Heikkila.....	36
3.3.4	Rahman and Krouglicof.....	38
3.4	Calibration Setup.....	40
3.4.1	Calibration cube.....	40
3.5	Calibration Results.....	43
3.5.1	Above Water	44
3.5.2	Above Water with Case	47
3.5.3	Below Water with Case.....	50

3.6	Calibration Comparison.....	53
3.6.1	Rahman and Krouglicof Data Analysis	53
3.6.2	Heikkila Data Analysis	56
3.6.3	Zhang Data Analysis	59
3.6.4	Algorithm Evaluation	62
Chapter 4.....		66
4.1	Stereoscopic Location	66
4.2	Stereoscopic theory	66
4.3	Point Correspondence.....	69
4.4	Stereo Location Evaluation	71
4.4.1	Testing setup.....	71
4.4.2	Measurements at 4.572 meters	72
4.4.3	Measurements at 6.858 meters	73
4.4.4	Measurements at 9.4488 meters	74
4.4.5	Measurements at 11.938 meters	75
4.4.6	Algorithm evaluation	76
4.5	Stereo Location Augmentations.....	78
4.5.1	Calibration Splitting	78
4.5.2	Iterative Solution Finding.....	79

4.5.3	Augmentation Testing.....	80
4.5.4	Stereo Augmentation Evaluation.....	85
Chapter 5.....		87
5.1	Mechanical and Hardware Design	87
5.2	Mechanical Overview and Requirements	87
5.2.1	Camera Frame.....	87
5.2.2	Camera Housing.....	88
5.2.3	Camera Mount	88
5.3	Material Analysis and Flame Tank Conditions	89
5.4	Mechanical Design	91
5.4.1	Camera Frame.....	91
5.4.2	Camera Container	96
5.4.3	Camera Mount.....	98
5.5	Mechanical Analysis	100
5.5.1	Mechanical Properties	100
5.5.2	Hydrodynamic Modeling.....	101
5.5.3	Flume Tank Flow Characteristics	104
5.5.4	System Modeling	106
5.5.5	Hydrodynamic Calculations	109

5.6.....	110
5.6.1 Bond Graph.....	110
5.6.2 System Response	112
5.6.3 Discussion and Recommendations.....	114
5.7 Hardware Overview and Requirements.....	115
5.7.1 Camera and Lens.....	115
5.7.2 Computer System.....	115
5.7.3 Power System	115
5.8 Hardware Design	116
5.8.1 Camera and Lens.....	116
5.8.2 Computer system.....	116
5.8.3 Power System	117
5.8.4 Completed Assembly	118
Chapter 6.....	120
6.1 Software Design	120
6.2 Remote Client.....	120
6.2.1 Software Design	120
6.2.2 Communication Design.....	121
6.3 Server Software.....	124

6.3.1	Software Design	124
6.3.2	User Interface	128
6.4	Stereo Location Implementation	133
6.5	Calibration Implementation	136
Chapter 7.....		138
7.1	Comparative Testing	138
7.2	Experiment Design	138
7.3	Data Collection	140
7.3.1	True Value of Distances	140
7.3.2	Testing Results of Old Camera System	141
7.3.3	Testing Results of New Camera System.....	141
7.4	System Evaluation	142
7.4.1	Comparison of Time Taken for Testing.....	142
7.4.2	Error Analysis of Old System.....	142
7.4.3	Error Analysis of New System	142
7.4.4	Evaluation of performance	142
7.5	Other Considerations	143
Chapter 8.....		145
8.1	Conclusion and Future Recommendations	145

8.2	Camera Calibration.....	145
8.3	Triangulation Methodologies.....	146
8.4	Comparative Testing	147
8.5	Future Work	147
	Bibliography	149
Appendix B	Camera Support Design.....	154

List of Figures

Figure 1 - Center for Sustainable Aquatic Resources Flume Tank Side Profile..... 21

Figure 2 - Center for Sustainable Aquatic Resources Flume tank Top Profile..... 21

Figure 3 - Pinhole Ray Projection..... 25

Figure 4 - Pinhole Camera Model 26

Figure 5 - Camera Model 26

Figure 6 - Radial Distortion 28

Figure 7 - Tangential Distortion 29

Figure 8 - Photogrammetric Calibration Target..... 32

Figure 9 - Highly Accurate Calibration target..... 42

Figure 10 - The 3D Location Problem..... 66

Figure 11 - Camera Frame Alpha Prototype 91

Figure 12 - Side Tank Mounting Option..... 92

Figure 13 - Top Tank Mounting Option..... 93

Figure 14 - Beta Camera Frame after Installation 94

Figure 15 - Corrosion Damage on Beta Support Frame..... 95

Figure 16 - Camera Container 97

Figure 17 - Camera Mount..... 98

Figure 18 - Camera Mount Holder 99

Figure 19 Reynolds number vs. Drag coefficient for common shapes [21]..... 103

Figure 20 Flow Profile of CSAR Flume Tank at 0.5 knots 104

Figure 21 Original Non-modal Bond Graph Model (5 Sections)	107
Figure 22 Horizontal Augmented Bond Graph	110
Figure 23 Vertical Augmented Bond Graph.....	111
Figure 24 Horizontal System Response.....	112
Figure 25 Vertical System Response	113
Figure 26 - Complete Hardware Assembly Diagram.....	118
Figure 27 - Remote Client Class Diagram.....	121
Figure 28 - Sever Network Class Diagram.....	124
Figure 29 - Server Processing Class Diagram	125
Figure 30 - Argus Data Class Diagram	126
Figure 31 - Stereo Processing GUI.....	128
Figure 32 - Stereo Data GUI	129
Figure 33 - Image Handling GUI	130
Figure 34 - Camera Calibration GUI	131
Figure 35 - Argus GUI class Diagram	132
Figure 36 - Example of Camera Target Underwater	133
Figure 37- Corner Detection Example.....	135
Figure 38 - Camera Comparison Experimental Rig.....	140
Figure 39 - Camera Container Technical Drawing 1	154
Figure 40- Camera Container Technical Drawing 2	155
Figure 41 - Camera Support Technical Drawing	156
Figure 42 - Camera Box Assembly Technical Drawing.....	157

Figure 43 - Camera Box and Support Technical Drawing 158

Figure 44 - Camera Box Support Technical Drawing 159

Figure 45 - Camera Support Frame Technical Drawing 160

List of Tables

Table 1 -Rahman and Krouglicof Camera Model Data above Water	44
Table 2 - Heikkila Camera Model Data above Water.....	45
Table 3 - Zhang Camera Model Data above Water	46
Table 4 - Rahman and Krouglicof Camera Model Data above Water with Case	47
Table 5 - Heikkila Camera Model Data above Water with Case	48
Table 6 - Zhang Camera Model Data above Water with Case.....	49
Table 7 - Rahman and Krouglicof Model Data below Water with Case	50
Table 8 - Heikkila Model Data below Water with Case	51
Table 9 - Zhang Model Data below Water with Case	52
Table 10 - Rahman and Krouglicof Model Analysis above Water	53
Table 11 - Rahman and Krouglicof Model Analysis above Water with Case.....	54
Table 12 - Rahman and Krouglicof Analysis below Water with Case	55
Table 13 – Heikkila Model Analysis above Water.....	56
Table 14 - Heikkila Model Analysis above Water with Case.....	57
Table 15 - Heikkila Model Analysis below Water with Case.....	58
Table 16 - Zhang Model Analysis above Water	59
Table 17 - Zhang Model Analysis above Water with Case.....	60
Table 18 - Zhang Model Analysis below Water with Case.....	61
Table 19 - Camera Model Focal Length Changes.....	62
Table 20 – Camera Model Image Center Change	63

Table 21- Camera model Distortion (Absolute Value) change	64
Table 22 - Camera Model Pixel Error	64
Table 23 - Flume tank Chemical Characteristics	89
Table 24 - Networking Commands	122
Table 25 - Network Command Structure.....	122
Table 26 - True Value of Calculated Distances	140
Table 27 - Results of Old Camera System Testing	141
Table 28 - Results of New Camera System Testing.....	141
Table 29 - Comparison of Testing Times (Seconds).....	142
Table 30 - Analysis of Error in Old System	142
Table 31 - Analysis of Error in New System	142

List of Equations

Equation 1 - Complete Distortion Model.....	30
Equation 2- Simplified Distortion Model	30
Equation 3 - Zhang Camera model	34
Equation 4 - Zhang Image Plane Homography	34
Equation 5 - Zhang Distortion Model.....	35
Equation 6 - DLT Translation Matrix	36
Equation 7 - Melen Back-Projection Solution.....	37
Equation 8 - Inhomogeneous Stereoscopic Equations.....	68
Equation 9 - Homogeneous Stereoscopic Equations.....	68
Equation 10 - Augmented Error Calculation	79
Equation 11 - Force of Gravity	101
Equation 12 - Force of Buoyancy on Submerged Objects	101
Equation 13 - Dynamic forces of Submerged Objects	102
Equation 14 - Reynolds Number of Submerged Objects	102
Equation 15 - Spring Constant of Translational Spring.....	106
Equation 16 - Spring Constant of Rotational Spring	106
Equation 17 - Shear Coefficient of a Rectangular cross section	106
Equation 18 - Inertia of Square Cross section.....	107

Chapter 1

1.1 Introduction

Computer vision is a field in which one or more digital images are analyzed, processed, and combined to extract useful information about an environment or object in the images. In modern times, with the automation of many aspects of day to day life, this field has become very important to engineers and computer scientists. This has allowed the theories to be applied to many fields from material inspection to transportation safety and security and as well as facial recognition. This field can be further subdivided into several topics such as image processing, machine vision and stereoscopic vision.

Stereoscopic vision is the process of using multiple images of a scene at multiple orientations and locations to reveal three dimensional information such as location and orientation of objects in the scene. In recent times stereoscopic camera work has become very popular in many fields from medicine to movie making to autonomous navigation with robots[1][2]. The majority of these applications are for above water applications with little attention paid to how this technology can be used in underwater environments. This project will analyze the effectiveness and challenges of using this technology in underwater environments.

1.2 Project Definition

The main objective of this research project is to develop a working system that uses the principles of machine vision and stereoscopy to measure and model objects in the flume tank

located at the Fisheries and Marine Institute, Memorial University, St. John's, NL. This system will need to meet several criteria for performance and accuracy:

The first is a simple and fast calibration protocol for the system. A proper calibration for the camera systems is important to ensure good accuracy and precision. This system should be both quick and easy to use, even for people with no training in machine vision.

The second is a simple and easy to use interface for the end user. This should hide all of the complex computations from the user and allow him or her to easily locate points in three dimensional space.

Finally and most importantly the system should be faster, more accurate and more precise than the existing system in the flume tank. The goal of which is to expand on the functionality of the flume tank and increase the accuracy of the existing functions to increase its life span, increase its competitiveness with other flume tanks and finally increase the customer base and profitability of the flume tank.

1.3 Challenges

Meeting the above criteria will require overcoming several important challenges: The first of which is housing the camera system in an underwater environment. Not only will the cameras be required to have a waterproof housing, they will also require power and a network connection to be able to return images and relevant information to the user. The housing will also need to minimize the effects of diffraction that are caused by the change in mediums as light travels through the water, housing, and air into the camera lens.

The process of determining the distance and position of a point in three dimensional space from multiple camera images will also be one of the main challenges of this project. The methods and equations of this process will need to be analyzed and compared to find the most accurate results.

Calibration of this system will pose additional challenges: The calibration will first need to function underwater to calibrate the camera system requiring a nontraditional calibration method, which typically relies on paper targets. Additionally, the various methods of calibration will need to be compared and testing for their performance and accuracy in underwater environments.

Finally, the system will be required to work over a large variety of distances and locations in the flume tank. The system should minimize the effects that distance and location will have on the error of the system.

1.4 Flume Tank

The flume tank at the Marine Institute in Memorial University of Newfoundland is the environment for the testing and installation of this project. The flume tank is an 8m x 4m x 22.5m circulating water channel designed to simulate the environment and conditions of the ocean. This is accomplished through the use of several water pumps to create water circulation and a moving belt for a floor to simulate moving over the ocean floor. The primary purpose of this is to test fishing gear for performance metrics before testing them in ocean environments[3].

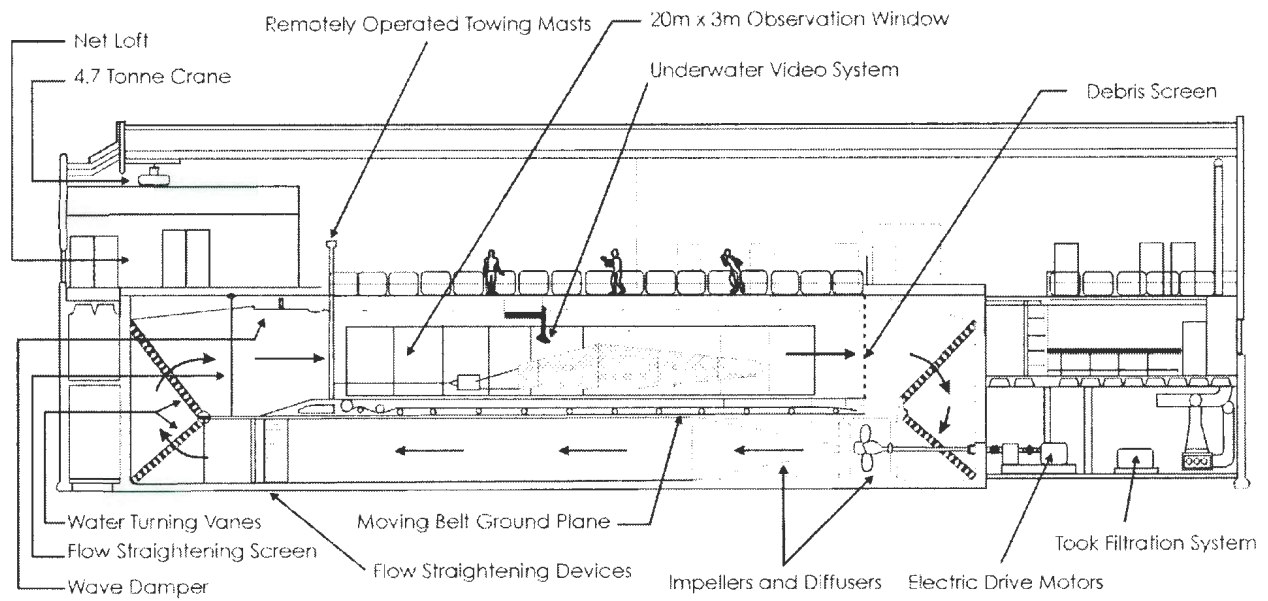


Figure 1 - Center for Sustainable Aquatic Resources Flume Tank Side Profile

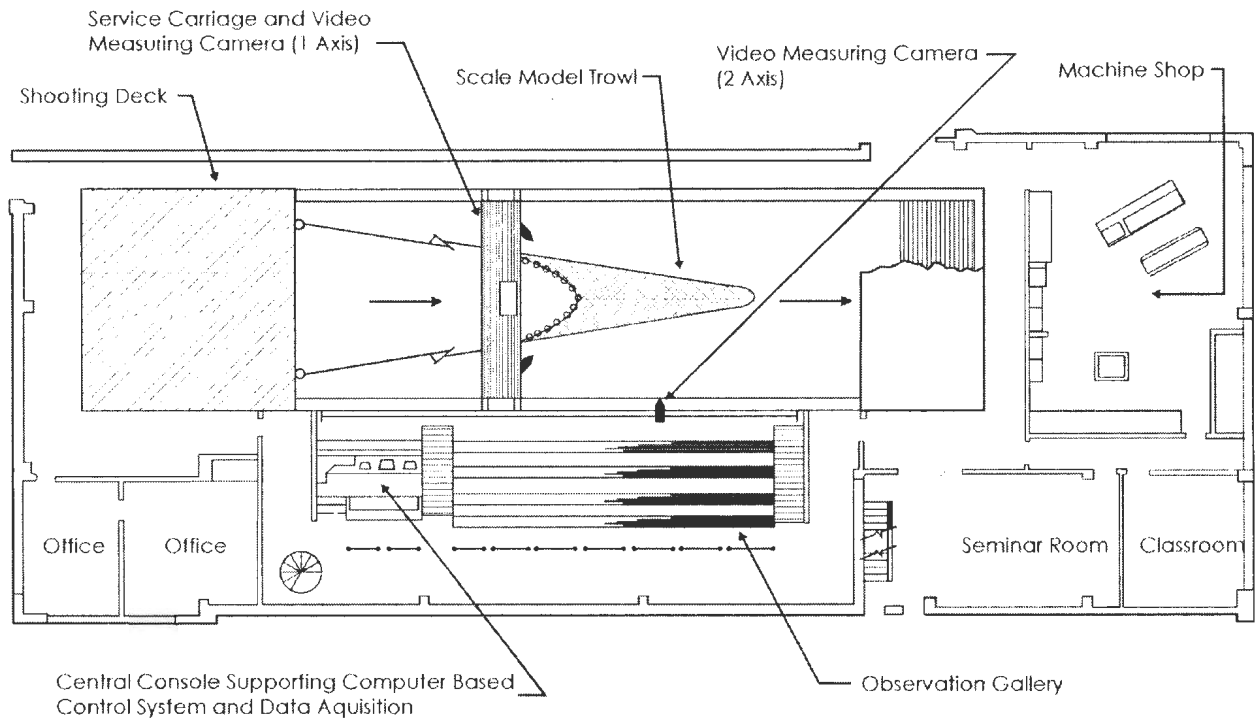


Figure 2 - Center for Sustainable Aquatic Resources Flume tank Top Profile

The existing system uses a series of analog cameras that are connected to encoders to determine movement. The system has 3 cameras: one for depth and vertical information and another two used for horizontal distance. These systems require the use of a crosshair to determine the position of an object in the tank. The cameras require slow mechanical chain systems to move the camera position to determine the position of an object in the tank.

The ultimate purpose of this project is to replace this existing system with a new stereoscopic camera system that will be faster, more accurate and more precise than the existing system.

1.5 Organization

This thesis contains the following 8 chapters:

Chapter 1: The introduction of the thesis, containing an overview of the purpose and scope of the project.

Chapter 2: A review of the theory and mathematics behind digital image capture. The modelling of a pinhole camera and image formation as a mathematical model will be described as well the theory and effects of distortion on this process.

Chapter 3: The theory and reasoning behind camera calibration will be described in this chapter. Modern calibration models and methods will also be compared to evaluate their performance and accuracy. Finally, this chapter includes an analysis of calibrating cameras in underwater environments.

Chapter 4: The theory of stereoscopic image processing will be reviewed. A comparison of several modern methods for stereoscopic location will be performed. Several novel

improvements of these methods are proposed and evaluated for performance versus other modern methods.

Chapter 5: The design of the mechanical and hardware support systems is included in this chapter. Additionally, this chapter contains an analysis of the effects that the water currents of the flume tank have on the camera support frame and its application for any camera system under the effects of movement.

Chapter 6: This chapter contains the software design of the project. Also included in this chapter is the implementation of the various algorithms used for camera calibration and feature recognition.

Chapter 7: The chapter has the comparative testing results of the old camera system versus the new camera system. The metrics of this testing, along with additional untestable benefits of the new system, will also be shown.

Chapter 8: The final chapter is the concluding remarks of the project as well as future recommendations for possible work and improvements to the system.

Chapter 2

2.1 Camera Model

The processes of translating a point from three dimensional space to the two dimensional space of an image can be described using a camera model. A camera model is a set of mathematical equations which represent the translation and rotation a point undergoes when moving from the world coordinate frame, through the camera coordinate frame and being projected on the image coordinate frame. The most common version of the camera model is the pinhole camera model used by many current camera calibration techniques[4][5][6].

2.2 Pinhole Camera Model

The pinhole Camera model is a simplified representation of the path that a ray will travel when being projected from a point in the world coordinate frame to being projected on the image coordinate frame. In this model the camera aperture is considered an infinitesimally small point through which all rays from the environment will pass and project on the image plane. The point through which all the rays pass is called the projection point or center of projection. The relationship between this point and the project plane is described by the intrinsic or internal camera parameters. The relation between the center of projection and a point in the environment is described by the extrinsic or external parameters.

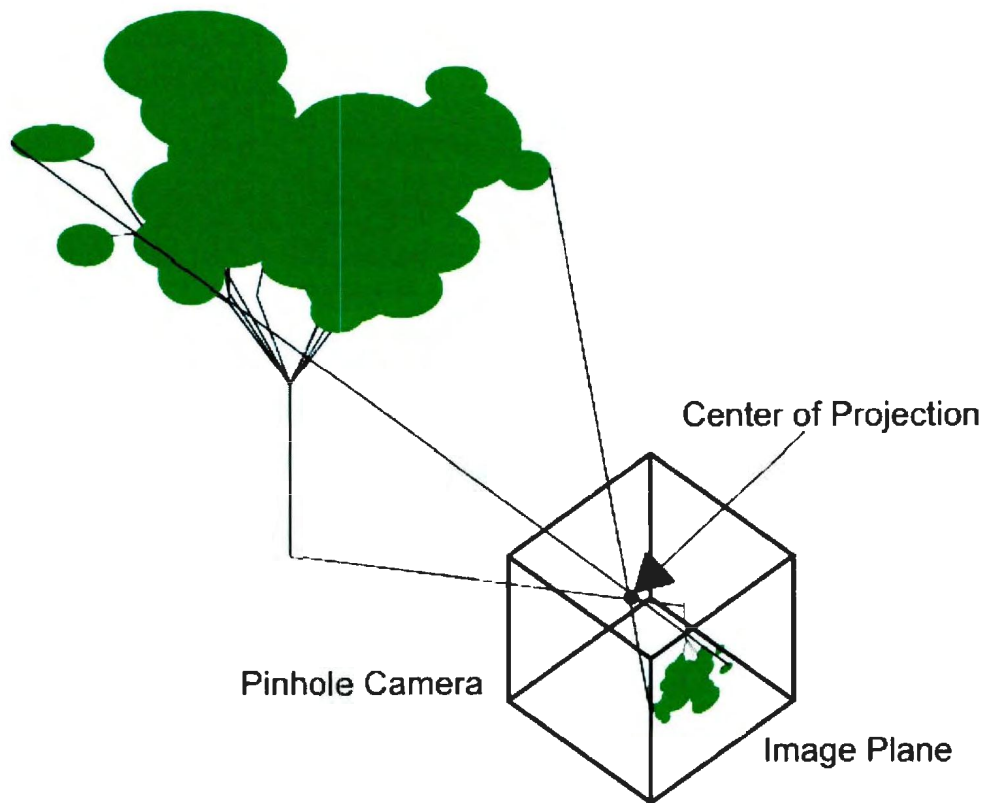


Figure 3 - Pinhole Ray Projection

2.3 Mathematical Model

The mathematical model can be divided into two distinct sections. The first section is the intrinsic parameters which describe the relation between the image plane and the center of projection. The first of the intrinsic parameters is the focal Length (f) which describes the translation distance between the image plane and the center of projection. The second is the scale factor (s) which relates the width and height of the camera pixels. If the pixels of the camera are square the scale factor is approximately one. The other two intrinsic parameters are the image center values (U_0 and V_0). These represent the offset between the center of the image and the center of projection.

The extrinsic parameters are described in two parts: The first is the rotation ($R_{3 \times 3}$) between the environment coordinate system which may be described by either a set of radian rotations or by quaternions. The second set is a translation ($T_{3 \times 1}$) vector between the center of projection and the environment coordinate system.

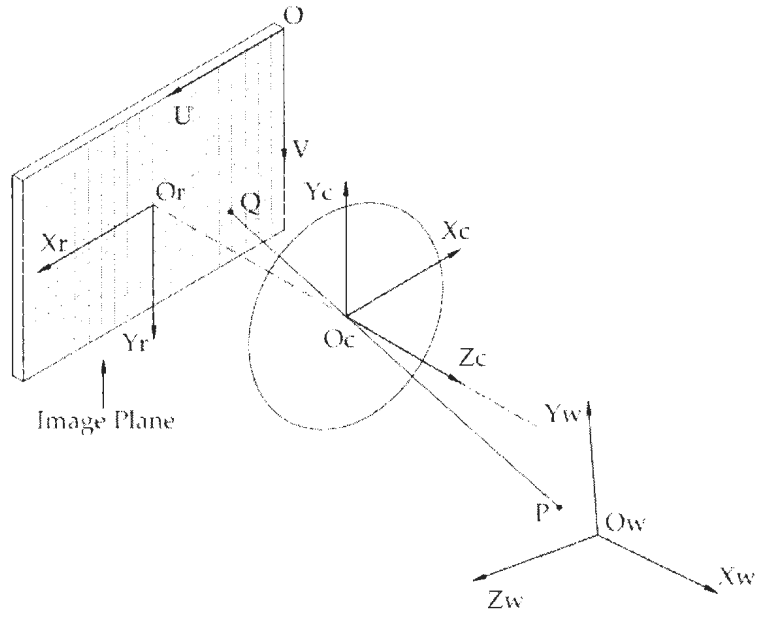


Figure 4 - Pinhole Camera Model[5]

A complete translation between the image plane and a point in the environment is described by the following equation:

$$\begin{bmatrix} u \\ v \\ 1 \end{bmatrix} = \begin{bmatrix} sf & 0 & u_0 & 0 \\ 0 & f & v_0 & 0 \\ 0 & 0 & 1 & 0 \end{bmatrix} \begin{bmatrix} r_{11} & r_{12} & r_{13} & t_x \\ r_{21} & r_{22} & r_{23} & t_y \\ r_{31} & r_{32} & r_{33} & t_z \\ 0 & 0 & 0 & 1 \end{bmatrix} \begin{bmatrix} P_x \\ P_y \\ P_z \\ 1 \end{bmatrix}$$

Figure 5 - Camera Model

Where s is the scale factor of the image sensor and f is the focal length of the camera. The variables u_0 and v_0 are the vertical and horizontal image centers. The matrices r and t

represent the rotation and transformation matrix. Finally P represents the world coordinates of the point.

2.4 Image Distortion

This equation however does not completely describe the translation due to the effect of distortion the camera lens and any other material between the environment and the image plane may cause. The distortions can be divided into two separate categories[5].

2.4.1 Radial Distortion

The first is radial distortion which is due to the refraction in the lens and is characterized by moving the points towards the center of the image or away from it depending on the distortion.

An image of this effect is shown below.

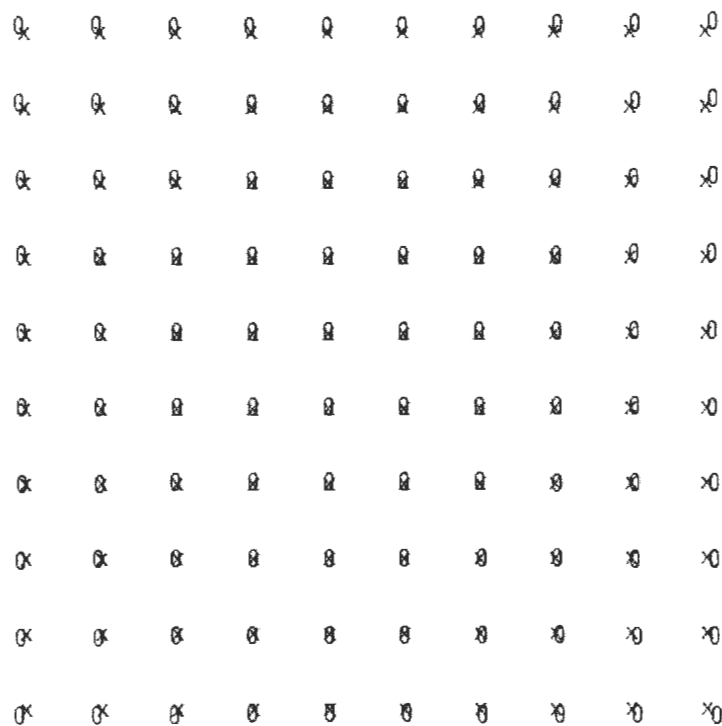


Figure 6 - Radial Distortion

In the image above the 'X' points indicate the image points that are undistorted and the 'O' marks indicate the points as they would appear due to radial distortion.

2.4.2 Tangential Distortion

Tangential distortion is due to an image plane that is not orthogonal to the lens. The image points may be closer together on top of the image and more distant on the bottom of the image or reversed depending on the distortion. An image showing this effect is displayed below.

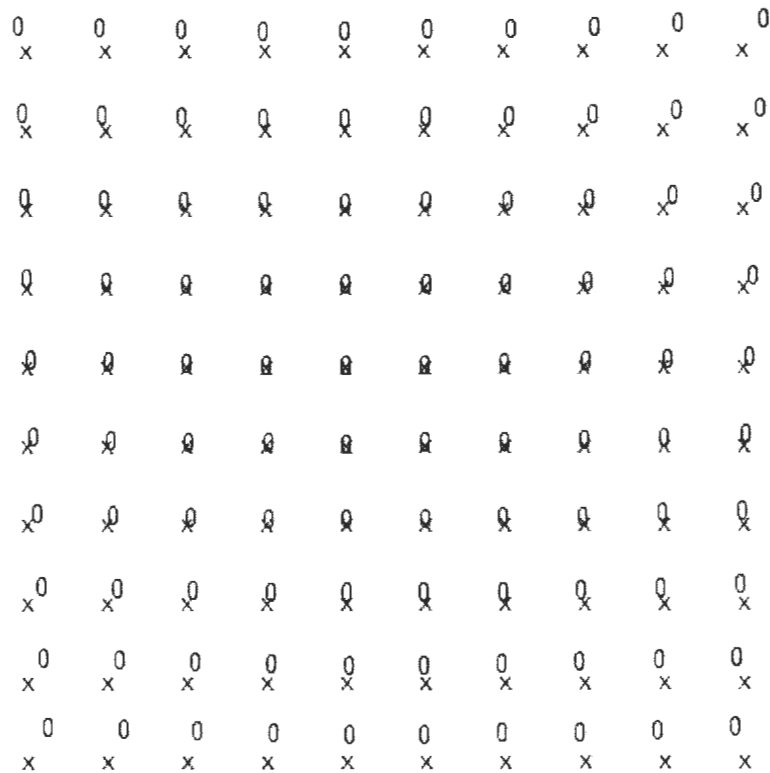


Figure 7 - Tangential Distortion

In the image above 'X' points indicate the undistorted points. The 'O' marks indicate the points as they would appear due to only tangential distortion. Here the image plane is closer on the

top of the lens and farther on the bottom, shifting the points upwards and farther apart on the top.

2.4.3 Complete Distortion Model

Distortion is described by the following equation:

$$\begin{bmatrix} u \\ v \end{bmatrix} = \begin{bmatrix} u_d \\ v_d \end{bmatrix} + \begin{bmatrix} \bar{u}_d(k_1 r_d^2 + k_2 r_d^4 + k_3 r_d^6 + \dots) + (2p_1 \bar{v}_d \bar{u}_d + p_2(r_d^2 + 2\bar{u}_d^2))(1 + p_3 r_d^2 + \dots) \\ \bar{v}_d(k_1 r_d^2 + k_2 r_d^4 + k_3 r_d^6 + \dots) + (p_1(r_d^2 + 2\bar{v}_d^2) + 2p_2 \bar{v}_d \bar{u}_d)(1 + p_3 r_d^2 + \dots) \end{bmatrix}$$

$$\text{Where, } \bar{u}_d = u_d - u_0, \bar{v}_d = v_d - v_0, r_d = \sqrt{\bar{u}_d^2 + \bar{v}_d^2}$$

Equation 1 - Complete Distortion Model

The variables k_1, k_2, k_3, \dots represent the radial distortion coefficients and p_1, p_2, p_3, \dots represent the tangential distortion coefficients. Any number of these coefficients may be included in the distortion model however, due to the higher order coefficients being small and having little effect on the model, they can be excluded. Reducing the equation to use 2 coefficients for each type of distortion produces the following equation:

$$\begin{bmatrix} u \\ v \end{bmatrix} = \begin{bmatrix} u_d \\ v_d \end{bmatrix} + \begin{bmatrix} \bar{u}_d(k_1 r_d^2 + k_2 r_d^4) + (2p_1 \bar{v}_d \bar{u}_d + p_2(r_d^2 + 2\bar{u}_d^2)) \\ \bar{v}_d(k_1 r_d^2 + k_2 r_d^4) + (p_1(r_d^2 + 2\bar{v}_d^2) + 2p_2 \bar{v}_d \bar{u}_d) \end{bmatrix}$$

Equation 2- Simplified Distortion Model

Chapter 3

3.1 Camera Calibration

Camera calibration is the process of determining a camera's intrinsic and extrinsic parameters through estimate and optimization of a model using a set of known points in three dimensional space. This process is essential for 3D reconstruction of an environment from one or more camera images. This process takes several steps and, depending on the methods used, will have greatly different degrees of accuracy, difficulty, stability and time spent on the calibration process.

3.2 Data Collection

The first step of calibration is collecting data for the calibration procedure. The data can be collected in several ways which require differing amounts of user interaction, number of points, and overall accuracy in the data collected. The various data collection methods and their advantages are collected below.

3.2.1 Photogrammetric Calibration

These techniques use highly accurate targets that consist of one or more planes in an orthogonal orientation. They typically have several hundred calibration points[5][4], either from one image or several images of the same target at multiple angles. These techniques produce highly accurate results however they require the construction of accurate targets and longer times for image collection.

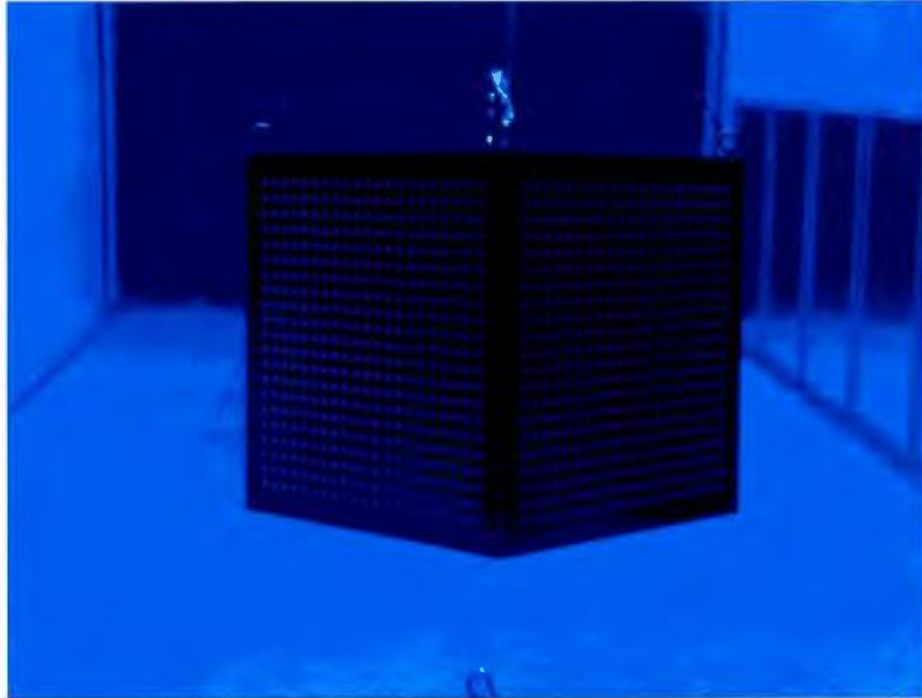


Figure 8 - Photogrammetric Calibration Target

The points collected from these targets can be refined through an iterative method to improve their accuracy. This is the technique used by this project.

3.2.2 Self-Calibration

These techniques use a static scene in order to calibrate the camera. The camera is moved around the environment and points for calibration are automatically chosen and the camera geometry is generated from these points. The advantage of this is that it is fully automated and takes very little user interaction for calibration and does not require the construction of an expensive or complicated target. However, data collected using these methods produce unstable and largely varying results [7]. Due to the high accuracy requirements of this project this method was not selected.

3.2.3 Calibration through Motion

This method uses a small target with only a few points, in a known geometry and orientation, which is moved through the environment. A series of images is taken during this motion which generates the points used in the calibration process. This process allows for a much simpler calibration target than those used by photogrammetric calibration and requires less expensive assembly. However, due to movement and rotation, this method can lead to missing calibration points which causes inaccuracy and instability in the camera model[8].

3.3 Calibration Methods

There are several techniques for camera calibration have that been proposed over the years[6][4][9]. All these techniques used the data collected from the previous methods to generate a camera model. The various techniques and their advantages are discussed below.

3.3.1 Tsai

In a paper by Tsai, the predecessor to the current paradigm of camera calibration was proposed[9]. His process divided camera calibration into two sections and used a simple linear camera model. The first step of this calibration process is to estimate the extrinsic camera parameter, ignoring the focal length and distortion. Here the forward camera model is used to estimate the location of the points on the image plane based on their location in three dimensional space. Next, this information is used to estimate the intrinsic parameters. The exact solution to these parameters can be found using iterative optimization.

This method was improved on by later algorithms developed by [4][6][5] and is therefore not used in current camera calibration techniques due to the poor optimization of camera parameters and simplified distortion modelling.

3.3.2 Zhang

Zhang proposed an improvement on the methodology proposed by Tsai. His method used three steps after the data is collected[6]. The first step estimates the intrinsic and extrinsic parameters using a closed form solution. The camera matrix and image plane homography are related by the following equations:

$$A = \begin{bmatrix} \alpha & \gamma & u_0 \\ 0 & \beta & v_0 \\ 0 & 0 & 1 \end{bmatrix}$$

Equation 3 - Zhang Camera model

$$s \begin{bmatrix} u \\ v \\ 1 \end{bmatrix} = A \begin{bmatrix} r_1 & r_2 & r_3 & t \end{bmatrix} \begin{bmatrix} X \\ Y \\ 0 \\ 1 \end{bmatrix}$$

$$s \tilde{m} = H \tilde{M}$$

$$H = A \begin{bmatrix} r_1 & r_2 & t \end{bmatrix}$$

Equation 4 - Zhang Image Plane Homography

Where α and β are the scale factors, γ is the image axis skew factor, s is the focal length and v_0 and u_0 are the principal point coordinates. The matrix above is used to write a set of homogenous equations used in the estimation of the camera parameters.

The parameters estimated above are used to estimate the distortion through the use of the following equations and a least squares analysis.

$$\begin{pmatrix} (u - u_0)(x^2 + y^2) & (u - u_0)(x^2 + y^2)^2 \\ (v - v_0)(x^2 + y^2) & (v - v_0)(x^2 + y^2)^2 \end{pmatrix} \begin{bmatrix} k_1 \\ k_2 \end{bmatrix} = \begin{bmatrix} \check{u} - u \\ \check{v} - v \end{bmatrix}$$

Equation 5 - Zhang Distortion Model

Where (u, v) are the real image coordinates and (\check{u}, \check{v}) are the distorted image coordinates.

Using the distortion and the estimates from above, these points are refined using maximum likelihood estimation to generate a full model[6].

This is the method implemented by OpenCV for their implementation of the camera calibration model[10]. However, the OpenCV implementation augments the distortion model to also include tangential distortion, something not included in the original modeling by Zhang. The performance of this method compared to other modern methods is discussed in section 3.5.

3.3.3 Heikkila

In [4] Heikkila suggested a four step calibration process that could determine all parameters of a camera. The first step of this process was to determine the focal length and image center of the camera, as well as estimates of the distortion using DLTs or direct linear transformations. This method was developed by Abdel-Aziz[11], in 1971, and uses only linear parameters to generate a model for the camera. This procedure generates a set of implicit camera parameters through the use of a homogeneous translation matrix.

$$\begin{bmatrix} u_i w_i \\ v_i w_i \\ w_i \end{bmatrix} = \begin{bmatrix} a_{11} & a_{12} & a_{13} & a_{14} \\ a_{21} & a_{22} & a_{23} & a_{24} \\ a_{31} & a_{32} & a_{33} & a_{34} \end{bmatrix} \begin{bmatrix} X_i \\ Y_i \\ Z_i \\ 1 \end{bmatrix}$$

Equation 6 - DLT Translation Matrix

By replacing the U_i and V_i with the observed points the parameters a_{11} through a_{34} are calculated through the least squares analysis. These values are then translated to explicit camera parameters through a decomposition technique described by Melen[12] which allows the image center, focal length and a distortion estimate to be extracted.

Next, a non linear estimate of the radial and tangential distortion is performed. The estimates of these parameters are calculated using an iterative technique [13] which attempts to minimize the error between the expected and measured points from the calibration target. The results from the DLT are also used as an initial estimation in this step. This provides two advantages: the first is that it speeds up convergence which reduces the number of iteration required for the process. Secondly it also prevents convergence on local minimums which may occur if an improper estimate is used as a first guess in the process.

The third step is the correction for asymmetric projection. This step will help correct errors that are introduced as a result of the target and camera being in non-orthogonal planes which may distort the image and, in particular, the circles which can be used for calibration. This part of the calibration introduces three (α , β and γ) skew coefficients which attempt to describe the effects of the asymmetric projection.

The fourth step is the image correction step where the model developed in the previous 3 steps is used to correct and relate the image points to real world coordinates. The problem, however, is that the equation describes the projection of the three dimensional points on to the image plane, and not the reverse. There is no exact numerical method to solve this back projection model. Heikkila uses the method described by Melen[12] which approximates the translation through the use of the following equations:

$$\begin{aligned}
 \mathbf{u}_i &= [-\tilde{u}'_i r_i^2, -\tilde{u}'_i r_i^4, -2\tilde{u}'_i \tilde{v}'_i, -(r_i^2 + 2\tilde{u}'_i{}^2), \tilde{u}'_i r_i^4, \tilde{u}'_i \tilde{u}'_i r_i^2, \tilde{u}'_i \tilde{v}'_i r_i^2, \tilde{u}'_i r_i^2]^T \\
 \mathbf{v}_i &= [-\tilde{v}'_i r_i^2, -\tilde{v}'_i r_i^4, -(r_i^2 + 2\tilde{v}'_i{}^2), -2\tilde{u}'_i \tilde{v}'_i, \tilde{v}'_i r_i^4, \tilde{v}'_i \tilde{u}'_i r_i^2, \tilde{v}'_i \tilde{v}'_i r_i^2, \tilde{v}'_i r_i^2]^T \\
 \mathbf{T} &= [\mathbf{u}_1, \mathbf{v}_1, \dots, \mathbf{u}_i, \mathbf{v}_i, \dots, \mathbf{u}_N, \mathbf{v}_N]^T \\
 \mathbf{p} &= [a_1, a_2, a_3, a_4, a_5, a_6, a_7, a_8]^T \\
 \mathbf{e} &= [\tilde{u}'_1 - \tilde{u}_1, \tilde{v}'_1 - \tilde{v}_1, \dots, \tilde{u}'_i - \tilde{u}_i, \tilde{v}'_i - \tilde{v}_i, \dots, \tilde{u}'_N - \tilde{u}_N, \tilde{v}'_N - \tilde{v}_N]^T
 \end{aligned}$$

Equation 7 - Melen Back-Projection Solution

The actual image coordinates are then interpolated from v_i, \tilde{u}_i and v'_i, \tilde{u}'_i . This, however, is an inexact calculation due to the interpolation and certain assumptions used to generate the above equations. The performance of this model compared to other modern techniques will be described in a later section.

3.3.4 Rahman and Krouglicof

The method developed by Rahman and Krouglicof is similar to the method developed by Heikkila but with several differences that improve the accuracy and stability of the generated model. The first difference is the introduction of quaternions into the calculation of the rotation matrix instead of the radian rotations used by previous methods. Using quaternions prevents the singularity and Gimbal lock that is characteristic of using radians. These require more computation but increase accuracy[5].

The second change is in the image correction process which handles the model optimization and error minimization in a different way. As described earlier, in the Heikkila method, the goal is to develop a numerically approximate model in which you attempt to minimize the difference between the measured points and the ideal points from the target distorted by the model. The Rahman and Krouglicof approach differs by using the model to correct the distorted points and compare them to the ideal points from the target.

The Rahman and Krouglicof method of developing a back projection model and not a forward model removes the error that is introduced by Heikkila's method. This model does not need to be reversed unlike Heikkila's method which allows it to be numerically exact instead of an

approximation[5]. The performance of this model will be compared to other modern calibration techniques in a later section.

3.4 Calibration Setup

The following section describes the calibration setup used for experimental comparison of algorithm performance and final project implementation. The calibration setup uses the photogrammetric data collection techniques described above.

3.4.1 Calibration cube

In order to ensure the most accurate data collection for the calibration process a highly accurate target is required for the calibration process. Most calibration implementations use a printed target for the purpose of calibration. This printed target is a checker board pattern in which the intersection points of the squares are used to locate the points. In a paper by Heikkila [4] it was suggested that these targets are inaccurate due to the effects of distortion. The transformation and distortion does not preserve the line and intersection points well. Circular control points, which are also used for calibration, suffer from the effects of this as well, but can be compensated for by treating the circles as ellipses and finding the centers. Using this information the target for calibration experimentation was designed and built to use circular control points.

The process of printing and mounting targets also introduces error into the calibration process. In a paper by Andrea Albarelli [14] a comparison of printer introduced error showed that laser printers can cause image error of up to 3 mm and inkjet printers introduce less but still significant error. For this reason regularly printed targets will not be used for the calibration process. To produce a highly accurate calibration image a computer numeric control (CNC) machine will be used to imprint a pattern on a metallic surface. This machine will lead to a

target accuracy of 0.001 millimeters with the most basic of CNC machines, results which are 1000 times more accurate than a printed target. The target is then attached to a 7 mm thick aluminium plate with metal screws and metal adhesive to ensure no target warping.

The calibration target also has the requirement of containing two nonparallel points in order to produce a proper calibration model. Multiple images of a singular target plane may be used instead of two orthogonal planes [15] to produce accurate results. However, in practice, this method would be more time consuming especially in an underwater environment and produce similar results as if a single multisided target was used.

The target was designed to have two orthogonal target planes at a know angle. This angle is achieved using the CNC machine to ensure a perfectly orthogonal plane by machining the aluminium plate before the target is attached. This method would ensure that the assembled cube faces would have error similar to that stated above.

The target cube was chosen to have a 21 x 21 grid of points to fit the two foot restriction of the plate size. This size is the maximum that can be purchased for the black anodized plate without connecting multiple panels. The holes were created using the CNC machine to ensure accuracy of the target. Originally a laser was used to remove the anodization, however, the resulting target had little contrast. The black anodized plate was chosen to increase the contrast between the circles and the background.

The completed calibration target is shown below.

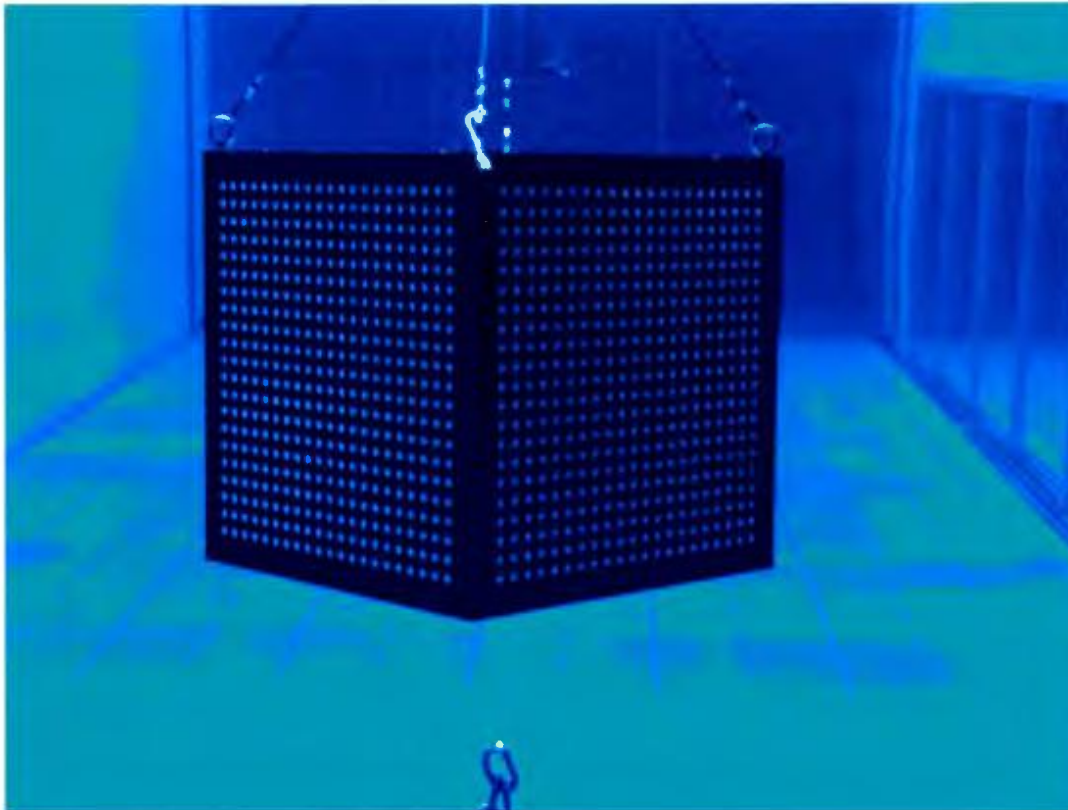


Figure 9 - Highly Accurate Calibration target

3.4.2 Data Acquisition and Algorithm Implementation

The Data, used for testing the above calibration methods, was captured using the calibration software used in section 6. The custom calibration software used an iterative circle correction algorithm to detect the best possible circle center for all points on the calibration cube. This data was then passed to a Matlab implementation of each algorithm used. The implementation of Zhang's camera calibration used was part of the Caltech Camera Calibration Toolbox for Matlab[16]. The implementation used for evaluating Heikkila's method of calibration was from his own camera calibration toolbox for Matlab[17]. The implementation used for the testing of

the Rahman and Krouglicof method was from the camera calibration toolbox Rahman published with his work[18].

3.5 Calibration Results

The following are camera models generated by their respective algorithms. All generated models use the same data set for image points, and all model differences are a result of the algorithms used. These models shown only use the intrinsic parameters, though these models produce extrinsic parameters as well, they cannot be compared directly due to the shifts in camera position and the representations of translation and rotation. The error shown below is the standard deviation of pixel error when the points are re-projected through the model.

Both the Rahman and Krouglicof method and the Heikkila method use the same calibration models [4][5], however, the implementation used for testing the Heikkila method averages pixels error across the X and Y directions before displaying the results. Zhang's method of calibration uses a slightly different model that includes no tangential distortion but includes an additional skew factor[6]. These changes are reflected in the models shown for Zhang Calibration Method.

3.5.1 Above Water

3.5.1.1 Rahman and Krouglicof

Parameter	1	2	3	4	5	6
Scale Factor	1.00026574	1.00030226	1.0002603	1.000528128	1.00023842	1.001456192
Focal Length	8.32742172	8.3090166	8.31608463	8.306763738	8.29806988	8.297457188
Image Center X	1321.69359	1323.09685	1319.52538	1328.199487	1331.90151	1328.326901
Image Center Y	910.331105	894.551629	912.962016	936.4398525	900.25375	930.007596
Radial Distortion 1	0.00131659	0.00111864	0.00120263	0.000978502	0.00076703	0.000947782
Radial Distortion 2	-6.11E-05	-4.10E-05	-5.30E-05	1.85E-06	2.04E-05	-1.89E-05
Tangential Distortion 1	0.00131659	0.000273	4.78E-05	-0.00024441	0.00024414	-0.00017937
Tangential Distortion 2	0.00016126	3.77E-05	0.00017465	0.00015214	-1.63E-05	0.00043476
Pixel Error Y	0.20207176	0.20657819	0.20500481	0.205934294	0.2071908	0.189158294
Pixel Error X	0.2650071	0.23360733	0.26139142	0.231761435	0.24379156	0.244885024

Table 1 -Rahman and Krouglicof Camera Model Data above Water

3.5.1.2 Heikkila

Parameter	1	2	3	4	5	6
Scale Factor	1.0003	1.0003	1.0003	1.0005	1.0002	1.0014
Focal Length	8.3278	8.3097	8.3166	8.3069	8.2988	8.2983
Image Center X	1321.8237	1323.2143	1319.907	1328.2213	1332.2115	1328.4701
Image Center Y	910.0301	894.4204	913.077	936.3319	900.1936	929.7921
Radial Distortion 1	1.33E-03	1.13E-03	1.22E-03	9.83E-04	7.79E-04	9.56E-04
Radial Distortion 2	-6.20E-05	-4.09E-05	-5.45E-05	2.87E-06	1.99E-05	-1.77E-05
Tangential Distortion 1	8.63E-05	2.76E-04	4.75E-05	-2.44E-04	2.45E-04	-1.79E-04
Tangential Distortion 2	1.60E-04	3.81E-05	1.71E-04	1.51E-04	-2.01E-05	4.28E-04
Pixel Error Y	0.235699	0.220698	0.234944	0.219465	0.226376	0.219141
Pixel Error X	0.235699	0.220698	0.234944	0.219465	0.226376	0.219141

Table 2 - Heikkila Camera Model Data above Water

3.5.1.3 Zhang

Parameter	1	2	3	4	5	6
Scale Factor	1.0003	1.00034	1.0003	1.00035	1.00031	1.00042
Focal Length	8.32188	8.30172	8.31093	8.31075	8.29909	8.32175
Image Center X	1330.867	1323.31	1329.886	1337.753	1331.435	1340.618
Image Center Y	914.8866	912.235	914.7343	919.0786	916.9579	916.023
Radial Distortion 1	-0.00015	-0.00013	-0.00014	-0.00012	-0.00011	-0.00014
Radial Distortion 2	7.6E-06	4.92E-06	7.3E-06	-1E-06	5.6E-07	2.86E-06
Skew Factor	0.00048	0.0005	0.0005	0.00051	0.00045	-0.00042
Pixel Error Y	0.19115	0.19375	0.19397	0.18596	0.19647	0.18801
Pixel Error X	0.24029	0.22549	0.23688	0.2245	0.22852	0.25089

Table 3 - Zhang Camera Model Data above Water

3.5.2 Above Water with Case

3.5.2.1 Rahman and Krouglicof

Parameter	1	2	3	4	5	6
Scale Factor	1.00082378	1.000607935	1.00070468	1.000763788	1.00074474	1.001237544
Focal Length	8.31329491	8.319168409	8.31432702	8.320816189	8.31276625	8.308460309
Image Center X	1327.3467	1330.214642	1334.20234	1337.672641	1330.78349	1332.717951
Image Center Y	931.737332	906.3922417	898.833601	910.0229545	913.157931	912.2215914
Radial Distortion 1	0.00105078	0.001361968	0.00115997	0.000803006	0.00095138	0.000897272
Radial Distortion 2	-1.96E-05	-8.62E-05	-7.69E-05	-6.38E-06	2.98E-06	-3.72E-06
Tangential Distortion 1	-0.00013235	9.19E-05	0.00013893	5.77E-06	5.09E-05	6.13E-05
Tangential Distortion 2	0.00016055	-3.15E-05	-8.31E-05	0.000100303	0.00012824	0.000245492
Pixel Error Y	0.21132119	0.190168343	0.21175306	0.202249849	0.18670391	0.179678147
Pixel Error X	0.4043873	0.2205956	0.47582481	0.49091584	0.22434023	0.23277432

Table 4 - Rahman and Krouglicof Camera Model Data above Water with Case

3.5.2.2 Heikkila

Parameter	1	2	3	4	5	6
Scale Factor	1.0008	1.0006	1.0007	1.0008	1.0007	1.0012
Focal Length	8.3144	8.3197	8.3171	8.3255	8.3131	8.3084
Image Center X	1328.0374	1330.3847	1332.9403	1333.5	1330.877	1333.1776
Image Center Y	931.0659	907.1027	899.5954	909.2888	912.9426	912.2002
Radial Distortion 1	1.06E-03	1.37E-03	1.18E-03	8.51E-04	9.54E-04	8.94E-04
Radial Distortion 2	-1.90E-05	-8.63E-05	-7.65E-05	-7.76E-06	4.23E-06	-2.06E-06
Tangential Distortion 1	-1.26E-04	8.65E-05	1.35E-04	2.81E-05	5.44E-05	6.26E-05
Tangential Distortion 2	1.46E-04	-3.32E-05	-6.16E-05	1.44E-04	1.27E-04	2.42E-04
Pixel Error Y	0.322795	0.206008	0.368368	0.3754	0.20648	0.208024
Pixel Error X	0.322795	0.206008	0.368368	0.3754	0.20648	0.208024

Table 5 - Heikkila Camera Model Data above Water with Case

3.5.2.3 Zhang

Parameter	1	2	3	4	5	6
Scale Factor	1.00055	1.00052	1.00059	1.00064	1.00053	1.00067
Focal Length	8.32004	8.31623	8.31415	8.32737	8.31591	8.32004
Image Center X	1336.534	1327.539	1328.312	1341.221	1337.617	1342.164
Image Center Y	921.5498	912.1176	908.3564	912.5452	917.5688	919.0994
Radial Distortion 1	-0.00013	-0.00016	-0.00013	-0.0001	-0.00011	-0.00012
Radial Distortion 2	1.68E-06	9.48E-06	7.71E-06	7.7E-07	-5.8E-07	4.2E-07
Skew Factor	0.00022	0.00004	0.00013	0.00019	-0.00001	0.00001
Pixel Error Y	0.20847	0.19049	0.21226	0.20156	0.18704	0.17909
Pixel Error X	0.40538	0.22114	0.47594	0.4902	0.22712	0.23923

Table 6 - Zhang Camera Model Data above Water with Case

3.5.3 Below Water with Case

3.5.3.1 Rahman and Krouglicof

Parameter	1	2	3	4	5	6
Scale Factor	1.00108941	1.000516513	1.00031477	1.00043359	1.00044628	1.000933543
Focal Length	11.1498052	11.10383382	11.1265633	11.13346304	11.1769577	11.17618091
Image Center X	1295.77022	1360.380405	1358.36299	1337.753511	1267.193	1269.765406
Image Center Y	954.571171	852.2596444	844.239703	896.8454246	979.382298	936.5652846
Radial Distortion 1	-2.52E-03	-3.15E-03	-2.69E-03	-1.87E-03	-2.29E-03	-2.54E-03
Radial Distortion 2	1.15E-04	2.07E-04	1.14E-04	-3.31E-05	8.30E-05	1.88E-04
Tangential Distortion 1	-5.84E-04	8.72E-04	8.80E-04	1.13E-04	-8.41E-04	-2.63E-04
Tangential Distortion 2	7.83E-04	-1.46E-04	-4.04E-05	2.41E-04	1.16E-03	1.07E-03
Pixel Error Y	0.15329564	0.157157675	0.14429398	0.180028998	0.20601263	0.141484589
Pixel Error X	0.12839447	0.132811681	0.14607391	0.142326279	0.17554819	0.148545089

Table 7 - Rahman and Krouglicof Model Data below Water with Case

3.5.3.2 Heikkila

Parameter	1	2	3	4	5	6
Scale Factor	1.0011	1.0007	1.0003	1.0004	1.0004	1.0009
Focal Length	11.151	11.1582	11.1277	11.1369	11.1796	11.1763
Image Center X	1297.9996	1272.1766	1358.1978	1335.4312	1267.6451	1270.3984
Image Center Y	954.897	983.5307	845.2576	896.8656	980.6605	937.1023
Radial Distortion 1	-2.52E-03	-4.08E-03	-2.68E-03	-1.85E-03	-2.27E-03	-2.52E-03
Radial Distortion 2	1.20E-04	8.63E-04	1.75E-05	-3.11E-05	8.27E-05	1.85E-04
Tangential Distortion 1	-5.87E-04	-8.53E-04	8.61E-04	1.08E-04	-8.49E-04	-2.67E-04
Tangential Distortion 2	7.47E-04	1.14E-03	-3.67E-05	2.57E-04	1.15E-03	1.06E-03
Pixel Error Y	0.14148	0.156472	0.145314	0.162365	0.19204	0.14515
Pixel Error X	0.14148	0.156472	0.145314	0.162365	0.19204	0.14515

Table 8 - Heikkila Model Data below Water with Case

3.5.3.3 Zhang

Parameter	1	2	3	4	5	6
Scale Factor	1.0006	1.00086	1.00065	1.0002	1.00032	1.00051
Focal Length	11.13026	11.13579	11.14561	11.14595	11.1551	11.1717
Image Center X	1355.33045	1354.33	1358.0654	1354.1255	1356.52553	1351.30976
Image Center Y	910.50366	913.29869	910.31599	906.61357	911.21711	916.27155
Radial Distortion 1	0.00025187	-0.0001553	0.0002354	0.0001661	0.00026044	0.00022325
Radial Distortion 2	-1.837E-05	9.48E-06	-1.052E-05	3.67E-06	-2.359E-05	-1.755E-05
Skew Factor	0.00051	0.00004	0.00045	-0.00008	0.00113	0.00093
Pixel Error Y	0.14315	0.19049	0.14896	0.18074	0.14621	0.13908
Pixel Error X	0.1318	0.22114	0.14792	0.14662	0.18808	0.14892

Table 9 - Zhang Model Data below Water with Case

3.6 Calibration Comparison

The following is a summary of the previous data to generate averages and deviations of data.

This data will allow the analysis of not only average performance of these algorithms, but also the effects that the water has on model generation.

3.6.1 Rahman and Krouglicof Data Analysis

3.6.1.1 Above Water

Parameter	Average	Standard Deviation
Scale Factor	1.00050851	0.000476344
Focal Length	8.30913563	0.011376701
Image Center X	1325.45729	4.737236523
Image Center Y	914.090992	16.37972628
Radial Distortion 1	0.0010552	0.000580129
Radial Distortion 2	1.09E-04	3.21489E-05
Tangential Distortion 1	0.00024295	0.000567023
Tangential Distortion 2	0.00015736	0.000156068
Pixel Error Y	0.20265636	0.006851883
Pixel Error X	0.24674064	0.013836976
Pixel Error Average	0.2246985	

Table 10 - Rahman and Krouglicof Model Analysis above Water

3.6.1.2 Above Water with Case

Parameter	Average	Standard Deviation
Scale Factor	1.00081374	0.000219644
Focal Length	8.31480551	0.004518721
Image Center X	1332.15629	3.569835529
Image Center Y	912.060942	10.95116089
Radial Distortion 1	0.0010374	0.000575151
Radial Distortion 2	2.22E-06	3.94665E-05
Tangential Distortion 1	3.6081E-05	9.36316E-05
Tangential Distortion 2	8.6671E-05	0.000122776
Pixel Error Y	0.19697908	0.013439011
Pixel Error X	0.34147302	0.129991242
Pixel Error Average	0.26922605	

Table 11 - Rahman and Krouglicof Model Analysis above Water with Case

3.6.1.3 Below Water with Case

Parameter	Average	Standard Deviation
Scale Factor	1.00062235	0.000476344
Focal Length	11.1444673	0.028922649
Image Center X	1314.87092	42.79909825
Image Center Y	910.643921	55.38073182
Radial Distortion 1	-0.0025114	0.001400889
Radial Distortion 2	7.08E-05	8.55828E-05
Tangential Distortion 1	2.9435E-05	0.000729415
Tangential Distortion 2	0.00051189	0.000569197
Pixel Error Y	0.16371225	0.024811952
Pixel Error X	0.1456166	0.016589632
Pixel Error Average	0.15466443	

Table 12 - Rahman and Krouglicof Analysis below Water with Case

3.6.2 Heikkila Data Analysis

3.6.2.1 Above Water

Parameter	Average	Standard Deviation
Scale Factor	1.0005	0.000451664
Focal Length	8.30968333	0.011241248
Image Center X	1325.64132	4.715350098
Image Center Y	913.974183	16.36269925
Radial Distortion 1	0.00106551	0.000585704
Radial Distortion 2	6.64E-06	3.26753E-05
Tangential Distortion 1	3.8655E-05	0.000213785
Tangential Distortion 2	0.00015463	0.000154387
Pixel Error Y	0.22605383	0.007642683
Pixel Error X	0.22605383	0.007642683
Pixel Error Average	0.22605383	

Table 13 – Heikkila Model Analysis above Water

3.6.2.2 Above Water with Case

Parameter	Average	Standard Deviation
Scale Factor	1.0008	0.000209762
Focal Length	8.31636667	0.005883423
Image Center X	1331.48617	2.12175774
Image Center Y	912.0326	10.48464587
Radial Distortion 1	0.0010528	0.000582172
Radial Distortion 2	4.42E-06	3.97494E-05
Tangential Distortion 1	4.0093E-05	8.9113E-05
Tangential Distortion 2	9.3831E-05	0.000116991
Pixel Error Y	0.28117917	0.083419043
Pixel Error X	0.28117917	0.083419043
Pixel Error Average	0.28117917	

Table 14 - Heikkila Model Analysis above Water with Case

3.6.2.3 Below Water with Case

Parameter	Average	Standard Deviation
Scale Factor	1.00063333	0.000320416
Focal Length	11.15495	0.020774865
Image Center X	1300.30812	38.3223739
Image Center Y	933.052283	53.52679627
Radial Distortion 1	-0.00265301	0.001593509
Radial Distortion 2	-2.92E-05	0.000330493
Tangential Distortion 1	-0.00026451	0.000662802
Tangential Distortion 2	0.00071962	0.00050302
Pixel Error Y	0.15713683	0.018839356
Pixel Error X	0.15713683	0.018839356
Pixel Error Average	0.15713683	

Table 15 - Heikkila Model Analysis below Water with Case

3.6.3 Zhang Data Analysis

3.6.3.1 Above Water

Parameter	Average	Standard Deviation
Scale Factor	1.000337	4.59E-05
Focal Length	8.31102	0.009612
Image Center X	1332.312	6.137927
Image Center Y	915.6526	2.310336
Radial Distortion 1	-0.00013	7.2E-05
Radial Distortion 2	1.70E-04	3.53E-06
Skew Factor	0.000337	0.000371
Pixel Error Y	0.191552	0.003971
Pixel Error X	0.234428	0.010244
Pixel Error Average	0.21299	

Table 16 - Zhang Model Analysis above Water

3.6.3.2 Above Water with Case

Parameter	Average	Standard Deviation
Scale Factor	1.000583	6.12E-05
Focal Length	8.318957	0.004753
Image Center X	1335.564	6.288181
Image Center Y	915.2062	4.99041
Radial Distortion 1	-0.00012	6.77E-05
Radial Distortion 2	5.00E-05	4.24E-06
Skew Factor	9.67E-05	9.71E-05
Pixel Error Y	0.196485	0.013008
Pixel Error X	0.343168	0.12828
Pixel Error Average	0.269827	

Table 17 - Zhang Model Analysis above Water with Case

3.6.3.3 Below Water with Case

Parameter	Average	Standard Deviation
Scale Factor	1.00052333	0.0002372
Focal Length	11.1474017	0.0147218
Image Center X	1354.94777	2.3086074
Image Center Y	911.370095	3.2327549
Radial Distortion 1	0.00016362	0.0001409
Radial Distortion 2	2.44E-04	1.324E-05
Skew Factor	0.00049667	0.0004759
Pixel Error Y	0.158105	0.0217801
Pixel Error X	0.16408	0.0336739
Pixel Error Average	0.1610925	

Table 18 - Zhang Model Analysis below Water with Case

3.6.4 Algorithm Evaluation

The differences in the algorithms make a direct comparison across all the camera models difficult, however, the main elements remain constant along with pixel error. Scale Factor appears unaffected by the camera case with changes of less than 0.1% for all camera models.

Algorithm	Above Water with Case	Underwater with Case
Rahman and Krouglicof	+0.06%	+34.12%
Heikkila	+0.08%	+34.24%
Zhang	+0.09%	+34.13%

Table 19 - Camera Model Focal Length Changes

The above table shows the percentage increase in focal length based of the above water without case condition. When the camera case is placed under water the focal length increases greatly with an approximate change of 34% for all camera models. In [19] it was theorized that all values of camera calibration can be found for above water conditions and accurately assumed for underwater conditions. While most values stay the same, the paper state that focal length must be increased by 33%. This finding however is not sufficiently accurate and causes an error of greater than 1% for focal length on average.

An analysis of the image center is shown below and shows minor shifts in image center, depending on the method used. In [19] it was stated that the water had no effect on the image center and could be ignored. This does not hold true especially for Heikkila's calibration method which produced a shift of 2% in both directions when calibrated under water.

Algorithm	Above Water with Case	Underwater with Case
Rahman and Krouglicof	X: +0.5%	X: -0.8%
	Y: -0.3%	Y: -0.4%
Heikkila	X: +0.4%	X: -2.0%
	Y: -0.3%	Y: +2.1%
Zhang	X: +0.2%	X: +1.6%
	Y: -0.1%	Y: -0.5%

Table 20 – Camera Model Image Center Change

Radial and Tangential distortion vary greatly across all models and image conditions. The first conclusion that can be drawn from this data is that the addition of mediums between the camera and the target tend to increase the distortion. The second is that the distortion model for the camera must be calculated in the medium in which it occurs since no estimation or approximation may occur based on in air conditions. Below are the changes that occur with the distortion models for the tested calibration methods. These changes are based on absolute values of distortion coefficients and percentage change from the above water without case condition.

Algorithm	Above Water with Case (Abs)	Underwater with Case(Abs)
Rahman and Krouglicof	K ₁ : -1.7%	K ₁ : +1.38%
	K ₂ : -98.0%	K ₂ : -35.1%
	P ₁ : -85.0%	P ₁ : -90.0%
	P ₂ : -45.0%	P ₂ : +225.0%
Heikkila	K ₁ : -31.9%	K ₁ : +76.6%
	K ₂ : -34.5%	K ₂ : +339.7%
	P ₁ : +3.8%	P ₁ : +583.1%
	P ₂ : -39.1%	P ₂ : +367.2%
Zhang	K ₁ : +7.7%	K ₁ : +25.3%
	K ₂ : +70.6%	K ₂ : +43.5%

Table 21- Camera model Distortion (Absolute Value) change

The most useful metric from the method comparison is the re-projection error. This is the standard deviation of error in pixels when the actual image points are compared with the calculated image points.

Algorithm	Above Water	Above Water with Case	Underwater with Case
Rahman and Krouglicof	0.2246	0.2692	0.1546
Heikkila	0.2260	0.2811	0.1571
Zhang	0.2130	0.2698	0.1611

Table 22 - Camera Model Pixel Error

The Rahman and Krouglicof method performs well under most conditions, and better than the other methods tested, as the calibration conditions become more difficult. Zhang's method performed slightly better under ideal conditions than the Rahman and Krouglicof method,

however, it quickly increases in error as the conditions become less ideal. Heikkila's method performs slightly worse than the Rahman and Krouglicof method for all testing conditions. The pixel standard deviation is lower for the underwater condition than the two above water situations which is due to the differing lighting conditions used in the calibration process. This shows that the calibration method is secondary to the calibration lighting and image quality.

The data presented shows that the paper presented by J.M. Lavest [19] is incorrect in the assumption that a system calibrated above the water can produce accurate results for underwater conditions. Any system required to produce accurate results must be calibrated below water if the system is to be used below water. For this reason, this project will use the underwater target to calibrate the system underwater using the Rahman and Krouglicof method for the most accurate camera model possible.

Chapter 4

4.1 Stereoscopic Location

Stereoscopic location is the process of locating a point in three dimensional space using two or more images. This section will describe the theory behind this process and the various challenges associated with this problem, as well as some novel improvements to existing methods for increasing accuracy.

4.2 Stereoscopic theory

The stereoscopic location problem involves trying to locate a point in three dimensional space in one coordinate system, using two or more points from two or more different two dimensional coordinate systems with a known geometry relating them.

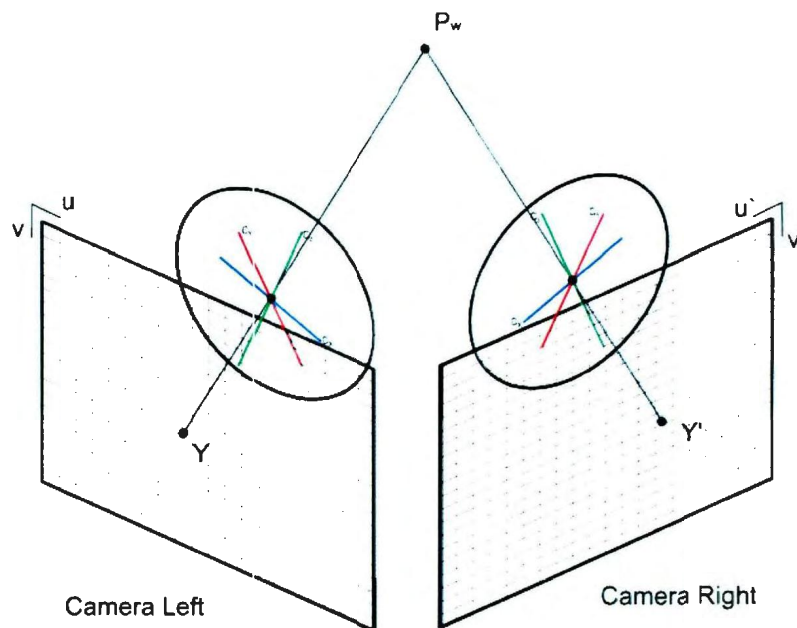


Figure 10 - The 3D Location Problem

The reason that two or more images are required to locate a point in three dimensional space is due to the way in which the camera is modeled. Starting with the original camera equation:

$$\begin{bmatrix} u \\ v \\ 1 \end{bmatrix} = \begin{bmatrix} sf & 0 & u_0 & 0 \\ 0 & f & v_0 & 0 \\ 0 & 0 & 1 & 0 \end{bmatrix} * \begin{bmatrix} r_{11} & r_{12} & r_{13} & t_x \\ r_{21} & r_{22} & r_{23} & t_y \\ r_{31} & r_{32} & r_{33} & t_z \\ 0 & 0 & 0 & 1 \end{bmatrix} * \begin{bmatrix} P_x \\ P_y \\ P_z \\ 1 \end{bmatrix}$$

This equation can be simplified and rearranged to solve for P :

$$\begin{bmatrix} u \\ v \\ 1 \end{bmatrix} = \begin{bmatrix} c_{11} & c_{12} & c_{13} & c_{14} \\ c_{21} & c_{22} & c_{23} & c_{24} \\ c_{31} & c_{32} & c_{33} & c_{34} \end{bmatrix} * \begin{bmatrix} P_x \\ P_y \\ P_z \\ 1 \end{bmatrix}$$

$$\begin{bmatrix} u \\ v \\ 1 \end{bmatrix} = \begin{bmatrix} c_1 P_w \\ c_2 P_w \\ c_3 P_w \end{bmatrix}$$

Where P_w is the column vector of P and c_i is the row vector of c . To make both sides equal, we normalize the right side:

$$u = c_1 P_w / c_3 P_w, \quad v = c_2 P_w / c_3 P_w$$

$$u c_3 P_w - c_1 P_w = 0, \quad v c_3 P_w - c_2 P_w = 0$$

Here we have 2 equations with 3 unknowns P_w (P_x, P_y, P_z). The inclusion of the other camera introduces an additional two equations:

$$u' c'_3 P_w - c'_1 P_w = 0, \quad v' c'_3 P_w - c'_2 P_w = 0$$

This generates a system of equations with four equations and three unknowns and can be extended to include multiple points in multiple camera coordinate systems.

These equations can be solved in two ways: The first is using a homogenous system of equations where the array is not assumed to be normalized. The second is an inhomogeneous solution solved using a least squares analysis.

The inhomogeneous system of equations has the following form:

$$\begin{bmatrix} c_3u - c_1 \\ c_3v - c_2 \\ c'_3u' - c'_1 \\ c'_3v' - c'_2 \end{bmatrix} * P = \begin{bmatrix} c_{34}u - c_{14} \\ c_{34}v - c_{24} \\ c'_{34}u' - c'_{14} \\ c'_{34}v' - c'_{24} \end{bmatrix}$$

Equation 8 - Inhomogeneous Stereoscopic Equations

Where $c_3u - c_1$ represents $(c_{31} \text{ to } c_{33}) * u - (c_{11} \text{ to } c_{13})$ and $c_{34}u - c_{14}$ is a singular value.

The homogeneous system of equations has the following form:

$$\begin{bmatrix} c_3u - c_1 \\ c_3v - c_2 \\ c'_3u' - c'_1 \\ c'_3v' - c'_2 \end{bmatrix} * P = 0$$

Equation 9 - Homogeneous Stereoscopic Equations

Where $c_3u - c_1$ represents $(c_{31} \text{ to } c_{34}) * u - (c_{11} \text{ to } c_{14})$. For this solution the array P is of the form:

$$\begin{bmatrix} P_x \\ P_y \\ P_z \\ P_s \end{bmatrix}$$

Where P_s is the scaling factor for the coordinates in 3 dimensional space and every dimension must be divided by this factor to find its true location.

The inhomogeneous solution to this problem will typically produce more accurate results than the homogeneous solution[20]. However, the inhomogeneous solution will break down in accuracy as the distance from the camera approaches infinity. These methods will be compared in a following section to compare the results for accuracy across multiple distances along with numerous other augmentations for increasing accuracy.

4.3 Point Correspondence

The problem of locating a point in space is further complicated when attempting to determine corresponding features across image pairs. Each point must be accurately matched to its pair in another image in order to ensure proper triangulation. This is called the correspondence problem and there are multiple methods for solving this problem[21] [22] ,all of which have their own advantages and disadvantages.

These methods can be divided into two main categories: local matching and global matching. Local matching uses the principle of epipolar geometry to search small sections of an image for corresponding points. Global matching algorithms do not limit searching scope to limited regions of the image. Instead, they use more complicated algorithms to search for matching points with more strict matching constraints[22]. Due to the complicated nature of implementing the Global matching algorithms, and the simplicity and open nature of the flume tank, a much simpler matching algorithm will be used for this project.

The local matching algorithms use a technique called stereo rectification to aid in the location problem. Stereo rectification is the re-projection of two images onto a common image plane. Using this technique, common points will appear on the same horizontal line. This line passes

through a point in the first image and it is matched to points in the second image. The point in the second image with the smallest distance to the line will be the best match. The smallest distance is used due to the error introduced from distortion and camera modeling and will prevent perfect matches.

The rectification process is not required and instead the epipolar geometry may be used to form a fundamental matrix. This matrix relates the transformation between the two camera coordinate systems. Epipolar lines represent a ray going from the center of projection of one camera to a point in three dimensional space which is then projected onto the image plane of the second camera using the fundamental matrix. This line can then be searched for a common feature or the detected features are compared to this line, and the one with the smallest distance to the line is chosen.

The advantage of the rectification technique over the older epipolar line generation is that it can be performed on uncalibrated systems[23]. This leads to much simpler and more flexible algorithm; however, the system for this project already has a fully calibrated system. The time taken to generate the equations for the epipolar lines is similar to that of the image rectification. Therefore, to simplify the system, epipolar lines will be used for the local stereo matching of this project.

4.4 Stereo Location Evaluation

4.4.1 Testing setup

Using the calibration data from the previous sections, various techniques were compared to evaluate their performance for three dimensional location. Along with the techniques described above, two additional methods for triangulation, as described in a paper by Hartley and Sturm[20] , are also included. The first is a method for triangulation which uses an optimization of points to reduce error before finding a homogeneous solution. The second is an iterative solution to the inhomogeneous system of equations which solves the equations multiple times with variable weights in order to minimize error.

For the following tests the calibration cube was positioned at increasing distances from the camera rig to evaluate performance of several stereoscopic triangulation algorithms. The length of each side of the cube is calculated using the corner circles of the calibration targets. Both sides of the cube are used producing 8 distances, 4 per side, using the 8 corner circles, again using 4 per side. Each circle is automatically detected using the calibration algorithm to remove human error. Each distance is measured from the center of the camera rig and each length calculated should be 508 millimeters.

4.4.2 Measurements at 4.572 meters

Sample	Homogeneous (mm)	Inhomogeneous (mm)	Iterative Inhomogeneous (mm)	Hartley-Sturm Optimal (mm)
1	359.3496	359.3565	365.2602	376.7973
2	415.8591	415.9022	413.0421	411.6639
3	357.1906	357.1284	362.5687	366.2121
4	540.5003	406.7063	405.9787	398.5824
5	405.5677	406.7379	367.6928	305.5260
6	412.6353	412.7545	405.0409	425.2519
7	402.5016	402.6381	373.1527	356.8913
8	417.0305	417.0710	413.4085	414.1724

	Homogeneous (mm)	Inhomogeneous (mm)	Iterative Inhomogeneous (mm)	Hartley-Sturm Optimal (mm)
Mean Error (mm)	102.2957	110.7131	119.7319	126.1128
Standard Deviation of Error (mm)	37.1550	24.5976	22.9360	39.3077
Speed (Seconds)	0.002398	0.108429	0.026827	0.197030

4.4.3 Measurements at 6.858 meters

Sample	Homogeneous	Inhomogeneous	Iterative	Hartley-Sturm
	(mm)	(mm)	Inhomogeneous (mm)	Optimal (mm)
1	535.2164	533.1224	520.5067	536.5824
2	514.7934	514.7429	511.5378	476.5530
3	542.3627	541.4595	520.9247	546.4529
4	756.0047	516.2194	511.2509	476.2101
5	484.6061	486.0958	496.6821	389.4053
6	528.8254	528.3681	510.7131	490.1853
7	539.8764	538.3855	492.1679	337.3430
8	514.4148	514.4291	509.0660	474.5536

	Homogeneous	Inhomogeneous	Iterative	Hartley-Sturm
	(mm)	(mm)	Inhomogeneous (mm)	Optimal (mm)
Mean Error (mm)	49.8610	19.0789	7.8937	58.8481
Standard Deviation of Error (mm)	80.7318	10.7632	5.7980	55.0517
Speed (Seconds)	0.000820	0.001900	0.004331	0.007004

4.4.4 Measurements at 9.4488 meters

Sample	Homogeneous	Inhomogeneous	Iterative	Hartley-Sturm
	(mm)	(mm)	Inhomogeneous (mm)	Optimal (mm)
1	663.0139	641.6503	573.1905	588.0141
2	564.5017	563.6820	521.9107	511.6011
3	1223.1591	1087.4502	572.7474	650.1040
4	753.6978	907.1786	572.9817	530.3919
5	490.7343	488.0110	467.5061	353.1799
6	531.8858	533.4366	516.8968	598.4524
7	519.8026	517.9720	481.4648	296.3819
8	524.5630	525.1081	513.8081	530.3145

	Homogeneous	Inhomogeneous	Iterative	Hartley-Sturm
	(mm)	(mm)	Inhomogeneous (mm)	Optimal (mm)
Mean Error (mm)	95.4152	64.5144	36.3205	83.2499
Standard Deviation of Error (mm)	91.7023	57.9548	26.0808	191.7245
Speed (Seconds)	0.000780	0.001848	0.002898	0.006181

4.4.5 Measurements at 11.938 meters

Sample	Homogeneous (mm)	Inhomogeneous (mm)	Iterative Inhomogeneous (mm)	Hartley-Sturm Optimal (mm)
1	555.0519	547.1288	526.2292	555.2573
2	532.2973	531.7018	518.0120	759.4298
3	655.9987	647.7304	615.3987	627.2656
4	773.4535	558.5407	521.3883	685.4110
5	502.5221	503.9531	495.5145	336.2157
6	600.7569	599.3661	521.5341	810.9142
7	675.1561	664.2546	566.0375	279.2570
8	526.6290	527.4545	508.5482	746.9929

	Homogeneous (mm)	Inhomogeneous (mm)	Iterative Inhomogeneous (mm)	Hartley-Sturm Optimal (mm)
Mean Error (mm)	94.7332	64.5162	29.2042	92.0929
Standard Deviation of Error (mm)	92.8135	58.5920	35.9184	197.8485
Speed (Seconds)	0.000763	0.011043	0.009865	0.008480

4.4.6 Algorithm evaluation

The first location at 4.572 meters is closer to the cameras than the calibration distance used for the cube. At this distance an incredibly high error can be seen for all methods. The inhomogeneous and homogeneous solutions perform slightly better than the other methods which attempt to optimize and correct these points.

When the distance is increased to 6.858 meters the error in all methods decreases for all methods tested. The inhomogeneous and iterative inhomogeneous solutions perform much better than the other tested methods. The iterative solution performs slightly better than the non-iterative method, showing error of less than one centimeter. The Hartley-Sturm optimization method performs better than the regular homogeneous solution with a lower standard deviation of error; however, it still produces a higher average error than the non optimized method.

At 9.4488 meters all the algorithms show an increase in error over the previous results. Again, the iterative inhomogeneous solution shows the most accurate results with the non-iterative solution producing slightly less accurate results. Both the homogeneous solution and optimal solution show the least accurate results and with the optimal solution performing less accurately than the regular homogeneous solution.

Finally, at 11.938 meters from the cameras, the iterative inhomogeneous solution is again closest to the correct solution and the homogeneous and optimized methods perform noticeably less accurately. The average error of the iterative solution is lower than the previous distance;

however, it has a larger deviation than the previous result. The Hartley-Sturm method performs even worse than the non-optimized homogenous method.

One important observation from this data is that the error does not steadily increase with distance. The error close to the cameras is higher than it is at larger distances. This may be due to the fact the first measured distance (4.572 meters) is closer than the calibration distance. This will lead to model instability as the distance to the cameras reaches zero. This problem will be further discussed in the next section.

Another observation is the large standard deviations experience by all of the calibration methods. This is most likely due to the non ideal conditions experienced in the flume tank. The water causes a great deal of distortion, especially over longer distances, which would account for the large standard deviation and error. The lighting of the flume tank may also attribute to part of the error. The overhead lighting does not perfectly illuminate the calibration target and may cause errors due to shadows.

Using this data, we can conclude that the most useful method for triangulation would be the iterative inhomogeneous method. This technique showed that it performed consistently and significantly more accurately than the other methods used. Since it performed less accurately than the regular homogeneous solution, the Hartley-Sturm method for optimization will not be used, even with the inhomogeneous solution.

4.5 Stereo Location Augmentations

This section will describe several novel augmentations that can be made to the above methods to improve performance and increase accuracy of the system.

4.5.1 Calibration Splitting

One of the main issues for the camera calibration, for the purpose of stereoscopic location, is producing accurate camera modeling, for the full image, while attempting to keep the calibration target in both images. In a paper by Heikkila[4] it is found that for proper camera calibration to take place a target should cover roughly 85% of the camera image. Depending on the angle of the cameras or the distance between them, an issue is created where the camera target used for calibration will not be centered or may only use a small section of the available target area, which leads to a poor calibration model. A novel method of splitting the calibration procedure into two sections is proposed where the intrinsic camera parameters are determined using one camera image with the target centered for each camera. A second image, with the calibration target shared between calibration images, is used to determine the extrinsic parameters of the camera. This method is designed so that the image distortion, camera center and focal length can be determined, and not affected by, off center images or small target area. This method will extend the calibration time for any system using this technique, however, if this technique increases accuracy of the system, and there is a long time between calibrations, this technique can be practical.

4.5.2 Iterative Solution Finding

The issue when using the least squares analysis for finding a solution to the inhomogeneous problem is that there is no proper criteria for what is being minimized. Instead, a proper error metric should be used and minimized based on re-projection error. Using the previous equations for the inhomogeneous system:

$$\begin{bmatrix} a_3u - a_1 \\ a_3v - a_2 \\ a'_3u' - a'_1 \\ a'_3v' - a'_2 \end{bmatrix} * P = 0, \quad P = \begin{bmatrix} P_x \\ P_y \\ P_z \\ 1 \end{bmatrix}$$

And the original equation for the camera model:

$$\begin{bmatrix} u \\ v \\ 1 \end{bmatrix} = \begin{bmatrix} c_{11} & c_{12} & c_{13} & c_{14} \\ c_{21} & c_{22} & c_{23} & c_{24} \\ c_{31} & c_{32} & c_{33} & c_{34} \end{bmatrix} * \begin{bmatrix} P_x \\ P_y \\ P_z \\ 1 \end{bmatrix}$$

We determine that:

$$u = P * c_1 / P * c_3$$

However, this equation also contains error so an error term is added:

$$(u + \varepsilon) = P * c_1 / P * c_3 = u_\varepsilon$$

Equation 10 - Augmented Error Calculation

The difference between the true u and the new u_ε is the value that should be minimized. The minimization of the difference is achieved through an iterative method. In [20] an iterative

method is proposed where error is associated with the value of $P * c_3$ which according to the assumptions of the equations should be equal to one. Therefore, the equations derived from the left and right hand sides, scaled by $1/P * c_3$ and the series of equations, is solved multiple times until the scaling value changes by less than a threshold, or a maximum number of iterations is reached. In practice this method works well, however, it assumes that error is uniform for both directions in an image which may not always hold true.

This method may be augmented to include direction for each image and the scaling factor may be broken down further. Instead of assuming the error may be simplified as $1/P * c_3$, we instead use the difference between u and u_ϵ where the scaling factor is equal to u/u_ϵ for the horizontal direction of the right image. This process can be extended to both directions for both images producing 4 scaling factors.

4.5.3 Augmentation Testing

4.5.3.1 Testing setup

The data used from the previous section was tested again using the new augmented techniques. The iterative solution was included again as a base line to show improvement.

4.5.3.2 Measurements at 4.572 meters

Sample	Iterative	Improved Iterative	Split Calibration
	Inhomogeneous (mm)	Inhomogeneous (mm)	Iterative Inhomogeneous (mm)
1	365.2602	365.2552	510.1599
2	413.0421	413.0017	508.1880
3	362.5687	362.5734	508.1933
4	405.9787	405.9326	509.0604
5	367.6928	367.6970	511.2259
6	405.0409	405.0270	508.7976
7	373.1527	373.1413	509.9467
8	413.4085	413.3735	508.7521

	Iterative	Improved Iterative	Split Calibration
	Inhomogeneous (mm)	Inhomogeneous (mm)	Iterative Inhomogeneous (mm)
Mean Error (mm)	119.7319	119.7498	1.2905
Standard			
Deviation of	22.9360	22.9183	1.0649
Error (mm)			
Speed (Seconds)	0.002607	0.060545	0.004688

4.5.3.3 Measurements at 6.858 meters

Sample	Iterative	Improved Iterative	Split Calibration
	Inhomogeneous (mm)	Inhomogeneous (mm)	Iterative Inhomogeneous (mm)
1	520.5067	520.5101	1321.6404
2	511.5378	511.5328	884.7672
3	520.9247	520.9378	1324.7685
4	511.2509	511.2270	922.7623
5	496.6821	496.6818	1320.6483
6	510.7131	510.7011	926.0973
7	492.1679	492.1639	1309.2704
8	509.0660	509.0408	880.2686

	Iterative	Improved Iterative	Split Calibration
	Inhomogeneous (mm)	Inhomogeneous (mm)	Iterative Inhomogeneous (mm)
Mean Error (mm)	7.8937	7.8880	603.2779
Standard Deviation of Error (mm)	5.7980	5.8099	222.7651
Speed (Seconds)	0.004413	0.064372	0.002930

4.5.3.4 Measurements at 9.4488 meters

Sample	Iterative	Improved Iterative	Split Calibration
	Inhomogeneous (mm)	Inhomogeneous (mm)	Iterative Inhomogeneous (mm)
1	573.1905	573.1849	3082.0844
2	521.9107	521.8098	1348.9658
3	572.7474	572.6665	3101.4879
4	572.9817	572.1397	1583.8408
5	467.5061	467.5064	2371.5044
6	516.8968	516.8721	1372.8329
7	481.4648	481.4611	2491.8389
8	513.8081	513.7869	1276.1900

	Iterative	Improved Iterative	Split Calibration
	Inhomogeneous (mm)	Inhomogeneous (mm)	Iterative Inhomogeneous (mm)
Mean Error (mm)	36.3205	36.1866	1570.5931
Standard Deviation of Error (mm)	26.0808	25.9559	777.2628
Speed (Seconds)	0.005303	0.071529	0.003028

4.5.3.5 Measurements at 11.938 meters

Sample	Iterative	Improved Iterative	Split Calibration
	Inhomogeneous (mm)	Inhomogeneous (mm)	Iterative Inhomogeneous (mm)
1	526.2292	526.2205	6847.0023
2	518.0120	517.9574	2650.1412
3	615.3987	615.3964	8786.1643
4	521.3883	521.3069	2416.4629
5	495.5145	495.5191	7479.3831
6	521.5341	521.4883	2816.3829
7	566.0375	566.0382	9633.2975
8	508.5482	508.5044	2211.2099

	Iterative	Improved Iterative	Split Calibration
	Inhomogeneous (mm)	Inhomogeneous (mm)	Iterative Inhomogeneous (mm)
Mean Error (mm)	29.2042	29.1741	4847.0055
Standard Deviation of Error (mm)	35.9184	35.9356	3141.7703
Speed (Seconds)	0.031879	0.082713	0.003093

4.5.4 Stereo Augmentation Evaluation

The measurements, at 4.572 meters, showed that the split calibration performed significantly better than the other methods, with an average error of only 1.29 millimeters. The improved iterative method, and normal iterative method, performed similarly well, the improved iterative method having a smaller standard deviation over the other method.

When the distance is increased to 6.858 meters the error for all methods increases. The improved iterative solution shows a better average error but a worst standard deviation of error than the original solution. Having been increased by several magnitudes, the split calibration method has a greatly increase standard deviation and average of error.

At 9.4488 meters the error of all the techniques is larger than the previous distance. The alternative iterative method performs better for average and deviation of error than the older method. Over the previous distance the split calibration method has a greatly increased error.

Finally, at a distance of 11.938 meters from the cameras, the non-split solutions show similar results to the previous testing, with a lower average error then the previous results but a higher deviation of error. The split calibration result shows an even greater error than the previous results, with an average error of several meters.

From these results it can be concluded that the improved method for iterative solutions provides a slight, but consistent, improvement in the accuracy of the algorithm and should be used for the final implementation of the camera system.

The most interesting result is from the split calibration procedure for camera calibration. The first interesting result was the divergence of accuracy and the increase in error. The split calibration showed significantly more accurate results at close range than the unified method. However, when the distance from the cameras was increased, the split calibration method diverged very quickly and became far less accurate than the unified method. The unified method became much more accurate once the target was further than the calibration distance and then diverged, but only slightly, compared to that of the split method. Using this information we can conclude that the split calibration technique is not feasible for use at longer distance. However, the split calibration technique did significant improvements at closer range than the traditional calibration method. This method should be further explored and more testing done on the subject to find if this method is truly better at closer distances and at which distances it is valid.

The second interesting result comes from the accuracy of the triangulation, with a calibration target covering a small amount of the image area. A paper by Heikkila [4] stated that camera calibration targets should cover the majority of the image in order to properly calibrate a camera. However, the original calibration method which covered approximately 18% of the image provided more accurate results at longer distance from the cameras. The split calibration method used a target which covered approximately 40% of the target but only provided more accurate results at short distances from the camera. These results contradict those of Heikkila[4] and it is possible that greater target coverage does not always lead to a better calibration model. These results show that further work should be done on the subject to determine target coverage requirements.

Chapter 5

5.1 Mechanical and Hardware Design

Due to the design constraints and requirements of both the hardware and software, a custom camera system was designed to house both the cameras and their supporting hardware. The design of the mechanical system and constraints will be discussed below.

5.2 Mechanical Overview and Requirements

The mechanical design of the camera system can be broken into three sections: The first is the frame, which holds the cameras in the flume tank, which will be referred to as the camera frame. The second is the waterproof container, which houses the cameras underwater and connects it to the camera frame, referred to as the camera container. The final is the mounting hardware inside of the camera container, which holds the camera and related hardware in place, referred to as the camera mount.

5.2.1 Camera Frame

The camera frame is designed to support the cameras and cables once the system is mounted in the flume tank. This support is required to not move or deform under normal operation of the flume tank and under the weight of the camera system. The design should also minimize its effects on the flume tank flow since the flow is highly calibrated and smoothed and small obstructions can have large effects on the flow quality. Finally, the camera frame needs to withstand the chemical environment of the flume tank and be resistant to corrosion, which will be discussed in depth in a later section.

5.2.2 Camera Housing

The camera housing is designed to protect the camera and related hardware from water and damage while in the flume tank. The most important constraint of the container is to protect the cameras and hardware from water for prolonged periods of time. The second is to allow a clear and non-distorted view of the flume tank. Thirdly, it should be easily adjustable to change orientation or position on the camera frame. The fourth requirement is that the container should have simple and waterproof connectors that can be removed, if removal of the entire system is required. Finally, similar to the camera frame, the container should also be resistant to the chemical conditions of the flume tank.

5.2.3 Camera Mount

The camera mount is configured to hold the camera in place inside of the camera container, as well as any needed hardware to power the cameras or process images. The camera mount should be easily removable in case repair or replacement is required for the camera system. Secondly, the camera mount should not penetrate or compromise the camera container in order to minimize the chance of leaks and damage. Finally, the mount should be non-conductive so that it does not interfere with the camera system by causing shorts or grounds.

5.3 Material Analysis and Flame Tank Conditions

The chemistry and conditions of the flume tank present several challenges that must be overcome when keeping objects immersed for long periods of time in chlorinated freshwater. The chemistry of corrosion can be described as an electrochemical reaction, similar to that of a battery. When a liquid, for example water, comes in contact with a metal, for example iron, a chemical reaction occurs. Using the materials the iron metal will lose electrons into the water and then start to exchange iron ions and hydrogen ions in an attempt to balance the electrical charge. This leads to the breakdown of the metal and the lost of material and mass into the surrounding water.

The flume tank uses several techniques to prevent this from occurring. The first is using a controlled tank chemistry to prevent damage. The exact chemical characteristics of concern and their values are shown below:

Characteristic	Value
Total Alkalinity	100 ppm
Calcium Hardness	220 ppm (mg/l)
Chlorine Concentration	>> 1.0 ppm
PH	7.5

Table 23 - Flume tank Chemical Characteristics

These concentrations are used to keep the water in balance and minimize the effects of the corrosion of metal in the tank and prevent the concrete walls from weakening. The chlorine concentration is much lower than that of a normal swimming pool due to the limited exposure

of the water to biological contamination. This level of chlorine is used to prevent algal growth in the tank and not make it suitable for recreational use.

Secondly, in conjunction to the balanced PH and low chemical concentrations, the tank also features sacrificial anodes to prevent corrosion of import flume tank components. These anodes are made from magnesium and corrode more easily than certain metals, such as stainless steel. During the previous flume tank maintenance cycle, these anodes lost 12 Kg of mass during a 24 month period[24].

Finally, through the use of the use of paints and non conductive separators, the flume tank electrically insulates all metallic components from the surrounding structural steel. This process also aids in limiting the corrosion of the metal components of the flume tank.

Using this information any metal placed into the tank, for extended periods of time should be stainless steel, or as corrosion resistant as stainless steel. Other materials, such as regular steel and aluminium, can be used for shorter periods of time, for testing purposes, but are not suitable for long term use.

5.4 Mechanical Design

5.4.1 Camera Frame

The camera frame went through several iterations before the final version which is currently installed in the flume tank.

5.4.1.1 Alpha Support Frame

This was a testing frame designed to test the containers underwater, as well as image quality.

This frame was constructed from aluminium 80/20 square stock and was suspended from the service carriage which moves across the top of the flume tank.



Figure 11 - Camera Frame Alpha Prototype

Once testing confirmed that the system worked, and image quality was determined, this testing framework was replaced with a more permanent solution.

5.4.1.2 Beta Support Frame

A permanent addition to the flume tank structure was designed next. Two options were considered when attaching the camera frame to the flume tank. The first is to mount the camera system on the side of the tank.

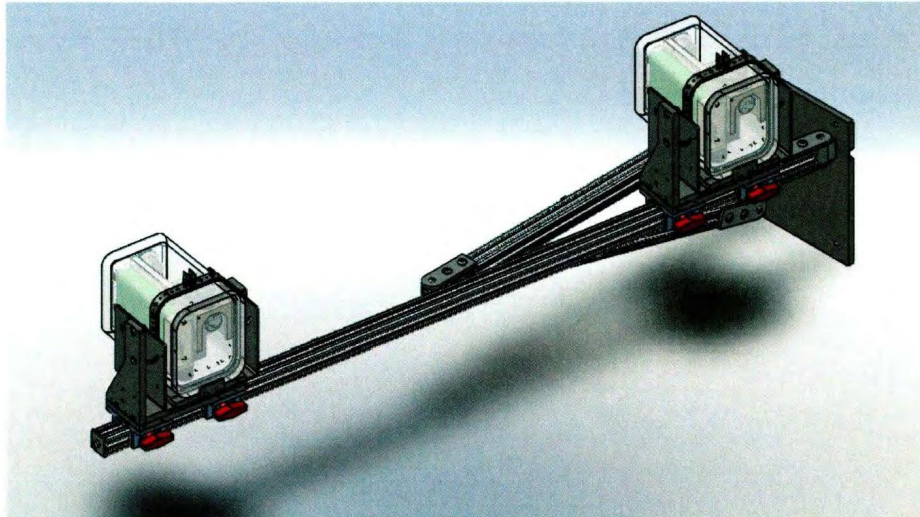


Figure 12 - Side Tank Mounting Option

This method would allow the camera to have minimal influence on the water flow and could be attached at any height in the flume tank. However, this model would also require drilling holes into the side of the flume tank, which is a time consuming process. Also, it has an increase chance of interfering with towed objects in the tank, such as model trawls, and wire warps.

The second option was to mount the cameras in the center of the tank and suspend them from the shooting deck. Under the deck are a series of I-beams which are well suited for mounting. This option would allow for easier mounting and less damage to the flume tank, as well not interfering with objects deployed for evaluation. This method, however, would place the

camera mount further back than the previous option, as well as increase the effect of the flow disturbance.



Figure 13 - Top Tank Mounting Option

The top mounting option was selected for installation since non-interference with the normal tank operation was the primary concern. The drawback of increased distance can be compensated for with the use of appropriate lenses and the increase flow disturbance can be handled by reducing the camera frame/containers flow profile.

The camera frame was constructed from 80/20 prototyping aluminum stock and attached to the shooting deck I-beams by a stainless steel plate. Cabling required for power and data was attached firmly to the frame, then suspended along the I-beam to ensure that it caused minimal drag in the water. The final installation is imaged below:

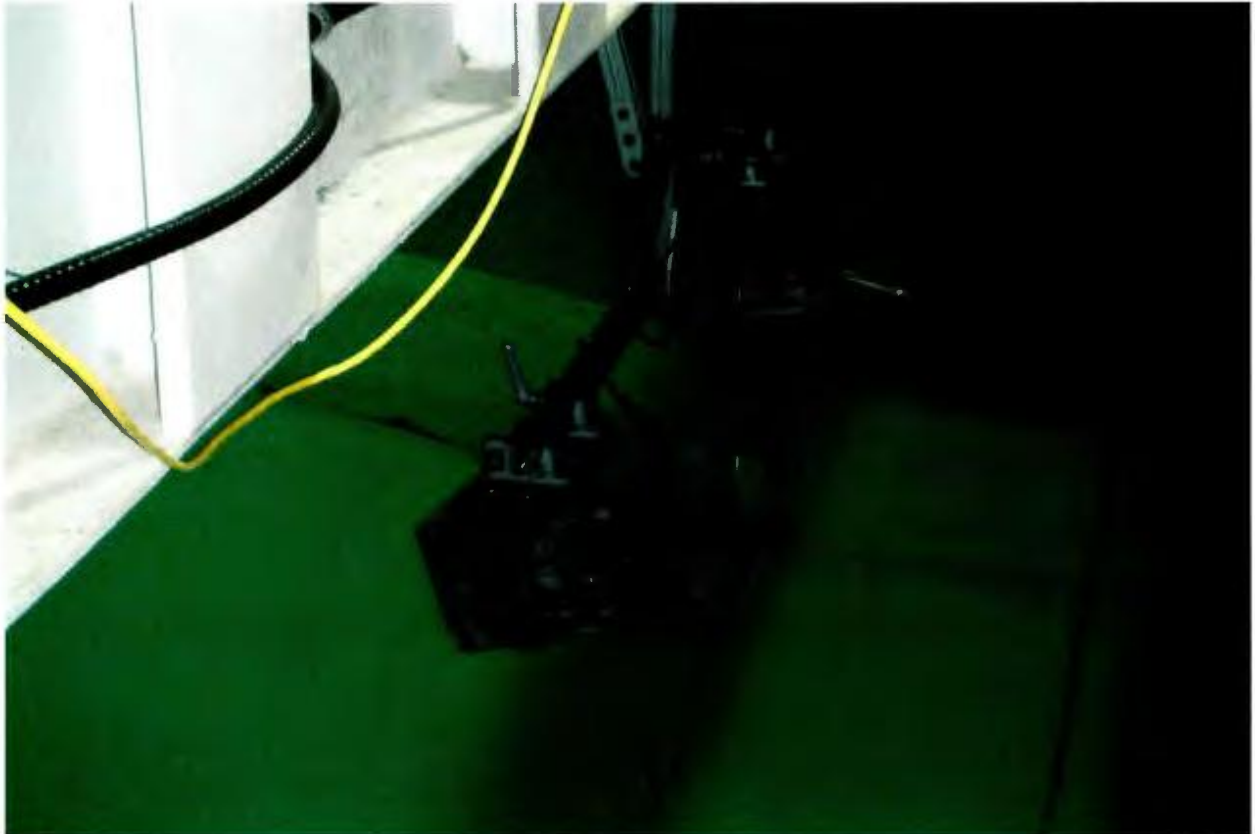


Figure 14 - Beta Camera Frame after Installation

Drawings of the Camera Frame can be found in Appendix A.

5.4.1.3 Production Support Frame

The final iteration of the camera frame is based on the beta support frame. Due to the chemical stress of the flume tank, the 80/20 prototyping aluminium would dissolve after prolonged use in the flume tank. The image below shows the pocketing of the aluminium and corrosion of the attaching hardware after only 3 months exposure to the tank conditions.

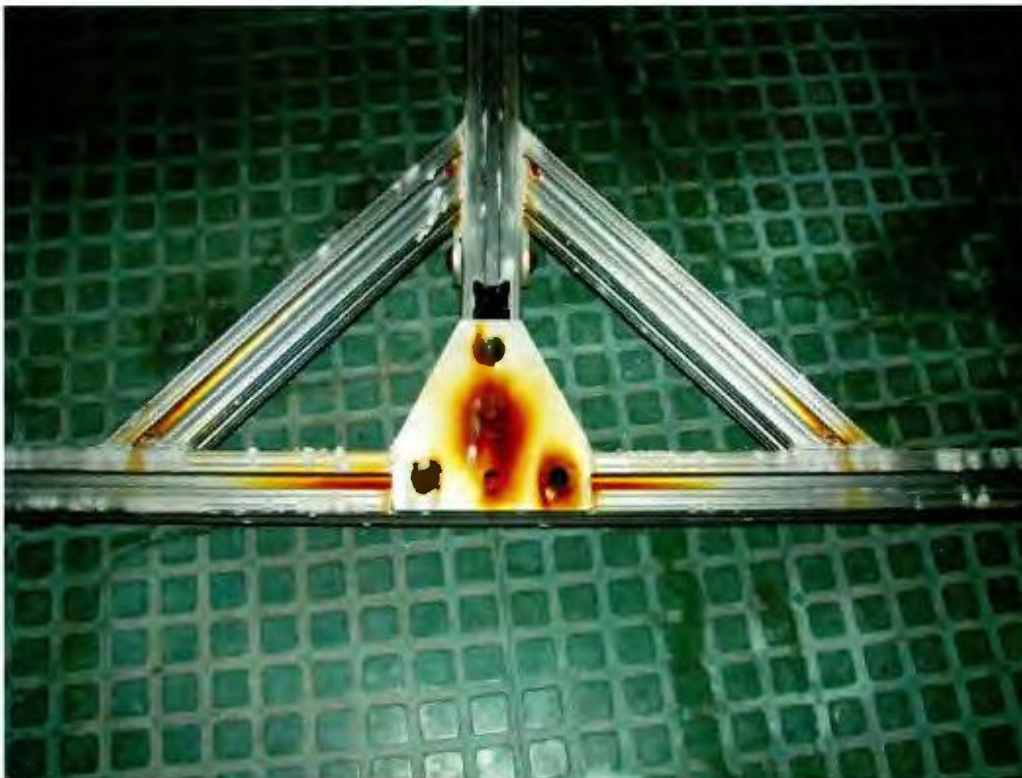


Figure 15 - Corrosion Damage on Beta Support Frame

This problem was solved when a new permanent frame was constructed from 316 stainless steel. This new version has the same geometry as the previous version but a much higher resistance to corrosion.

5.4.2 Camera Container

The camera container is composed of two sections: The first is the waterproof housing which houses and protects the cameras. The second is the housing support which connects the container to the camera frame and allows for changes of position and orientation.

5.4.2.1 *Waterproof Housing*

The primary design concerns of the camera container is that it remains waterproof for long periods of time and that the cameras have a non-obstructed, and non-distorted, view of the flume tank. In order to accomplish both of these constraints there are two options: the first is a stainless steel container and the second is an acrylic container. Due to the high cost of a custom stainless steel container, it was decided that an acrylic container should be used. While the acrylic containers may only be used in depths of five to ten meters, this was sufficient for the flume tank.

The container used was a clear acrylic P4.6x6.75 PrevCo subsea housing[25]. The original housing was modified to accommodate the underwater power and data connectors. A drawing of these modifications can be found in Appendix A.

On the back side of the camera container are the connectors for power and data. These connectors are Bulgin IP68 compliant connectors. These connectors are waterproof approved for environments deeper than five meters. These connectors allow for simple connection and removal of the camera container, when installing or removing the camera frame.

5.4.2.2 Housing Support

The housing support system is designed to allow for easy attachment to the camera support frame and for simple, and fast, adjustment of the camera position and orientation. The adjustment of the position is accomplished through the use of a sliding connector, which connects to the 80/20 prototyping frame work in the beta frame and to the stainless steel crossbar in the final production frame.

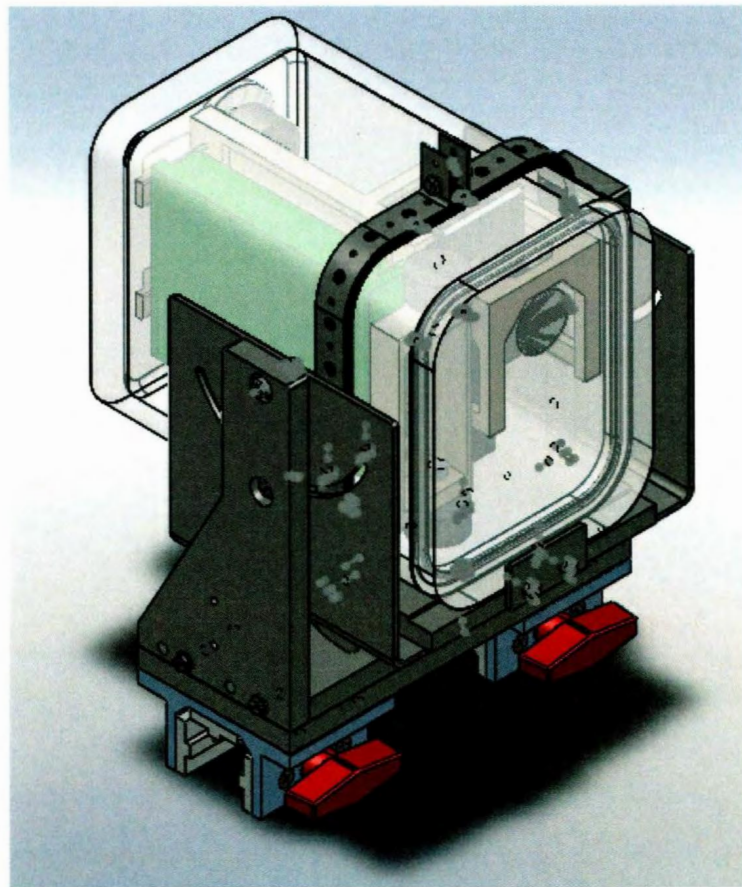


Figure 16 - Camera Container

The rotation requirement is solved through the use of several rotation points at different locations on the mount. The Frame is capable of rotating in 180 degree arcs in two degrees of

freedom, pitch and yaw. Roll was not included since it would have overly complicated the camera support frame without increasing the viewable area.

5.4.3 Camera Mount

The camera mount is designed to hold the camera and supporting hardware in place within the small volume constraints of the camera container. To accomplish this, a custom support was designed and fabricated using a 3D printer provided by the Faculty of Engineering and Applied Science at Memorial University.

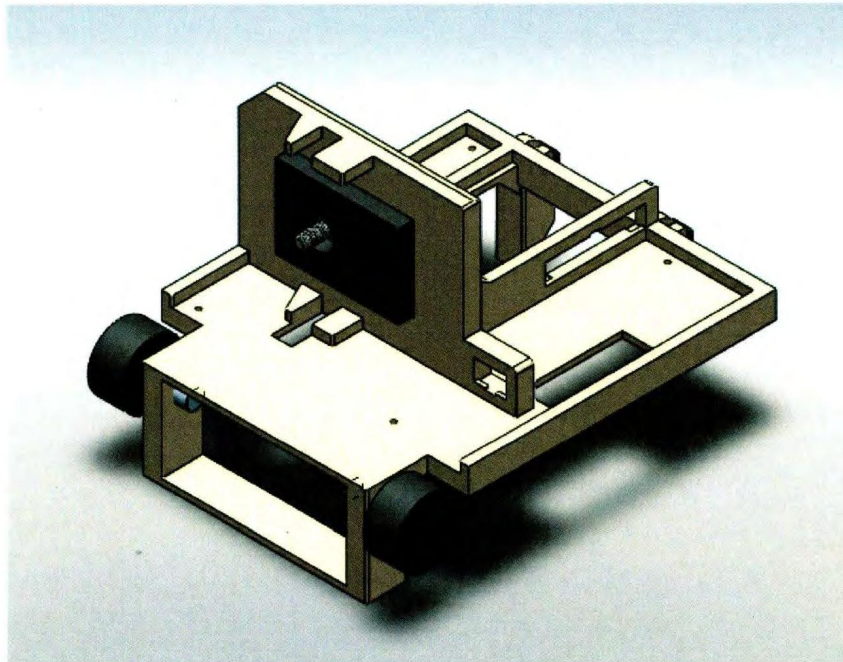


Figure 17 - Camera Mount

The camera itself is held by a special camera holder which is attached to the rest of the mount. This holder ensures that there is no direct contact between the camera lens and the camera container to prevent damage. To prevent damage, the camera holder is mounted on the front of the support and padded with a small layer of rubber foam. The purpose of this is to

accommodate any misalignments in the container and mount, and to ensure the camera is parallel to the camera container. The holder is held in place with a Teflon screw to ensure that there is no possibility of grounding out any wires with the camera case and the screw.

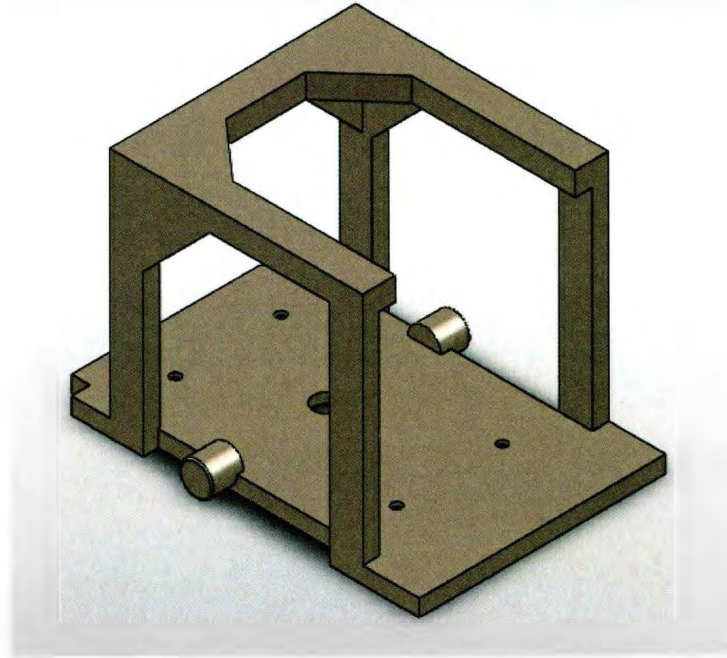


Figure 18 - Camera Mount Holder

In addition to the camera, the mount also houses a small single board computer, used for computations and networking. This board is mounted on the underside of the camera mount and is held in place with four metal offsets.

On the topside of the holder is the mount for the power supply. The power supply has no casing and exposed wires. Due to this, all other components surrounding the power supply are insulated and non-conductive. The extra lengths of wires are also held in place in this area.

5.5 Mechanical Analysis

A mechanical analysis of the performance of the camera frame was performed using bond graph modeling. The purpose of this modeling is to determine if the water flow of the flume tank will have any effect on the camera frame.

5.5.1 Mechanical Properties

The beta prototype frame has been constructed using 80/20 prototyping framework. This material is 6105-T5 aluminium, which is described as having a weight of 0.5097 lbs per foot, and a modulus of elasticity of 10.2×10^6 lbs per square inch. The frames are slotted, but will be considered a flat surface for the purpose of calculating the Reynolds number and drag coefficients.

The final version of this frame will be constructed using stainless steel tubes, which will be both more hydrodynamic and stiffer than the aluminium prototype. If testing reveals that the aluminum will be too soft and deflect too much, more testing will need to be performed using these final materials and support frame shapes.

5.5.2 Hydrodynamic Modeling

5.5.2.1 Forces on Immersed Objects

Forces on immersed objects are split into two categories: dynamic which is a result of the water moving passed the object, which causes shear stress. The second type is static, which are the gravity and water buoyancy affecting the object.

5.5.2.2 Static Forces

The forces of gravity follow the standard equations:

$$F_g = m g$$

Equation 11 - Force of Gravity

Where m is the mass of the object and g the force of gravity. The force of buoyancy on an object is based on the mass of water displaced by the object[26]. For simplicity we will assume that the metal beam is a solid rectangular prism.

$$F_b = V \rho g$$

Equation 12 - Force of Buoyancy on Submerged Objects

Where V is the volume of the water displaced, ρ is the density of the water and g the force of gravity.

5.5.2.3 Dynamic Forces

To calculate the dynamic forces the following equation[27] is used:

$$F_k = \frac{C_d A \rho u^2}{2}$$

Equation 13 - Dynamic forces of Submerged Objects

Where C_d is the drag coefficient, ρ is the water density, A is the projected surface area of the object, and u is the relative velocity of the object and the flow of the water. Since we are using a square beam, the projected surface area will be:

$$A = LD$$

This will be based off the size of the sections we use for force calculations. The drag coefficient can be calculated using the Reynolds number which is calculated using the following equation:

$$Re = \frac{D u \rho}{\mu}$$

Equation 14 - Reynolds Number of Submerged Objects

Where D is the particle diameter or characteristic length of the object, ρ and μ are fluid properties and u is the fluid velocity. To get the drag coefficient from the Reynolds number a graph such as the one below is used:

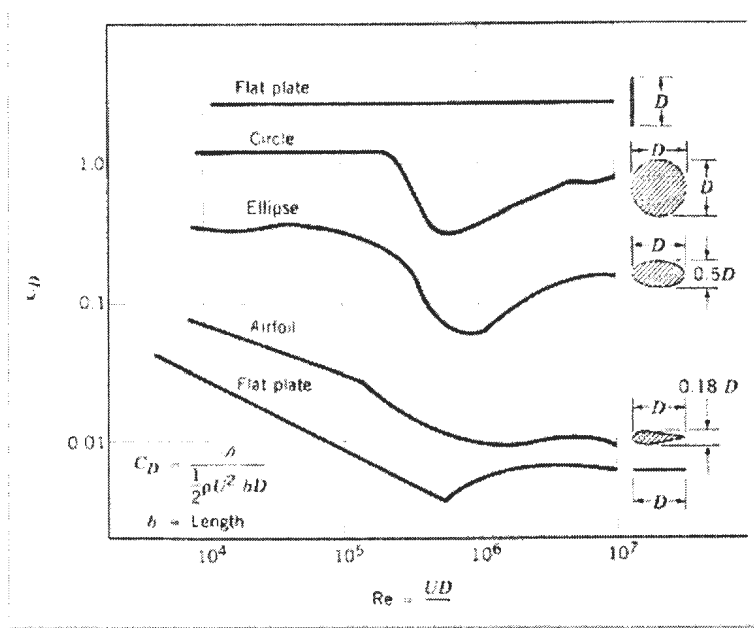


Figure 19 Reynolds number vs. Drag coefficient for common shapes[28]

From the above graph the drag coefficient will not only depend on the shape of the object, but also the speed of the fluid.

5.5.2.4 Total Forces

The total forces on the object will be:

$$F_t = F_k + F_b + F_g$$

However, the direction of the forces have to be taken into account since the forces of gravity and buoyancy will be in the y axis and the forces of water drag will be in the x-axis, due to the nature of the water flow. It should also be noted that, due to the nature of the system, there are no z axis forces, and it will not need to be included in the modeling.

5.5.3 Flume Tank Flow Characteristics

Accurately modeling the System response of objects in the tank will require an accurate model of the flow characteristics of the flume tank. Fortunately, in an effort to produce uniform flow throughout the tank there have been multiple projects to model the flow of the water. While these projects have improved flow quality in recent years, by their nature, flume tanks always have some degree of turbulence. The following graph shows a representation of the horizontal flow profile in terms of depth and distance across the width of the tank:

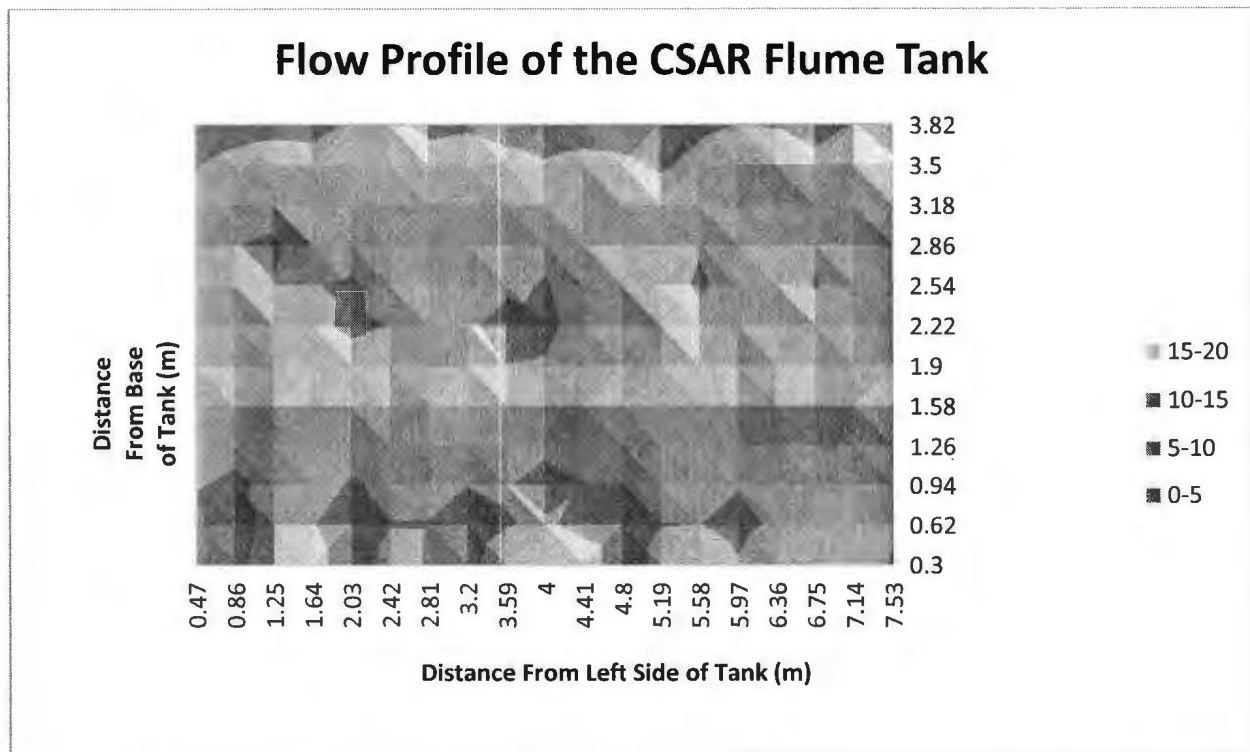


Figure 20 Flow Profile of CSAR Flume Tank at 0.5 knots

The total depth of the tank is 4m above the belt, excluding the pumping area below the tank, so the 3.82m height is 18cm below the surface of the water. The tank is approximately 8m across and the measurements are from the left side of the tank. The colour profile notes speed and the lighter the colour the faster the flow. This profile is taken from a low pump speed with a

nominal water speed of 0.5 knots or 0.257 m/s. These measurements were taken in March, 2013, the last time the flow profile of the flume tank was changed, and are assumed to still be accurate.

The flow turbulence is incredibly low and is considered laminar since the flow is smooth and the speed varies by less than 0.001 knots. To model this for the bond graph the force applied to the system will be considered constant; however, the profile will be used so that different forces will be applied to different points across the tank. Since accurate speeds are not available for every point, which will be used for the bond graph, the speed will have to be interpolated between the available data points.

5.5.4 System Modeling

5.5.4.1 Aluminum Beam Modeling

Modeling of the aluminum supports is done using a non-modal lumped segment approach. This method approximates the beam and its deflection by approximating a beam in multiple segments that are connected by both lateral and rotational springs which are connected to lateral and rotational translating masses[29]. The spring constant of the translational spring is described by the equation:

$$K_{ti} = \frac{EI}{l}$$

Equation 15 - Spring Constant of Translational Spring

Where E is the modulus of elasticity, I is the moment of inertia and l is the length of the beam Segment. The rotational spring is described using the equation:

$$K_{ri} = \frac{x A G}{l}$$

Equation 16 - Spring Constant of Rotational Spring

Where A is the cross sectional area, G is the shear modulus, l is the length of the beam Segment and x is the shear coefficient. The shear coefficient for a rectangular cross section is described using the following equation:

$$x = \frac{10(1 + \nu)}{12 + 11\nu}$$

Equation 17 - Shear Coefficient of a Rectangular cross section

Where ν is Poisson's ratio. There are also damping elements added to each of the springs to dampen all the spring effects and simulate a real beam. As well, each segment is approximated via an I element, which is simply the mass of the object for the translation forces. The rotational I element is described via the following equation for a square cross section:

$$J_i = \frac{M_i}{12}(l^2 + h^2)$$

Equation 18 - Inertia of Square Cross section

Where M_i is the mass of the element. Each of the rotational and translating elements is connected via transformers. The transformers for the bond graph are based off the unit length of each segment, where the transformer constant is $l/2$.

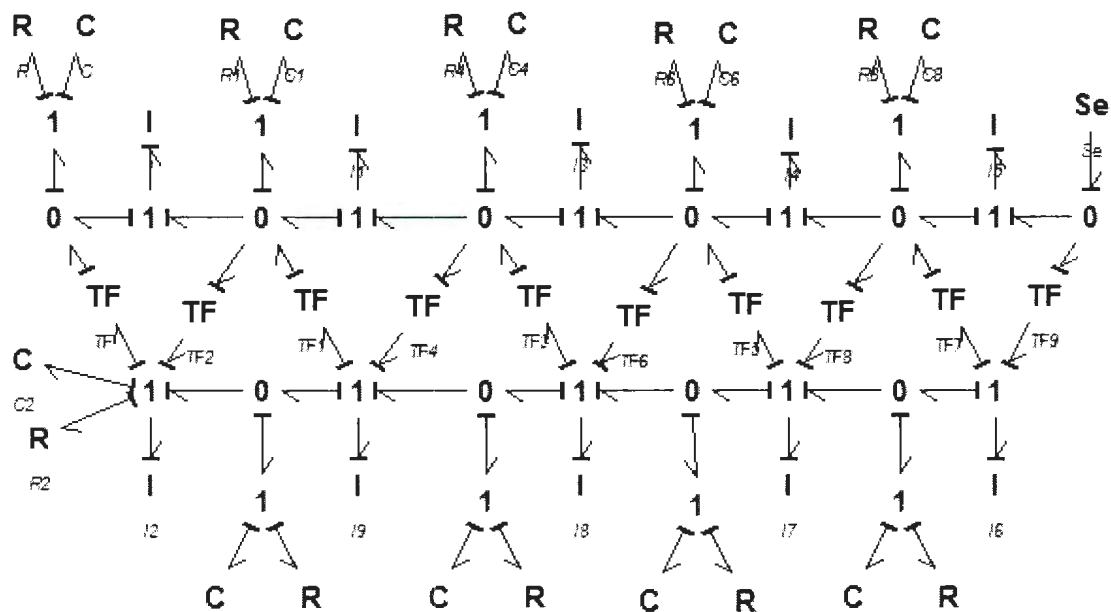


Figure 21 Original Non-modal Bond Graph Model (5 Sections)

The above modal is from Ibrahim's[29] paper which models a cantilever beam with a point force on the far end of the beam. Applications of these principles to the camera frame are done

by dividing the frame into two distinct components. The first is a free-free beam modeling, the horizontal camera support with two point forces at the far ends of the frame. The second is a cantilever beam that is suspended vertically. The connection of these two beams will be achieved by modeling the horizontal beam and calculating the forces required to keep the center from moving, then by applying this calculation for the vertical beam and finding maximum deflection. An estimate of the maximum deflection of the camera frame can be determined by adding these deflections together.

5.5.5 Hydrodynamic Calculations

Using the principles derived above, the forces of water flowing over the frame can be calculated. The forces on the camera containers are calculated as follows:

$$F_k = \frac{C_d A \rho u^2}{2}$$

$$A = \text{Area} = L \times W = 0.0255\text{m}^2$$

$$\rho = \text{Water Density} = 1,000 \text{ kg/m}^3$$

$$u = \text{water velocity}^1 = 0.700 \text{ m/s (left), } 0.669 \text{ m/s (right)}$$

$$C_d = \text{Flow Coefficient of a cube}^2 = 1.05$$

$$F_k = 6.55\text{N (left), } 5.99\text{N (Right)}$$

The force of flow across the cross section area of the metal beam is calculated as follows:

$$F_k = \frac{C_d A \rho u^2}{2}$$

$$A = \text{Area} = L \times W = 0.038\text{m} \times \text{Sectional Length}$$

$$\rho = \text{Water Density} = 1,000 \text{ kg/m}^3$$

$$u = \text{water velocity} = \text{Position Dependent}$$

$$C_d = \text{Flow Coefficient of a cube} = 1.05$$

¹ This velocity is based off the maximum velocity of the flume tank (approx. 60 cm/s) since this will also produce the greatest displacement of the metal frame.

² The flow coefficient for a cube is approximately constant for all speeds of fluid flow.

$$F_k = 199.5 \times (\text{Section Length}) \times u^2$$

$$F_k = 1.492N$$

Position	-0.685	-0.533	-0.381	-0.228	-0.076	0.076	0.228	0.381	0.533	0.685
	(m)	(m)	(m)	(m)	(m)	(m)	(m)	(m)	(m)	(m)
Speed	70.06	70.03	69.77	68.54	67.32	66.95	67.43	67.91	67.65	67.22
	cm/s	cm/s	cm/s	cm/s	cm/s	cm/s	cm/s	cm/s	cm/s	cm/s
Force	1.492	1.490	1.479	1.428	1.377	1.360	1.381	1.402	1.390	1.373
	N	N	N	N	N	N	N	N	N	N

5.6

5.6.1 Bond Graph

Adding the wave forces and a free-free beam design to the non-modal bond graph for the horizontal bar, the following bond graph is generated:

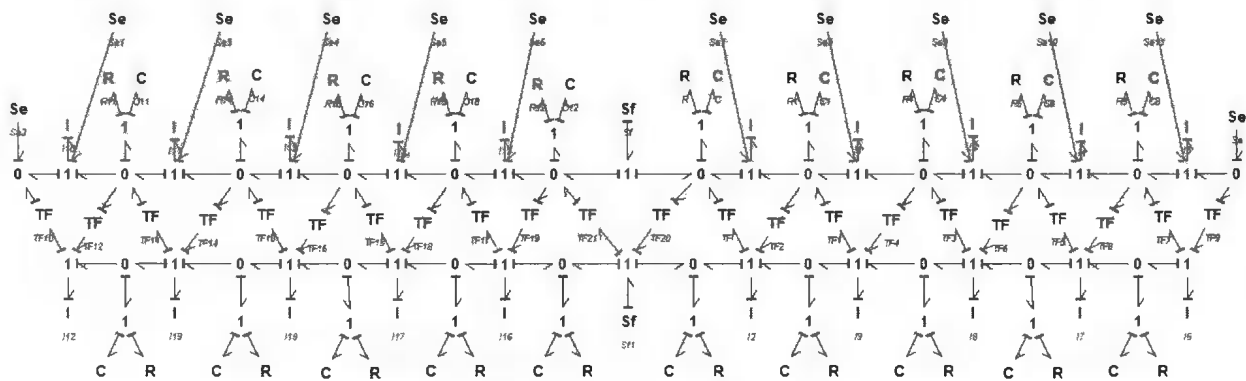


Figure 22 Horizontal Augmented Bond Graph

The flow sources in the center will be forced to be zero and forces calculated from them to keep them at zero. The upper effort sources are generated from the previous wave force calculations and the forces at the end are a result of the camera boxes. The values of the R/C/I elements are derived from the previous equations. The bond graph of the vertical bar is shown below:

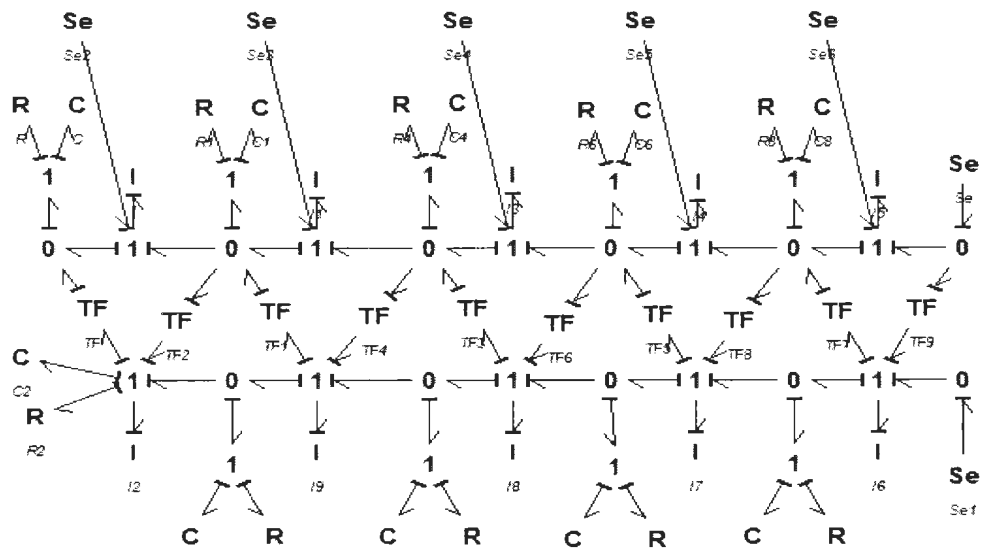


Figure 23 Vertical Augmented Bond Graph

5.6.2 System Response

5.6.2.1 Horizontal System Response

Running a simulation for 30 seconds shows the following response. The constant force application leads to a fast settling time to a steady state response. Below is the graph of the system response:

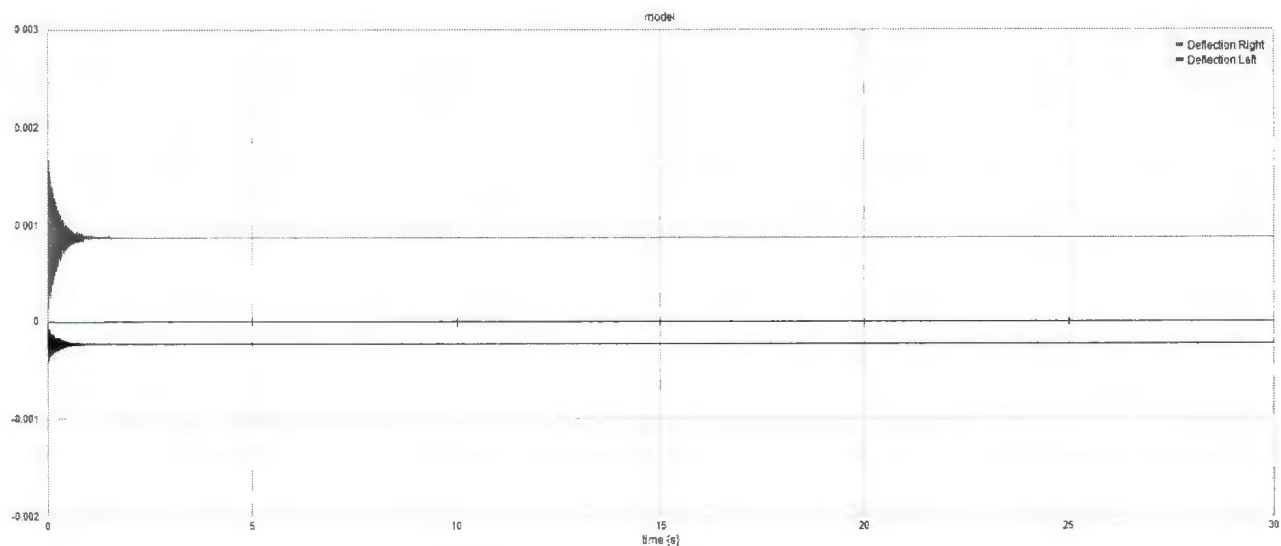


Figure 24 Horizontal System Response

Due to the large difference in responses for the values of interest, a table that summarizes the results is below:

	Max	Steady State
Deflection Right	1.66 mm	0.87mm
Deflection Left	-0.41 mm	-0.23 mm

5.6.2.2 Vertical System Response

Using the results of the previous system for a rotational and translation force, the vertical response of the system is calculated. The graph of the system response for a 30 second run is down below:

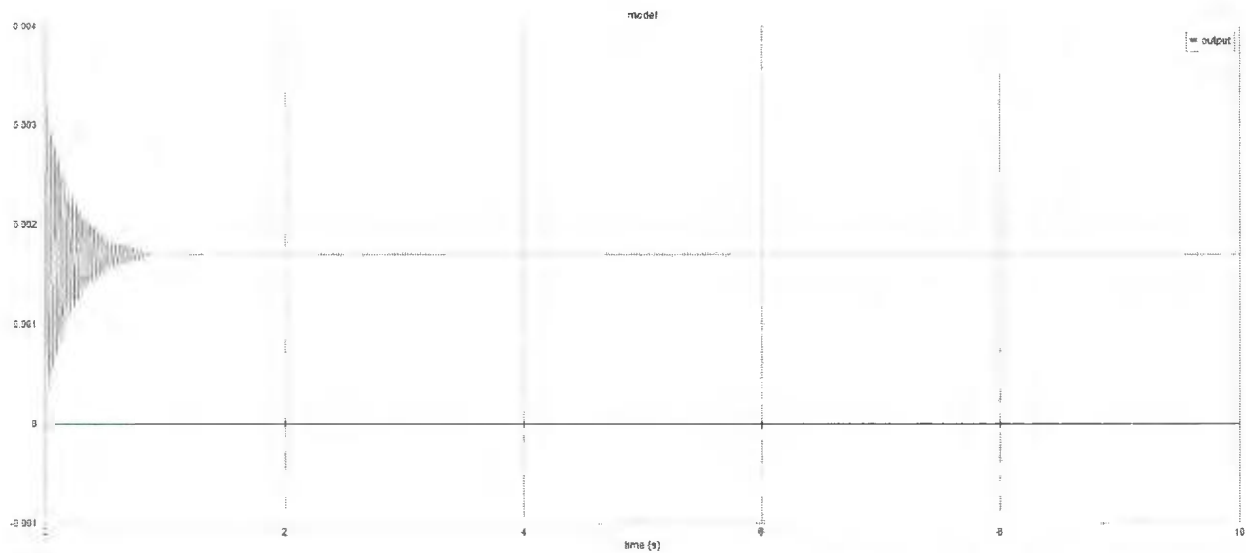


Figure 25 Vertical System Response

A summary of the results can be seen below:

	Max	Steady State
Vertical Deflection	3.2 mm	1.7 mm

5.6.3 Discussion and Recommendations

The data from the testing reveals a steady state translation of the camera by 0.87mm horizontally and 1.7mm vertically. The vertical displacement greater than 1 mm is concerning for the final System. This shift may cause problems for the calibration of the final system; however, the final resulting shift will be less than the calculated maximum. The first reason for this is that the model does not include the cross bracing for the horizontal and vertical bars. Due to the larger cross brace used in this direction, the greater displacement in the vertical direction will also be better compensated. Secondly, this displacement is for the maximum velocity of the flume tank which is rarely used, typical usage of the system will be at lower speed and thus less deflection of the camera support system. Overall the displacement of the vertical and horizontal bar will not need to be taken into account for the final system.

The testing also reveals a settling time for the metal frame once a force is applied. The system does settle quickly, less than 5 seconds, which must be taken into account when performing image processing. When operators of the flume tank change the velocity of the water flow it will have to be recommended that they must wait 30 seconds before starting the image processing system in order for the system to settle properly.

5.7 Hardware Overview and Requirements

The hardware system consists of three parts: The first is the camera and lens used to capture images. The second is the computer used to power the camera, process images and send information. The third is the power system which powers the board and the computer.

5.7.1 Camera and Lens

The camera and lens, for the system, are required to capture high quality images of at least 5 megapixels. The camera should also be developer friendly and have an application programming interface (API) that should be assessable through most major programming languages. Finally, the lens should be easily removable and selectable by the user for testing purposes.

5.7.2 Computer System

The supporting computer is needed to power and control the connect camera and be able to communicate with a central computer, to send and process images, as well as adjust camera settings. Secondly, it should be able to provide power to the camera through USB or other supporting cables. Thirdly, the enclosed conditions of the underwater environment require that the computer be low power or produce little heat during normal operation. Finally, due to the space constraints, the computer should have a small footprint in order to be accommodated in the camera container.

5.7.3 Power System

The power system is essential in providing power to the camera and the computer system, and should provide sufficient amperage and appropriate voltage for the system. Secondly, the

power system should be low power or produce little heat due to the small volume of the camera container. Finally, the power system should have a small footprint in order to fit into the enclosed space of the camera container.

5.8 Hardware Design

5.8.1 Camera and Lens

The camera that was selected for the design is a Lumenera LW575. The camera provides a 2592x1944 pixel image, creating a 5.03 megapixel image, at a frame rate of 7 fps full resolution and up to 60 fps with x4 sub-sampling[30]. The camera features a full API for multiple programming languages with multiple modes of operation. Finally, the camera provides a small footprint of 57.15 x 94.325 x 38.22 mm and removable lenses.

The lens selected for this application was an Edmund Optics 8mm fixed focal length lens. The high quality and low distortion of these scientific lenses, along with the size and short barrel length, are why this lens was chosen.

5.8.2 Computer system

The computer system chosen for the project was an Advantech PCM-9361 single board computer. This platform offers a small size of 146 x 102 x 28.2 mm which allows for containment in small areas. The power requirements of the board are a 12v connection which draws between 0.07 and 0.09 amps, or a draw of between 10.34 and 12.98 watts, which is low enough to produce little heat and easily meet the power concerns of the system. The board also features 4 USB and 1 serial port capable of powering any number of cameras. Finally, the board uses windows embedded for an operation system allowing for features such as remote

access, wake on LAN and easy software installation, all of which speed up development time and increase the capabilities of the system.

5.8.3 Power System

The power system chosen for the project is the Mini-Box PicoPSU-120. This is a small power supply designed to provide power in low power situations. This power supply provides a 12 volt and 120 watt output which meets the 12 volt requirement of the computer system and provides ten times the required wattage. The power supply is fanless, caseless and measures only 31 x 45 x 20mm, which fits the size requirements of the design. Finally, the low power requirements of the power supply lead to low temperature outputs that will not overheat the camera container.

5.8.4 Completed Assembly

The following diagram represents the final hardware assembly:

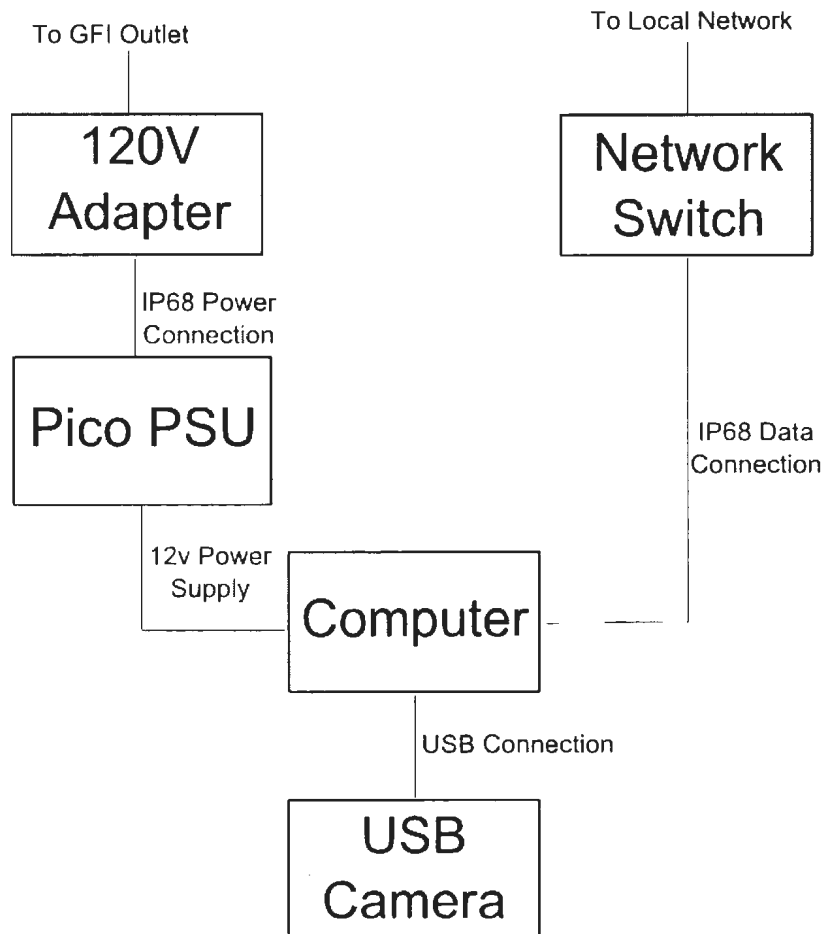


Figure 26 - Complete Hardware Assembly Diagram

The camera is connected to the computer board via a USB 2.0 connection. The computer is then connected to a local network switch in order to communicate with the server via an IP68 compliant underwater network connection. The computer board is also connected to the pico power supply for power. The power supply is connected to 120 volt adapter via an IP68 compliant underwater power cable. To prevent damage and electrocution in case the camera

case is compromised or other damage is sustained by the system, the power supply adapter is connected to the local power supply through a ground fault interrupter (GFI) outlet.

Chapter 6

6.1 Software Design

The software can be broken into two main sections: The first is the remote client software which operates on the computer system within the camera container. There are multiple copies of this software running, one per camera which communicates to the server. The second section is the server which is the interface for the flume tank operator. The majority of the processing is completed on the server, including the camera calibration and the stereo location. A detail explanation of the implementation of these processes will be described later in this chapter.

6.2 Remote Client

6.2.1 Software Design

The software for the remote client follows a small and simple design. The class diagram showing the major class design is shown below:

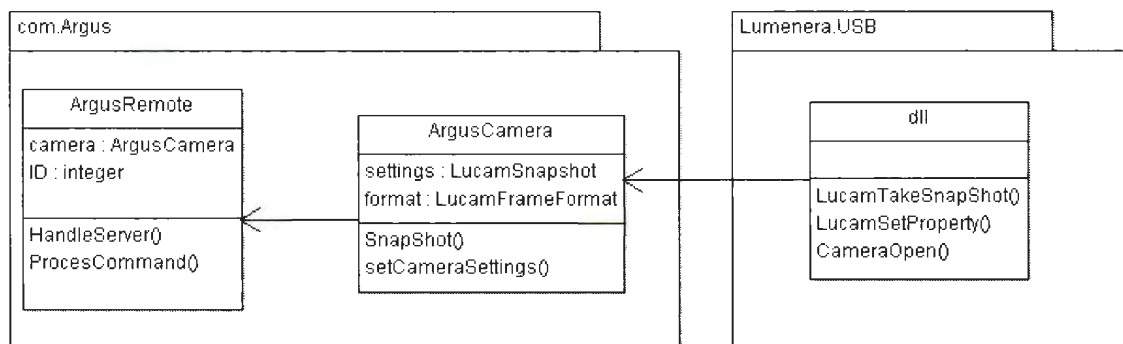


Figure 27 - Remote Client Class Diagram

An instance of the ArgusRemote class is created on program start up and it handles all of the commands sent by the server software. The ArgusRemote class will create an instance of ArgusCamera during start which is used to capture images and communicate with the connected Camera. ArgusCamera uses the application programming interface (API) through the dynamically linked library (DLL) provided by Lumenera with the camera. The API allows for direct control of the camera settings and capturing images.

Due to the computer system being directly inaccessible, it is designed to turn on when a LAN connection is detected. The remote client software will also start once the computer has finished its boot process and has loaded the embedded version of windows. This setup allows for the remote camera system to be reset remotely in case of an error and to restart automatically in the case of a power failure.

6.2.2 Communication Design

Each client is connected to the server using a unicast routing scheme. Each client is given the server IP address when the server software is installed and the server is setup on the network to have a static network address, to remove the need to constantly change the software settings remotely.

When the server software is connected, the remote client software will attempt to connect to the server every 30 seconds until a successful attempt is made. Once a successful attempt is made, the server and client will exchange important information such as the cameras unique ID and camera settings. Once the client and server are ready the client can accept commands that

the user has issued from the server software. As well, during this time, the client and server will exchange acknowledgement commands every five seconds. If the client does not receive a message in 30 seconds it assumes that the server has been closed and it returns the connection attempt state. The server performs a similar check so that if the client does not respond to the acknowledgement during the 30 second window, it assumes there was a client error and discards the connection.

The following are the available commands the server and client may exchange:

Command	Description
GetPicture	Gets the client software to capture an image from the connected camera and send it back to the server via bit stream in bitmap format.
NoOp	The acknowledgement command to ensure that the server is still connected to the client.
Settings	Allows the server to remotely adjust the camera settings.
Close	Remotely stops the client software.

Table 24 - Networking Commands

Each of these commands follows a similar structure which is shown below:

Command	Delimiter	Message Length	Delimiter	Message Data ³
---------	-----------	----------------	-----------	---------------------------

Table 25 - Network Command Structure

³ The message section may contain additional delimiters and sections depending on the message used.

The message command is one of the commands from the table above. This is followed by a delimiter used to easily parse the message. The delimiter used for the messages is the “|” symbol. The message length is the next section and used to verify that the entire message is sent. If the server, or the client, receives a message with a different actual and expected length the message is resent. The length is followed by another delimiter then finally the message data. The data can be a few bytes, image data or several additional sections separated by delimiters.

6.3 Server Software

6.3.1 Software Design

The software design for the server software can be split into several distinct sections. The first is the networking section which handles the communication with the connected camera clients.

The major class design is as follows:

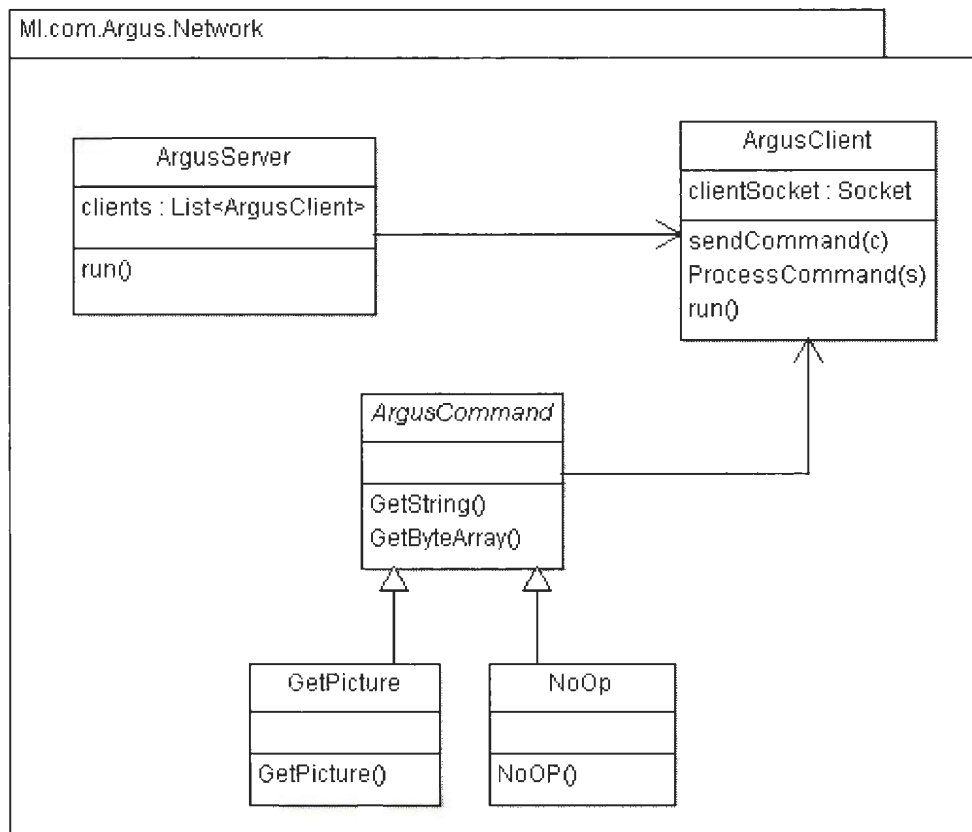


Figure 28 - Sever Network Class Diagram

The `ArgusServer` Class is instanced on program start up and opens a socket to listen for client connection attempts. When a client connects to the server an instance of the `ArgusClient` Class

is created, to handle the connection between the server and the client. As commands are issued by the users, implementations of the ArgusCommand abstract class are sent to the ArgusClient which issue commands to the remote clients. These commands are the implementation of the messages from the previous section.

The next section handles image processing, calibration and the stereoscopic location. The major classes for this section are shown below:

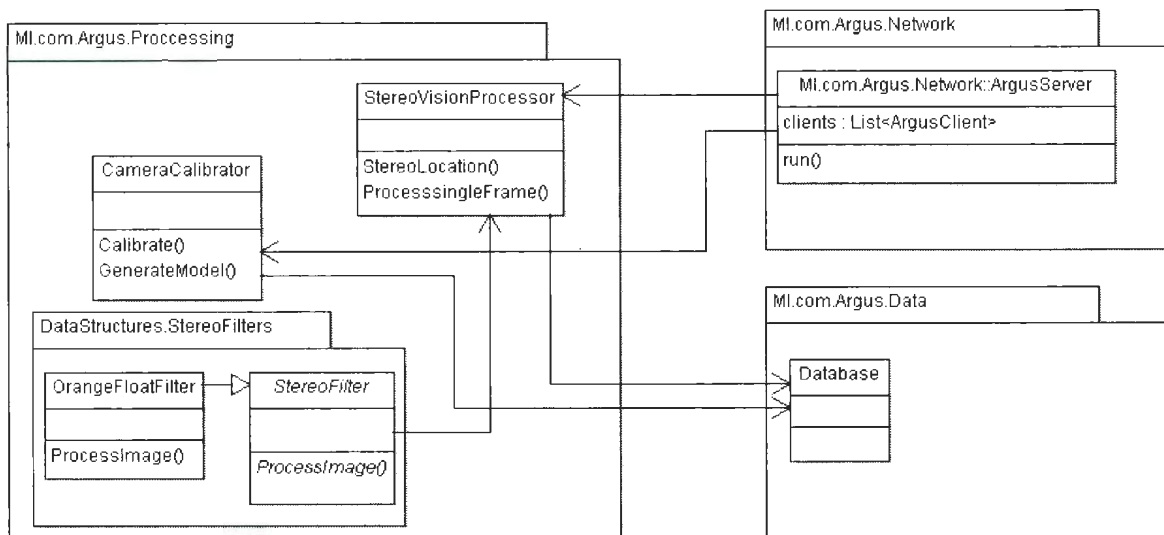


Figure 29 - Server Processing Class Diagram

The ArgusServer Class handles input from the user and creates an instance of the CameraCalibrator or StereoVisionProcessor class as needed. The CameraCalibrator class handles the camera calibration in two steps. A detailed explanation of this process will be described later in sections 6.4 and 6.5. The StereoVisionProcessor uses the StereoFilter class and its implementations to aid it in generating point location data used in the 3d location process. Once data is generated by the CameraCalibrator, or the StereoVisionProcessor, the data is then

saved to the Database class. This class will permanently save the data using XML files, if necessary, and help display it to the user.

The Final major section handles all of the data stored by the program and makes it available to the rest of classes. The layout of the major classes is as shown below:

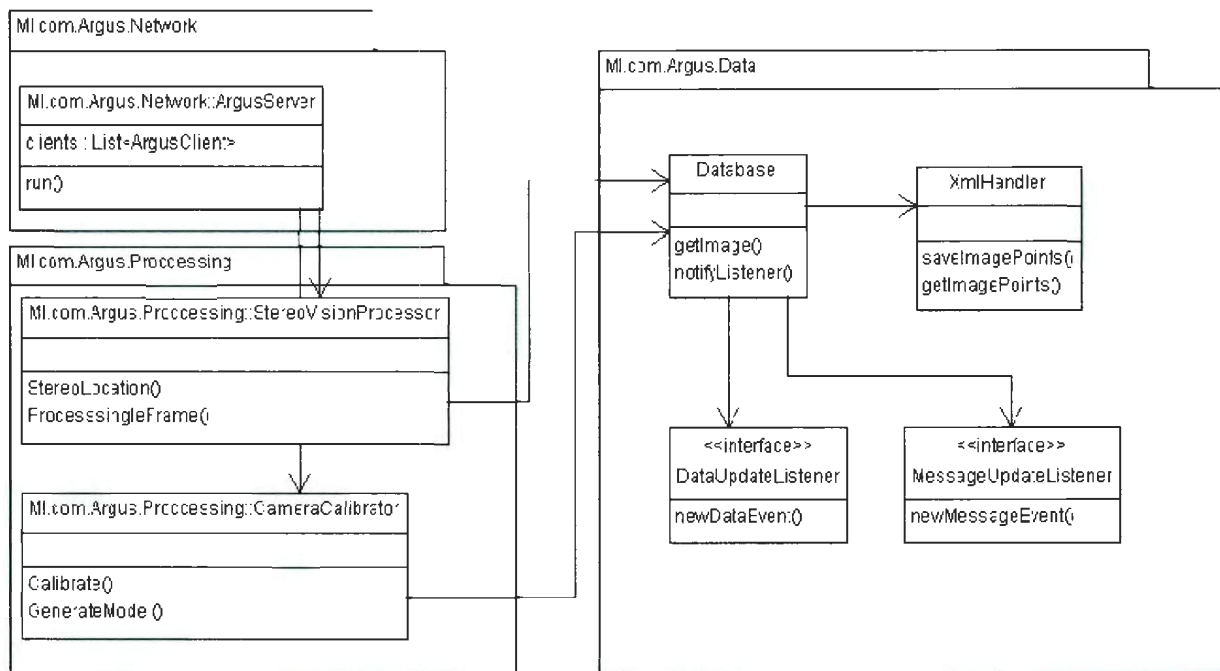


Figure 30 - Argus Data Class Diagram

The Database class handles, and stores, all of the programs information. An instance of this is created on program start up and passed to the ArgusServer class, as well as the GUI classes and any data processing classes as needed. Once new data is received the Database class uses an observer pattern to notify all listeners to new data being received by the Database. When it is required the Database can permanently save data to be used later. There are two methods for doing this, the first of which uses xml files. One instance the XmlHandler class can be used to

read and write data to custom xml files. This is typically used when large amounts of similar data are saved such as calibration point data. The second method is by using applications settings, which is a feature of c# and .net applications. This method allows for simple and fast access of persistent files, anywhere in the program. This method, however, has the drawback of requiring unique identifiers for each piece of information, making it unsuitable for large quantities of similar information and more suited for smaller data segments, such as the camera model and camera settings.

6.3.2 User Interface

The graphical user interface (GUI) is how the user interacts with the program during regular usage. A description of the features and its interaction with the rest of the program are described below.

6.3.2.1 Interface Design

The user interface has two main sections: The first, shown on the left below, is the tabbed section which allows for behaviour selection. The Second, on the right below, is the status section which monitors the software status and allows for image data to be updated.

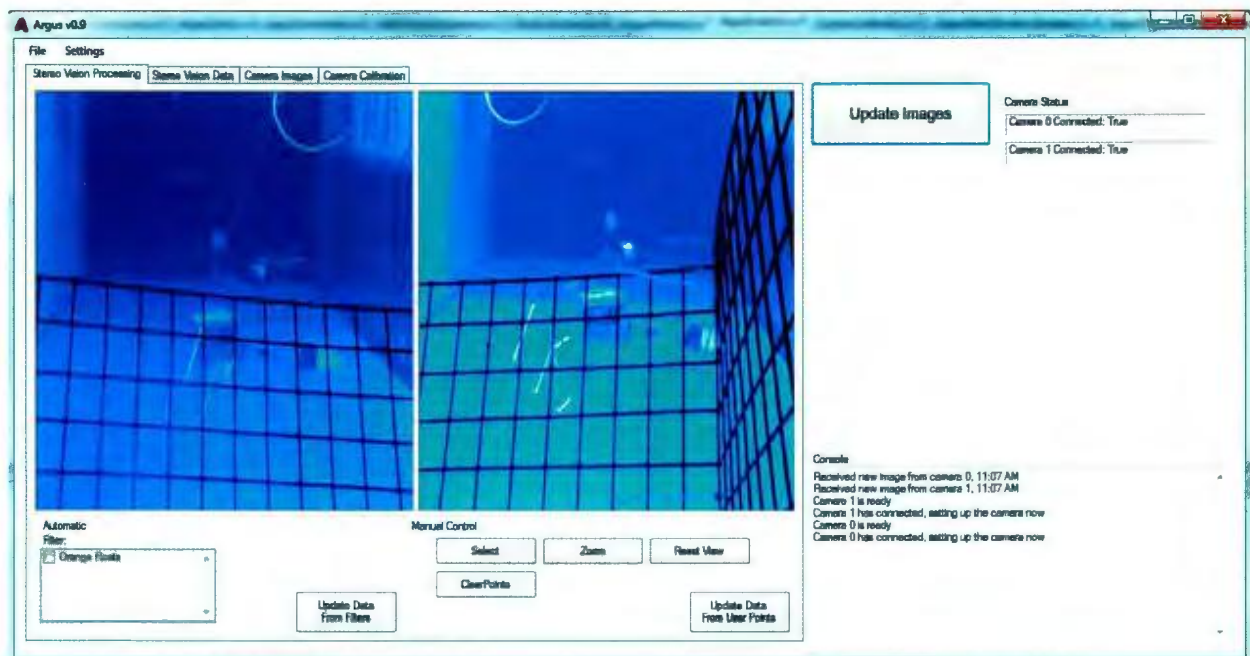


Figure 31 - Stereo Processing GUI

The tabbed section of the GUI has 4 sections: The first, shown above, is the stereo processing tab which provides the main functionality. There are two ways in which users can select a location to generate a point in 3D space. The first is to use the automatic point selection using the filters provided. For example, the orange float filter shown will automatically look for small

orange circles and attempt to locate their centers. This method uses several iterations to optimize the location, and is therefore the most accurate. The Second method is a user selected method, where the user may select the point that will be used for location. The user may select any number of points at once and may zoom in on the image to increase accuracy. This method is less accurate than the automatically generated points, however, it is more flexible since the user may select any location for triangulation.

The second tab features the positional data from the stereo vision processing tab. This tab will show the Id of the point and its coordinate in 3D space. This was separated from the previous tab to allow greater amounts of information to be shown and easily copied, and to remove clutter from the display.

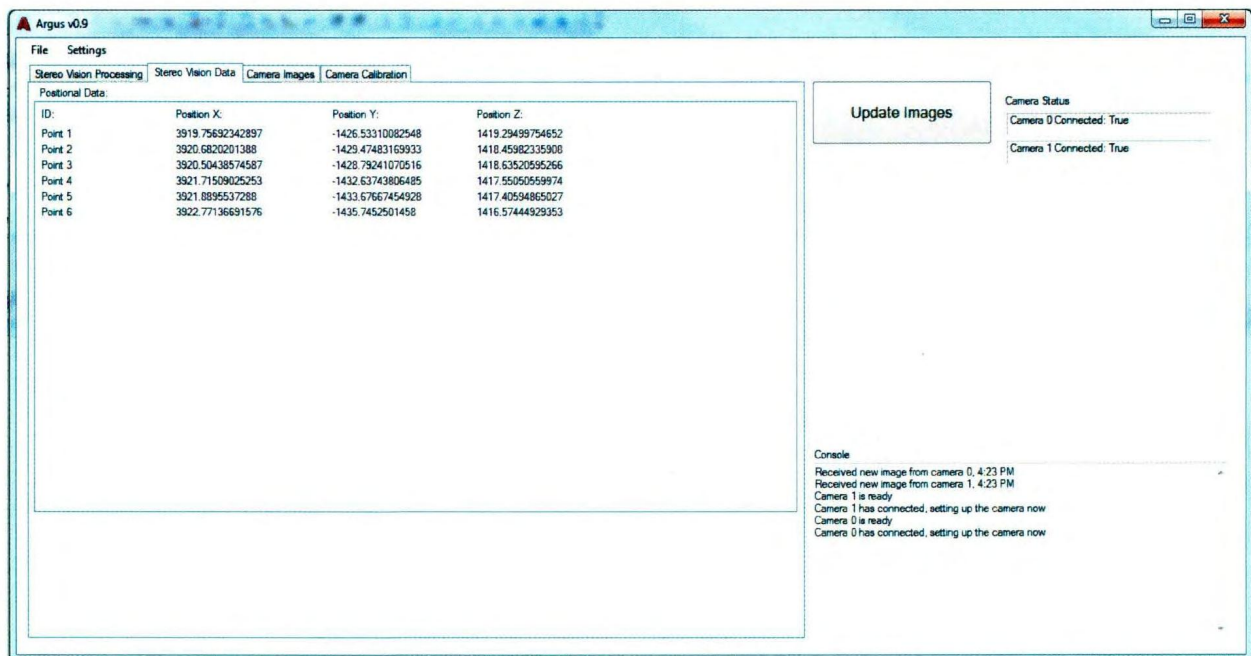


Figure 32 - Stereo Data GUI

The third tab features the ability to load and save images captured from the connected cameras. Though this is not required by the project, this feature aided in program debugging and development, as well as giving a new view of objects that will be tested in the flume tank. A view of this interface is shown below:

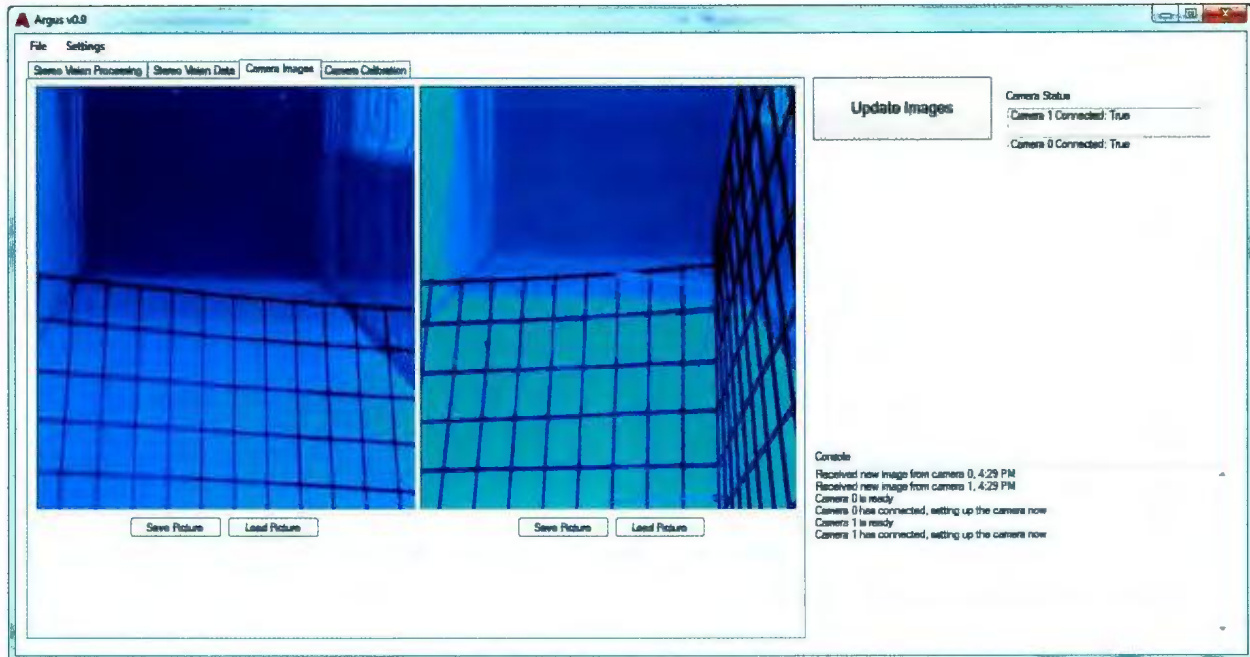


Figure 33 - Image Handling GUI

The final tab handles the camera calibration procedure. From the explanation in the calibrations section, the calibration process has been broken into several sections. The first step is getting the points for calibration, which is done using the select and zoom options below. The user selects the get points option. If the user is content with the selected points the user can then generate and save the calibration information. The “generate int.” option saves the intrinsic camera parameters and “generate ext.” generates the extrinsic parameters. An in depth implementation of this process is described later in the chapter. A view of this interface is shown below:

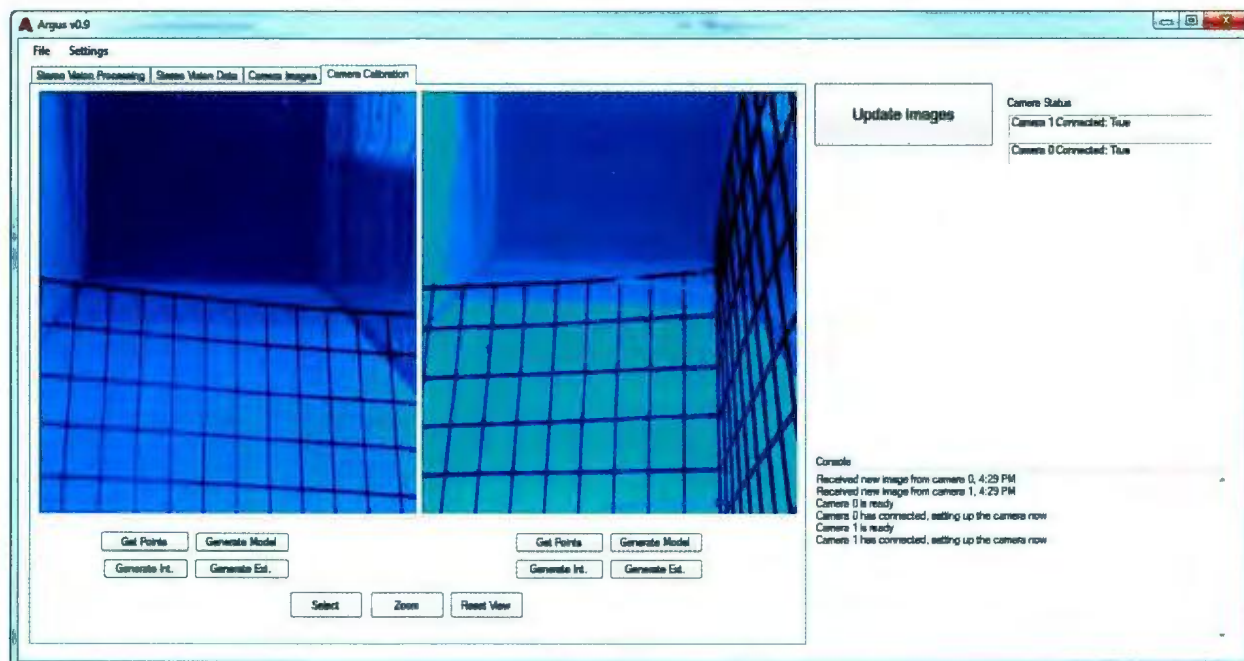


Figure 34 - Camera Calibration GUI

The right section does not change, depending on the selected behaviour of the program. The first part of this section shows the connected status of the cameras. As the cameras connect to the server their ID number and status is shown. The next section is the Update image option. Using this option the user can update the images, used by the rest of the program, and that are displayed on the screen. The final section is the Console which reports errors in user input, important calibration information and any other important information important to the user.

6.3.2.2 Software Integration

The GUI classes interact with the rest of the program, as shown in the following diagram:

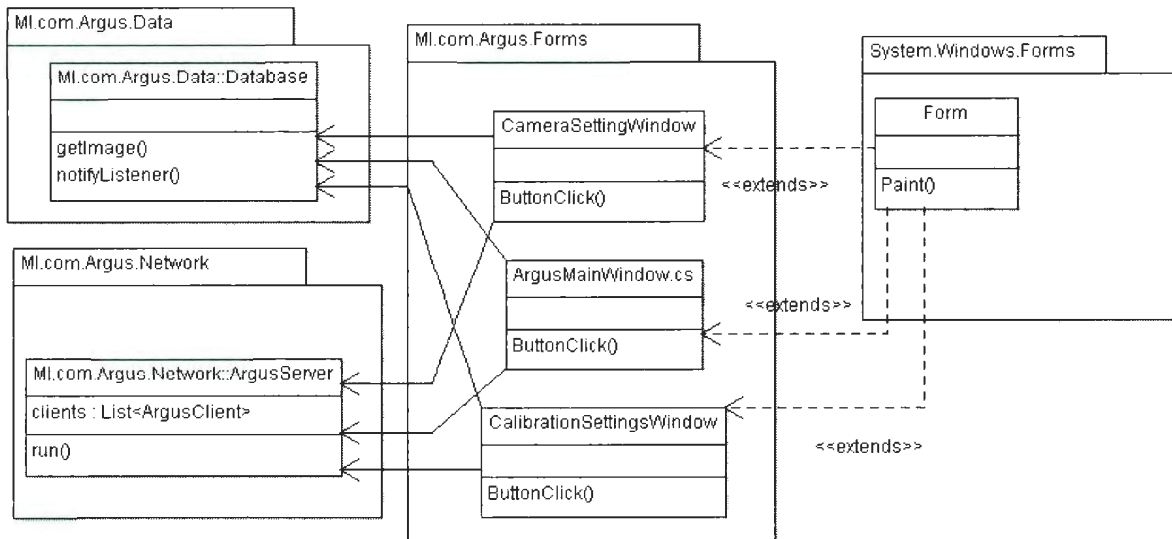


Figure 35 - Argus GUI class Diagram

The GUI is implemented using .net forms and Microsoft Visual Studio form designing software to automatically generate the look and layout of the program. This is implemented in the code by extending the Form class from windows .net library for the three main windows. ArgusMain Window is the window described above while the Calibration and Camera settings windows are minor windows used when the user adjusts the various settings of the window. All the windows contain references to both the ArgusServer and Database classes in order to retrieve data or send it for processing, when the appropriate settings are selected by the user.

6.4 Stereo Location Implementation

This section will describe in depth the implementation of the point location algorithm and its iterations. The first step of the calibration procedure is locating the points that will be used by the calibration routine in order to generate the camera model. This process needs to be automated, due to the large number of points involved, and accurate in order to increase the accuracy of the generated camera model. This process is further complicated by being underwater which not only decreases the available light and contrast, but also blurs images and reduces edge sharpness. An example of these effects is shown below:

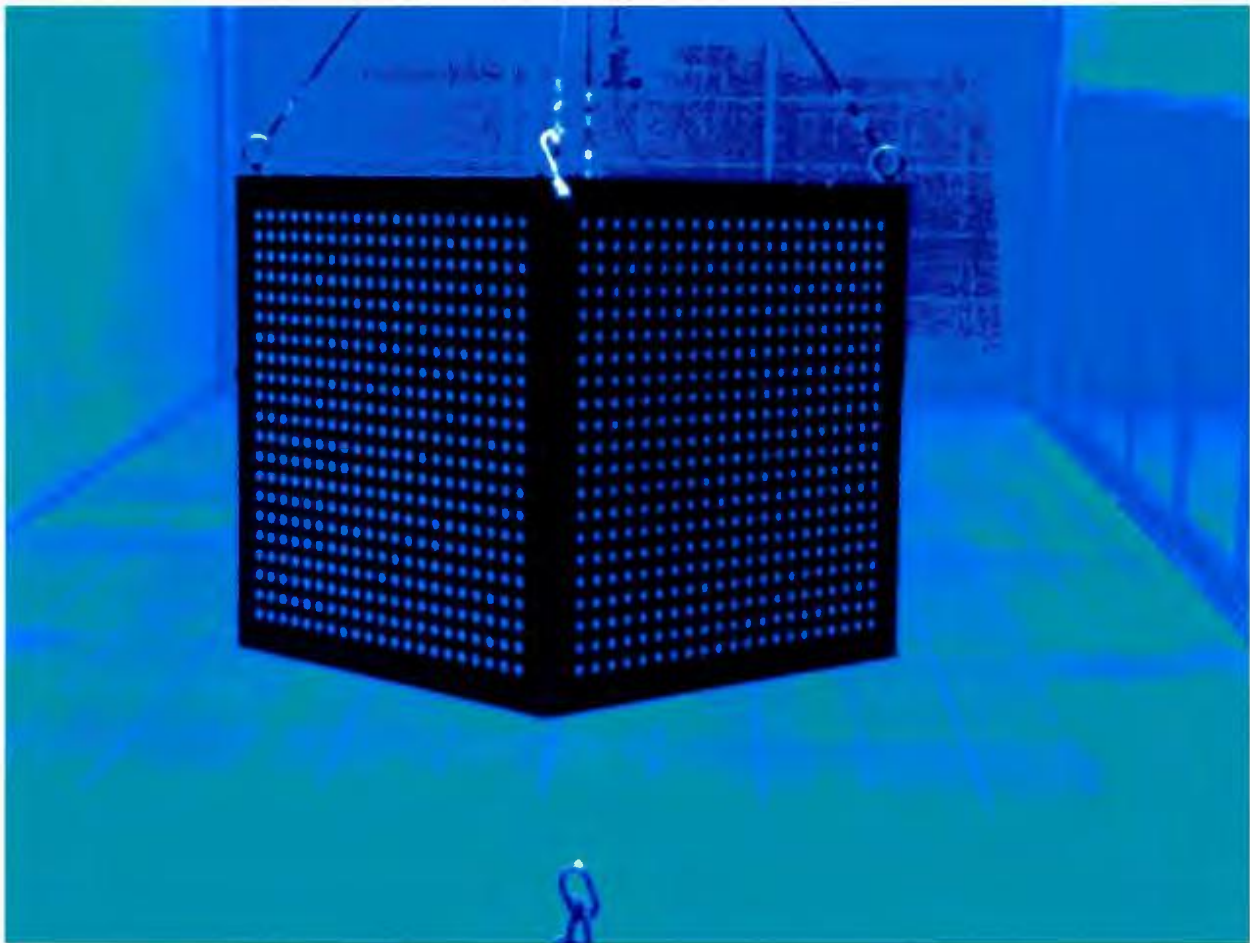


Figure 36 - Example of Camera Target Underwater

The first challenge, after the images are passed through a set of dilatation and erosion transformations to remove image noise, is for the location process to discover the target in the environment. The first iteration of this process used an automatic blob detection method. This would search the scene, after a black filter had been applied and looked for the largest target with similar features to that of the cube. This method worked well above water, however when submerged the black of the tank background caused errors in the detection of the target. The second, and current, iteration uses user input to select the four corners of the two sides of the cube. This improved the accuracy and reduced error with only a small inconvenience to the user. These selected points are used in the next step.

The second step is to calculate the orientation of the object and find the four corner circles of each side. This step is done automatically by the algorithm using an arc search and circle center optimization. The four corner points are used to estimate the slope at the top, bottom and side of the cube, if a line were drawn through two points. This information will be used later to find all the points on the target in an organized fashion. Next, the four corner circles are discovered using the knowledge that a line between the two opposing corners should also intersect the corner circles. However, due to the orientation of the cube, and the blur of the target it can be difficult to detect the circle exactly so an arc search is performed. The search uses a ten degree arc to each side of the corner to corner line. The following arc shows the arc searched to find the top left corner of the target. The red circles are points tried until the white circle is discovered and the blue circle is the corner after it has been corrected.

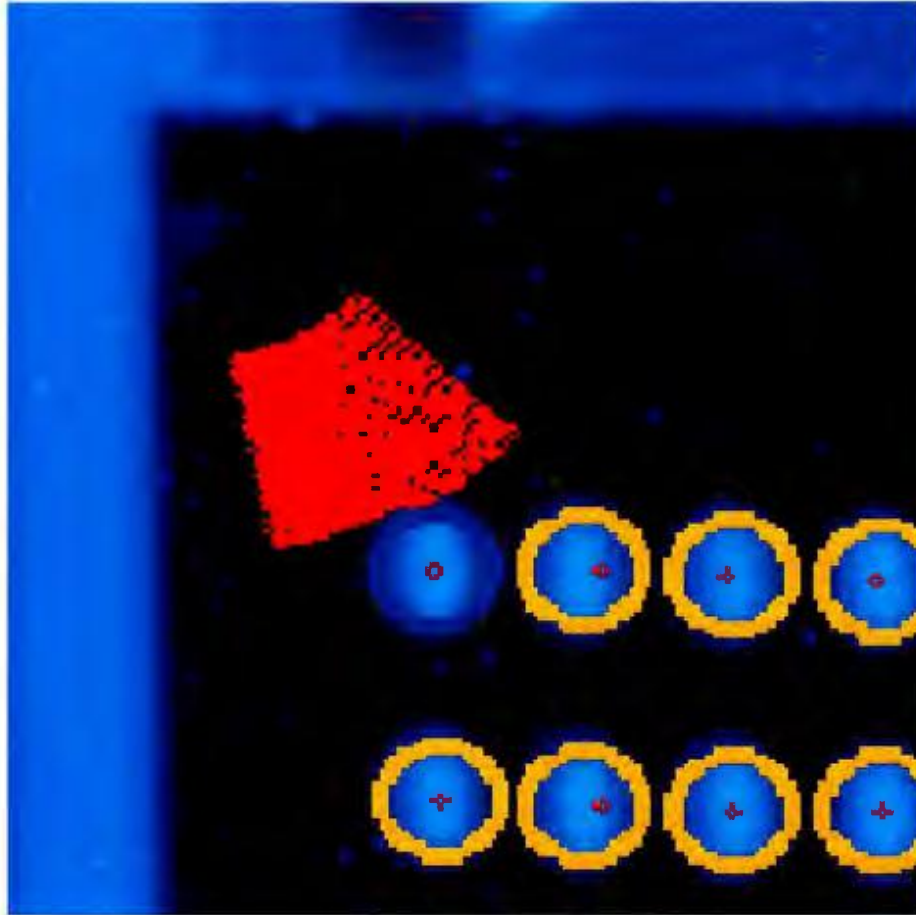


Figure 37- Corner Detection Example

This process is continued for all four corners, and two sides, of the target during which the circle center is also corrected. If the algorithm fails to discover an appropriate corner an error is reported to the user.

Using this fact there are 21 points in each column and row, the approximate distance between all the points is calculated in pixels. This information, in conjunction with the four discovered corners, the first and last column of the target are found using a line projected from the top circle to the bottom circle. These are then used to calculate a series of horizontal lines used to find all the points. When locating all the points on the horizontal line the spacing is used to find an approximate location which is then corrected and a new spacing is calculated between the

current point and the previous point. Updating the distance between points improved performance of the algorithm and reduced error in circle detection. Once all the points are corrected, they are saved in an xml file for use later by the camera model generation routine.

Previous versions of the circle detection did not use the ordered circle detection method described above. The earlier versions of this algorithm used a canny circle detection algorithm to find all possible circles on the target. However, this method would miss detecting certain circles and discover certain non-circles. This method was augmented with a grid repair algorithm which would remove circles if they did not have the appropriate colour and search to the left, right, top and bottom in an attempt to repair the grid and discover all circles. While this method proved effective to detect all circles in the grid, the circles detected would be in no known order and organizing them proved inefficient and ineffective so the method was discarded in favour of the currently used algorithm.

6.5 Calibration Implementation

This section describes the implementation of the calibration routine, described in the previous camera calibration chapter in detail. The calibration routine can be broken into several distinct steps, the first of which is loading the points saved by the previous circle detection algorithm.

Next, a set of points is generated for the real world coordinates, in millimeters, where the top center corner of the target is considered $(0, 0, 0)$. This has the result of placing the coordinate system of the camera system in a non-intuitive orientation and location based off the location of the cube when the image was taken. However, all points can be placed into a more intuitive coordinate frame by a simple rotation and transformation done on the final calculated points.

Using the image points, world points, and known camera parameters such as pixel size and resolution, an estimation of the camera's extrinsic parameters is found. Rahman and Krouglicof's method of camera calibration is used in conjunction with this information to iteratively generate a camera model. A mathematical explanation of this process can be found in chapter 3.

This model is then reversed and the data from the world coordinates are used to calculate the pixel coordinates and the error between the actual coordinates, and the model coordinates, is calculated and displayed to the user, along with important model information.

Chapter 7

7.1 Comparative Testing

One of the main goals of this project was to produce a functional system that could calculate the location and distance of features in the flume tank faster, more accurately and more precisely than the existing system. Using the techniques and research from the previous chapters, the newly developed system will be evaluated under real world conditions for performance versus the old camera system.

The old camera system, consisting of three cameras, is used to locate a point in three dimensional space. Above the water there are two cameras that give a horizontal distance between two points in the centers of the cameras. This system uses a mechanical gear and encoder to determine distances. Below the water is another camera with two encoders to determine the vertical and horizontal location of a point, as seen from the side of the flume tank. These systems only reliably allow for a maximum accuracy of 1 centimeter and must be aligned by hand.

7.2 Experiment Design

The evaluation of the new system against the old system was conducted using a metal testing rig with orange plastic floats attached to the rig, with high tension twine, to prevent stretching. This rig had 6 points, at fixed distances from each other, and floats at different heights in the water column. The exact distances, and lengths, of the testing rig were unknown to the testers before calculating distances. The experiment measured three distances between three sets of

points on the rig. This will be repeated several times over various locations and orientations in the tank.

For the experiment, the testers were evaluated for the time, accuracy and precision of their measurements. The time taken for the old system was the total time taken from the start of the measurement process to the time in which the measurements are entered into a spread sheet. The time taken to setup the spread sheets, and do the calculations, was not included in the testing. The time for the new system was the time taken to acquire a new image and enter the calculated distances into a spread sheet. When the measurements were compared to the true results after testing, the accuracy and precision of the systems were evaluated based on average error and standard deviation of error.



Figure 38 - Camera Comparison Experimental Rig

7.3 Data Collection

7.3.1 True Value of Distances

Data Point	Distance(mm)
1	1720.01
2	3516.80
3	1835.21

Table 26 - True Value of Calculated Distances

7.3.2 Testing Results of Old Camera System

Data Point	Trial 1 (mm)	Trial 2 (mm)	Trial 3 (mm)	Trial 4 (mm)
1	1759.891	1738.032	1742.378	1747.77
2	3582.396	3616.12	3617.12	3622.118
3	1899.358	1923.589	1935.854	1922.646
Time (Seconds)	245	211	210	161

Table 27 - Results of Old Camera System Testing

7.3.3 Testing Results of New Camera System

Data Point	Trial 1 (mm)	Trial 2 (mm)	Trial 3 (mm)	Trial 4 (mm)
2	1682.735	1680.421	1687.258	1686.723
2	3572.275	3577.991	3569.602	3567.154
3	1888.153	1899.069	1898.606	1902.671
Time(Seconds)	53.4	54.4	64.0	51.9

Table 28 - Results of New Camera System Testing

7.4 System Evaluation

7.4.1 Comparison of Time Taken for Testing

	Average Time (Seconds)	Standard Deviation (Seconds)
Old System	206.75	34.5676
New System	55.9250	5.4805

Table 29 - Comparison of Testing Times (Seconds)

7.4.2 Error Analysis of Old System

Data Point	Average Error (mm)	Standard Deviation (mm)
1	27.0177	9.4615
2	92.6385	18.2183
3	85.1517	15.2403

Table 30 - Analysis of Error in Old System

7.4.3 Error Analysis of New System

Data Point	Average Error (mm)	Standard Deviation (mm)
1	35.7158	3.2719
2	54.9555	4.6534
3	61.9147	6.2511

Table 31 - Analysis of Error in New System

7.4.4 Evaluation of performance

Overall the new system performs better than the old system in all respects. The time taken to gather data for the new system is approximately four times less than the old system. While the operators of the old camera system improved their time during the testing, the new system was consistently faster.

The new system was also more accurate as well as more precise than the old camera system. The new camera system had an overall average error of 50.862 millimeters while the old camera system had an average error of 68.2693 millimeters, which is an improvement of 25%. Along with the overall increase in accuracy the standard deviation of error for the new system was much lower, approximately one third to one fourth of the old system. This increase in precision will lead to more consistent results in the data captured as well as a greater ability to detect small changes in the position of an object in the flume tank.

7.5 Other Considerations

One of the advantages that is not immediately shown by the above results is that of the static images used by the new camera system of the video feed. When fishing gear and other objects are placed in the flume tank they typically drift back and forth over a position. The solution used by the older flume tank system is to use the average position of an object over time to calculate distances. This method was done manually and was left up to the best judgement of the operator to determine this average position. Not only would this immediately lead to a greater inaccuracy and less precision, this would cause the operator to 'chase' the position of the object in the tank leading to a much longer time to capture the location of a point. The new system overcomes this issue by computing distances from static images

Another advantage of the new system is the ease in which the data is collected. The new system requires only one person using a single workstation to gather locations and distances of objects in the flume tank. The old system by comparison requires multiple operators at multiple workstations in the flume tank. The results for time above were the time required for a

pair of operators to collect such data. Under normal conditions there is often only typically be one operator for the entire system requiring at least twice the time to capture the needed data.

A final advantage of the new system comes from the custom software. The old system required the creation of spread sheets to manually enter the data captured from the old camera system by hand. Further calculations were then needed to calculate distances between points which again needed to be done by hand. The new system creates a table of the location of all points automatically when the points are chosen by the user and distance calculation is done automatically by selecting two points. This allows for a much shorter time between capturing data and determining distances than the old system, something which was not included in the testing times above.

Chapter 8

8.1 Conclusion and Future Recommendations

The goal of this project was to design a functional and accurate system for measuring and locating objects in an underwater environment. This led to an analysis of modern calibrations methodology and how these process were affected by underwater environments.

Methodologies for triangulation were also compared, in an effort to increase the accuracy of the camera system in the challenging conditions of an underwater environment. Finally, the designed system was evaluated against the older existing camera system to measure increases in efficiency and accuracy.

8.2 Camera Calibration

The comparison of several modern calibration techniques showed that the Rahman-Krouglicof method performed the best in the challenging underwater environments. The Rahman-Krouglicof method showed a 3% increase in accuracy over Heikkila's method and 6% over Zhang's method.

Underwater testing also revealed that calibration of systems to be used underwater must also be calibrated underwater. The paper by J. Lavest[19] on using above water calibration for underwater use, was proven incorrect. The equations and theories he used to approximate an underwater camera model were incorrect in all aspects, and creating any camera model using these approximations will be very inaccurate.

The testing also revealed that a proper calibration system such as, the calibration cube used for this project, can lead to a much more accurate system and it is worth the expense and time required to implement it. This is especially true when used in conjunction with the previous findings, where the properly designed target allowed for testing in underwater conditions, something that would be impossible with traditional paper targets.

8.3 Triangulation Methodologies

The goal of developing a system that uses stereo location, to locate the position of objects in an underwater environment, was also achieved. The experimentation revealed the accuracy of these systems is heavily dependent, not only on the calibration of the system, but also the techniques used for solving the stereo location problem. Testing revealed that the techniques developed by Hartley and Sturm [20] did not always improve triangulation accuracy but often significantly lowered the accuracy of the triangulation.

The novel improvements to the iterative inhomogeneous solution showed small but consistent improvements in accuracy. The results from this method were significantly more accurate than the optimized location methods by Hartley and Sturm. The testing also revealed that, even at longer distances, approximately twelve meters from the camera; this algorithm can still perform accurately and have error of approximately two to four centimeters.

The novel concept of calibration splitting showed interesting results that varied greatly in accuracy. Results from testing in close proximity to the cameras, approximately four to five meters; showed a large increase in accuracy over traditional calibration methods. However, when the distance increased, the accuracy of this calibration method fell quickly to where the

results were not usable past six meters. The method showed promise for close range triangulation in wide set cameras but more work must be done to determine its usefulness in longer distance scenarios.

8.4 Comparative Testing

Comparative testing between the new camera system and the older human operated system showed significant improvements. The new system showed increased accuracy over the older system with less average error and more consistent results with less deviation. The new system is also considerably faster than the older system and required fewer operators to use. The new system also showed several other immeasurable benefits over the older system such as, better handling of gear drift and reduction in the number of calculations handled by the operators.

8.5 Future Work

As it currently exists, the system is functional and useful but there is still room for increased functionality. The system currently handles basic object identification and matching across images, however, there is room for improvement and identification of more complicated objects. There is also room for improvement in the handling of the captured data. The system currently only handles the position of objects in one frame; the system could be adapted to handle movement across multiple frames. This could be used to monitor not only fishing gear size and position, but its movement over time to model drift and movement.

The experimentation and modeling of the effects of splitting calibration could also be further investigated. The testing from this project revealed much better results of triangulation when the split calibration model was used for objects in close proximity to the cameras. More testing

should be conducted over a wider range of locations and distances, in the camera's viewable area. Additionally, to monitor the effects of target size on calibration, more testing should be conducted with calibration targets using more and less of the image area.

This project has shown that high precision stereo location is possible in underwater environments. Though the effort required to make the system accurate in challenging environments is high, the results and functionality of such a system are worth the investment.

Appendix A Bibliography

- [1] L. Su and F. Zhu, "Design of a novel stereo vision navigation system for mobile robots," in *Robotics and Biomimetics (ROBIO). 2005 IEEE International Conference on* , Shatin , 2005.
- [2] L. Pisani, R. Comeau, B. Davey and T. Peters, "Incorporation of stereoscopic video into an image-guided neurosurgery environment," in *Engineering in Medicine and Biology Society, 1995., IEEE 17th Annual Conference*, Montreal, Que. , 1995 .
- [3] P. D. Winger, H. Delouche and g. Legge, "Designing and Testing New Fishing Gears," *Marine Technology Society Journal*, vol. 40, no. 3, pp. 44-49, 2006.
- [4] J. Heikkila, "Geometric camera calibration using circular control points," *Pattern Analysis and Machine Intelligence, IEEE transactions on*, vol. 22, no. 10, pp. 1066-1077, 2000.
- [5] T. Rahman and K. N, "An Efficient Camera Calibration Technique Offering Robustness and Accuracy Over a Wide Range of Lens Distortion," *Image Processing, IEEE Transactions on*, vol. 21, no. 2, pp. 626-637, 2012.
- [6] Z. Zhang, "A flexible new technique for camera calibration," *IEEE Transactions on Pattern Analysis and Machine Intelligence*, vol. 22, no. 11, pp. 1330-1334, 2000.
- [7] S. bougnoux, "From projective to Euclidean space under any practical situation, a criticism of self-calibration," in *Computer Vision, 1998. Sixth International Conference on*, INRIA,

Sophia-Antipolis, France , 1998.

- [8] D. Jacobs, "Linear fitting with missing data: applications to structure-from-motion and to characterizing intensity images," in *Computer Vision and Pattern Recognition, 1997. Proceedings., 1997 IEEE Computer Society Conference on*, NEC Res. Inst., Princeton, NJ, USA , 1997.
- [9] R. Tsai, "A versatile camera calibration technique for high-accuracy 3D machine vision metrology using off-the-shelf TV cameras and lenses," *Robotics and Automation, IEEE Journal of*, vol. 3, no. 4, pp. 323-344, 1987.
- [10] "OpenCV," itseez inc., 2013. [Online]. Available: <http://opencv.org/>.
- [11] Y. I. & K. H. M. Abdel-Aziz, "Direct linear transformation into object space coordinates in closer-range photogrammetry," in *Proc. Symposium on Close-Range Photogrammetry*, Urbana, Illinois, 1971.
- [12] T. Melen, "Geometrical modelling and calibration of video cameras for underwater navigation," Institutt for teknisk kybernetikk, Norges tekniske høgskole, 1994.
- [13] K. Levenberg, "A Method for the Solution of Certain Non-Linear Problems in Least Squares," *Quarterly of Applied Mathematics*, vol. 2, pp. 164-168, 1944.
- [14] A. Albarelli, E. Rodolà and A. Torsello, "Robust Camera Calibration using Inaccurate Targets," in *British Machine Vision Conference 2010*, Aberystwyth , 2010.

- [15] P. Sturm, "On plane-based camera calibration: A general algorithm, singularities, applications," in *Computer Vision and Pattern Recognition, 1999. IEEE Computer Society Conference on.*, Maybank, S.J. , 1999.
- [16] J.-Y. Bouguet, "Camera Calibration Toolbox for Matlab," [Online]. Available: http://www.vision.caltech.edu/bouguetj/calib_doc/htmls/example2.html. [Accessed 5 march 2013].
- [17] J. Heikkila, "Camera calibration toolbox for Matlab," 17 October 2000. [Online]. Available: <http://www.ee.oulu.fi/~jth/calibr/>. [Accessed 8 March 2013].
- [18] T. Rahman, "Camera Calibration," 2012. [Online]. Available: <http://www.engr.mun.ca/~taufiqur/calcam.php>. [Accessed 2 March 2013].
- [19] J. Lavest, G. Rives and J. Lapresté, "Dry camera calibration for underwater applications," *Machine Vision and Applications*, vol. 13, pp. 245-253, 2003.
- [20] S. Hartley and S. Hartley, "Triangulation," GE-CRD, Schenectady, NY, 1994.
- [21] M. Z. Brown, D. Burschka and G. D. Hager, "Advances in Computational Stereo," *IEEE Transactions on Pattern Analysis and Machine Intelligence*, vol. 25, no. 8, pp. 1222-1239, 2003.
- [22] D. Scharstein and R. Szeliski, "A taxonomy and evaluation of dense two-frame stereo correspondence algorithms," *International Journal of Computer Vision* , vol. 47, no. 1/2/3,

pp. 7-42, 2002.

- [23] N. Ayache and C. Hansen, "Rectification of images for binocular and trinocular stereovision," in *Pattern Recognition, 1988., 9th International Conference on* , Rome , 1988.
- [24] G. Legge, *Person Communication on Tank Maintenance*, St. John's, NL, 2013.
- [25] L. PrevCO, "PrevCo Subsea Housings," PrevCo Subsea, LLC., [Online]. Available: <http://prevco.com/>. [Accessed 2013].
- [26] T. Smid, "The Dynamics of Buoyant Objects," [Online]. Available: <http://www.physicsmyths.org.uk/buoyancy.htm>. [Accessed 26 11 2012].
- [27] J. S. Swinnea, "Flow Around Immersed Objects CHE 354," 2012. [Online]. Available: http://www.google.ca/url?sa=t&rct=j&q=&esrc=s&source=web&cd=1&cad=rja&ved=0CD AQFjAA&url=http%3A%2F%2Fcapsicum.me.utexas.edu%2FChE354%2Ffiles%2FLectures%2FChE354_Immersed.ppt&ei=hbCzULPWAtGBOQHwrIDgAg&usg=AFQjCNGZlp9bhh5DxuH3j7JgEQg-1RVR4A. [Accessed 26 09 2012].
- [28] Y. a. O. Munson, *Fundamentals of Fluid Mechanics*, John Wiley & Sons, 1998.
- [29] F. I. H. M. A. Ibrahim, "Modeling of the Dynamics of a Continuous Beam Including Nonlinear Fatigue Crack," *International Journal of Analytical and Experimental Modal Analysis*, pp. 76-82, 1987.

- [30] L. Corporation, "Lumenera Corporation," 2013. [Online]. Available:
<http://www.lumenera.com>. [Accessed 2013].
- [31] W. Faig, "Calibration of Close-Range Photogrammetry: Mathematical Formulation,"
Photogrammetric Engineering Remote Sensing, vol. 41, pp. 1479-1486, 1975.
- [32] E. Technology, "Bulgin Inc.," Elektron Technology, [Online]. Available:
<http://bulgin.co.uk/>. [Accessed 2013].
- [33] D. Karnopp, D. Margolis and ,. R. Rosenberg, System Dynamics 5th edition, John Wiley &
Sons, 2012.

Appendix B Camera Support Design

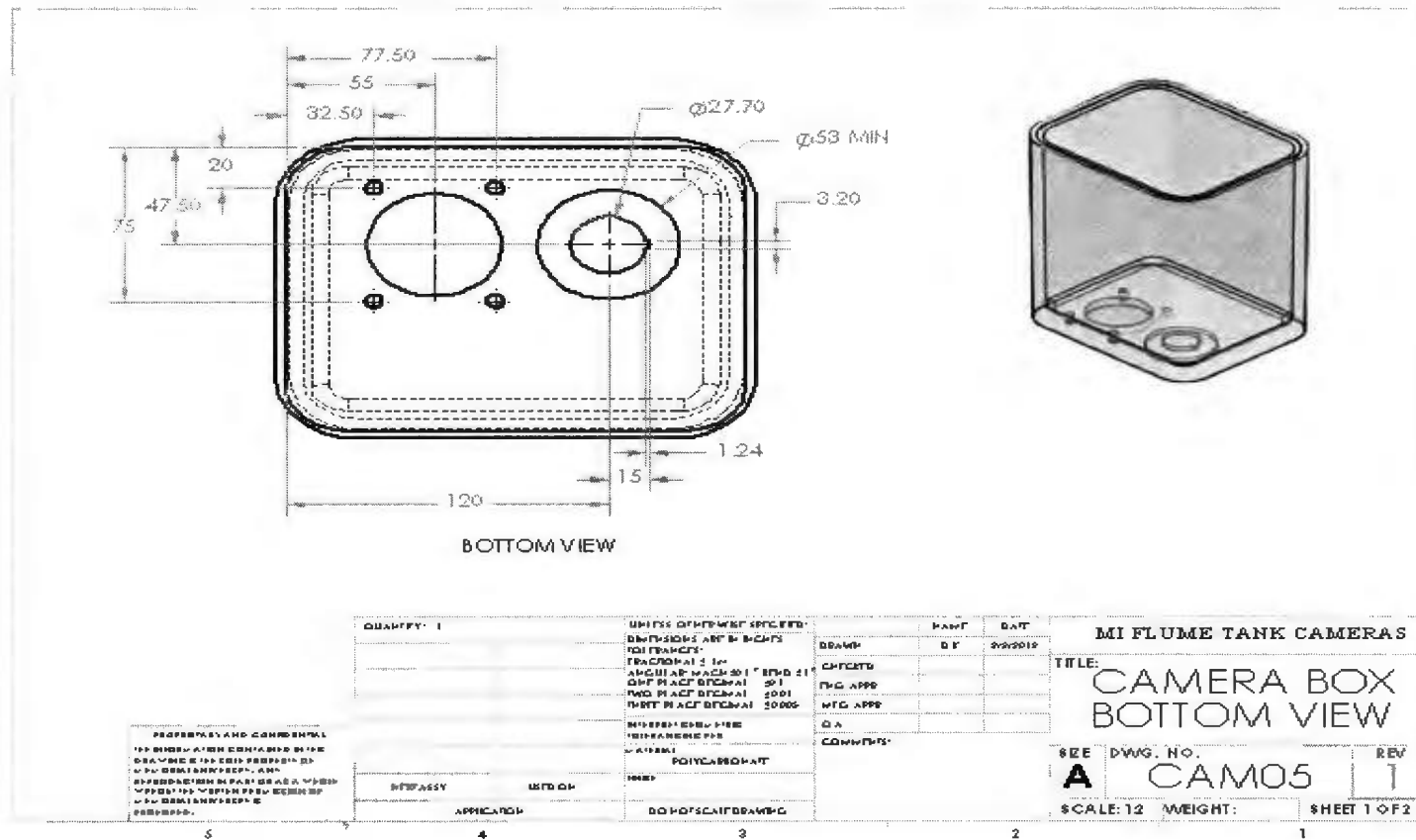
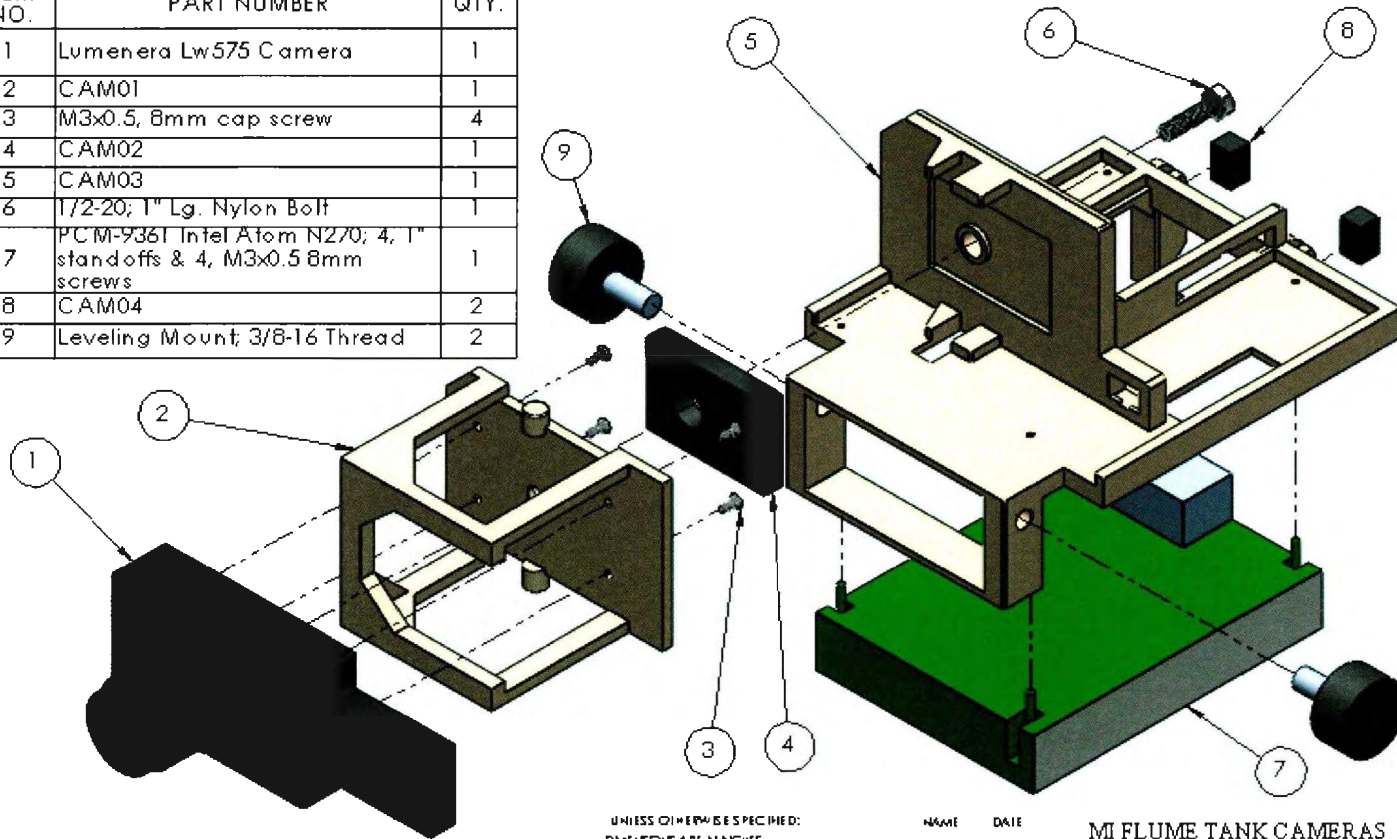


Figure 39 - Camera Container Technical Drawing 1

ITEM NO.	PART NUMBER	QTY.
1	Lumenera Lw575 Camera	1
2	CAM01	1
3	M3x0.5, 8mm cap screw	4
4	CAM02	1
5	CAM03	1
6	1/2-20; 1" Lg. Nylon Bolt	1
7	PCM-9361 Intel Atom N270; 4, 1" standoffs & 4, M3x0.5 8mm screws	1
8	CAM04	2
9	Leveling Mount; 3/8-16 Thread	2



QUANTITY: 2

PROPRIETARY AND CONFIDENTIAL
THE INFORMATION CONTAINED IN THIS
DRAWING IS THE SOLE PROPERTY OF
MWH GLOBAL. UNLESS ANY
OTHERWISE INDICATED BY A REPORT
WITHOUT THE WRITTEN PERMISSION OF
MWH GLOBAL, UNLESS OTHERWISE
PROHIBITED.

HWY ASSY

ASSEMBLY

APPLICATION

5

4

UNLESS OTHERWISE SPECIFIED:

DIMENSIONS ARE IN INCHES

TOLERANCES:

FRACTIONAL ± 1/16

ANGULAR: MAX ± 0.1° BEND ± 1°

ONE PLACE DECIMAL ± 0.1

TWO PLACE DECIMAL ± 0.01

THREE PLACE DECIMAL ± 0.005

PROPERTY OF MWH GLOBAL

FOR FURNISHING PER-

MATERIAL

FINISH

DO NOT SCALE DRAWING

3

NAME DATE
D/C 23/03/12

DRAWN

CHECKED

END APPR.

MHC APPR.

O.A.

COMMENTS:

CIRCUITRY INCLUDES
4 STANDOFFS

DATE

MI FLUME TANK CAMERAS

TITLE:

CAMERA FRAME
WITHOUT BOX

SIZE DWG. NO.

A ASSEM06 1

REV

SCALE: 1:2 WEIGHT:

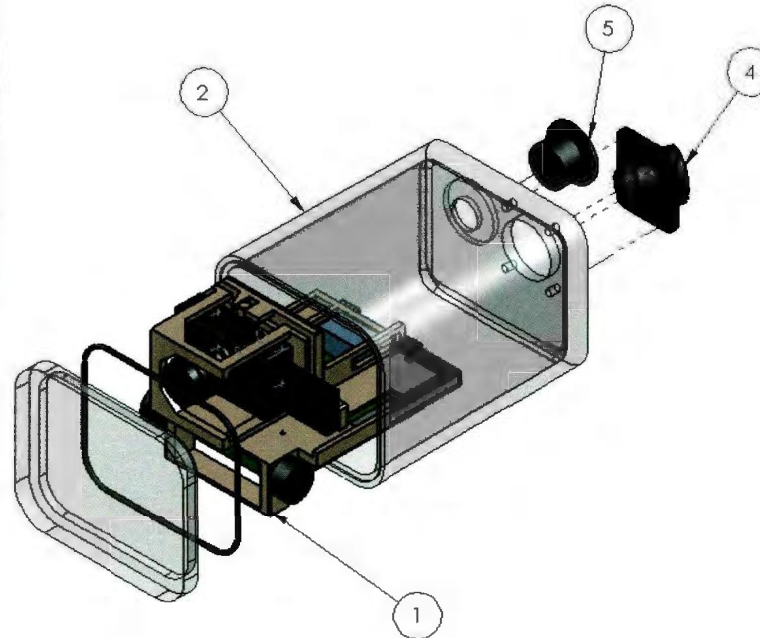
SHEET 1 OF 1

2

1

Figure 41 - Camera Support Technical Drawing

ITEM NO.	PART NUMBER	QTY.
1	ASSEM06	1
2	Leveling Mount; 3/8-16 Thread	2
3	CAM05; PREVCO POLYCARBONATE UNDERWATER HOUSING	1
4	EXP series EXPlora flange mounting connector part no. EXP-0941/03/S	1
5	Buccaneer Ethernet panel mounting connector part no. PX0833	1



PROPRIETARY AND CONFIDENTIAL
 THE INFORMATION CONTAINED IN THIS
 DRAWING IS THE SOLE PROPERTY OF
 MEMORIAL UNIVERSITY. ANY
 REPRODUCTION IN PART OR AS A WHOLE
 WITHOUT THE WRITTEN PERMISSION OF
 MEMORIAL UNIVERSITY IS
 PROHIBITED.

5

QUANTITY: 2

NEXT ASSY

APPLICATION

4

USED ON

UNLESS OTHERWISE SPECIFIED:

DIMENSIONS ARE IN INCHES

TOLERANCES:

FRACTIONAL ± 1/4

ANGULAR: MACH ± 0.1° BEND ± 1°

ONE PLACE DECIMAL ± 0.1

TWO PLACE DECIMAL ± 0.01

THREE PLACE DECIMAL ± 0.005

INTERPRET GEOMETRIC

TOLERANCING PER:

ASME Y14.5

FIRRH

DO NOT SCALE DRAWING

3

DRAWN

CHECKED

ENG APPR.

MFG APPR.

Q.A.

COMMENTS:

NAME

DK

DATE

29/03/12

MI FLUME TANK CAMERAS

TITLE:

CAMERA FRAME
 AND BOX

SIZE DWG. NO.

A ASSEM05

REV

1

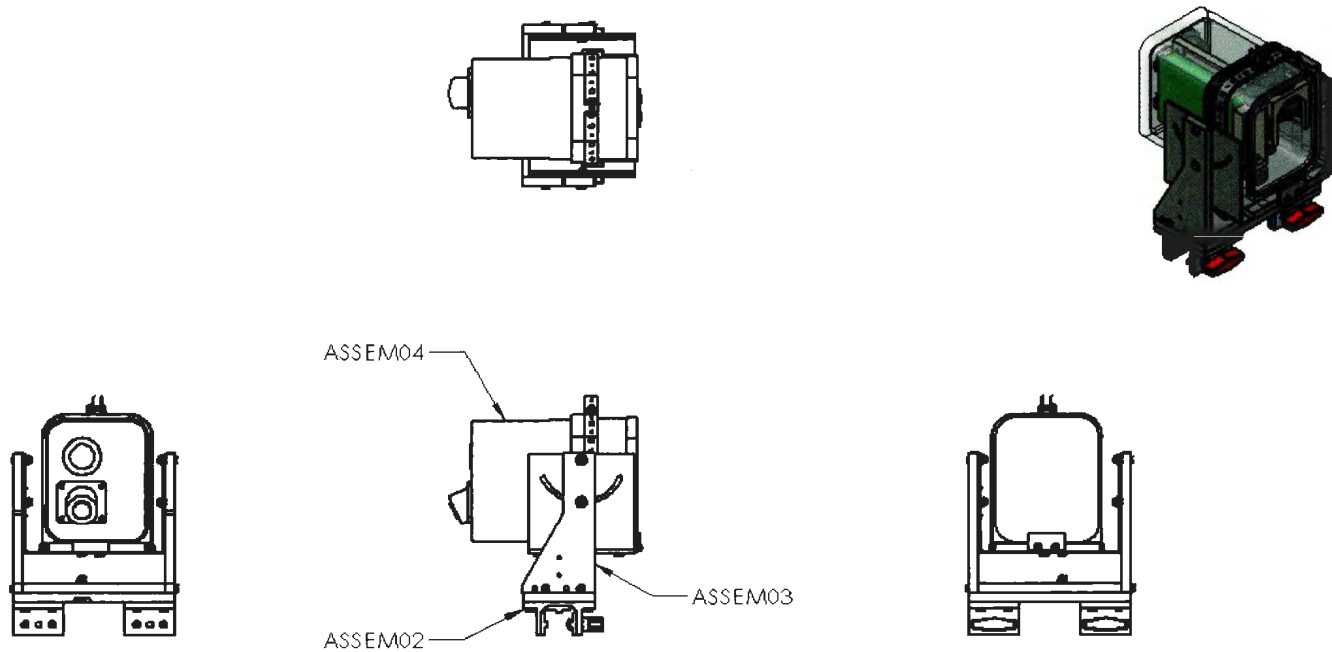
SCALE: 1:4 WEIGHT:

SHEET 1 OF 1

2

1

Figure 42 - Camera Box Assembly Technical Drawing



QUANTITY: 2

UNLESS OTHERWISE SPECIFIED:

DIMENSIONS ARE IN INCHES

TOLERANCES:

FRACTIONAL ± 1/4

ANGULAR: MACH ± 0.1° BEND ± 1°

ONE PLACE DECIMAL ± 0.1

TWO PLACE DECIMAL ± 0.01

THREE PLACE DECIMAL ± 0.005

INTERPRET GEOMETRIC

TOLERANCING PER:

MATERIAL

DRAWN

CHECKED

ENG APPR.

MFG APPR.

Q.A.

COMMENTS:

NAME

DATE

DK

24/04/12

MI FLUME TANK CAMERAS

TITLE:
CAMERA BOX
& SUPPORTS

SIZE DWG. NO.

A ASSEM01

REV

0

SCALE: 1:8 WEIGHT:

SHEET 1 OF 1

PROPRIETARY AND CONFIDENTIAL
THE INFORMATION CONTAINED IN THIS
DRAWING IS THE SOLE PROPERTY OF
MEMORIAL UNIVERSITY. ANY
REPRODUCTION IN PART OR AS A WHOLE
WITHOUT THE WRITTEN PERMISSION OF
MEMORIAL UNIVERSITY IS
PROHIBITED.

NEXT ASSY

USED ON

FINISH

APPLICATION

DO NOT SCALE DRAWING

5

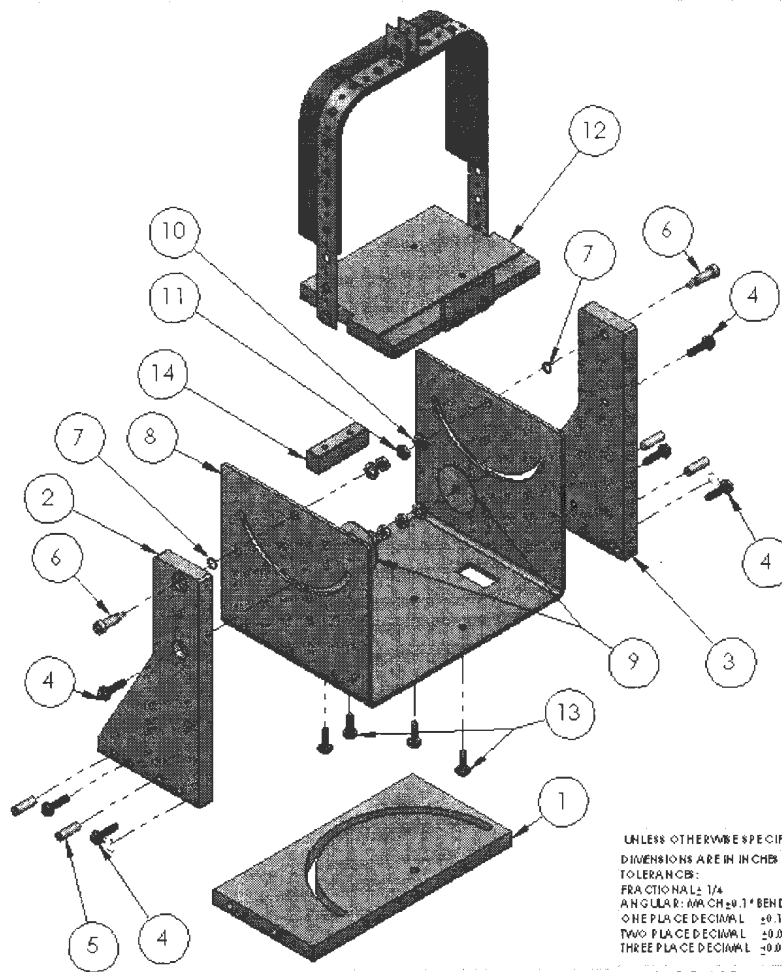
4

3

2

1

Figure 43 - Camera Box and Support Technical Drawing



ITEM NO.	PART NUMBER	QTY.
1	SYS03; ASSEM02	1
2	SYS06	1
3	SYS05	1
4	3/4" 10-32 HEX MACHINE SCREW	6
5	1/4" DIA. 3/4" LG. DOWEL PIN	4
6	1/4" DIA. 5/8" LG. SHOULDER SCREW, 10-32 THREAD	2
7	PTFE LOW FRICTION WASHER	2
8	SYS07	1
9	#10, LARGE DIA. WASHER	2
10	1/4" LOCK WASHER	4
11	10-32 HEX NUT	4
12	ASSEM03; SYS08	1
13	10-32, 5/8" LG. MACHINE SCREW	4
14	SYS10	1

PROPRIETARY AND CONFIDENTIAL
 THE INFORMATION CONTAINED IN THIS
 DRAWING IS THE SOLE PROPERTY OF
 MEMPHIS UNIVERSITY. ANY
 REPRODUCTION IN PART OR AS A WHOLE
 WITHOUT THE WRITTEN PERMISSION OF
 MEMPHIS UNIVERSITY IS
 PROHIBITED.

QUANTITY: 2

NEXT ASSY

USED ON

APPLICATION

MATERIAL

DO NOT SCALE DRAWING

UNLESS OTHERWISE SPECIFIED:
 DIMENSIONS ARE IN CHS
 TOLERANCES:
 FRACTIONAL: 1/4
 ANGULAR: MAX CH ±0.1° BEND ±1°
 ONE PLACE DECIMAL ±0.1
 TWO PLACE DECIMAL ±0.01
 THREE PLACE DECIMAL ±0.005

INTERPRETOMETRIC
 TOLERANCING PER:
 MATERIAL

FINISH

NAME DATE
 D.K. 16/02/12

MI FLUME TANK CAMERAS

TITLE:

X-AXIS ASSEMBLY

SIZE DWG. NO.

A ASSEM03

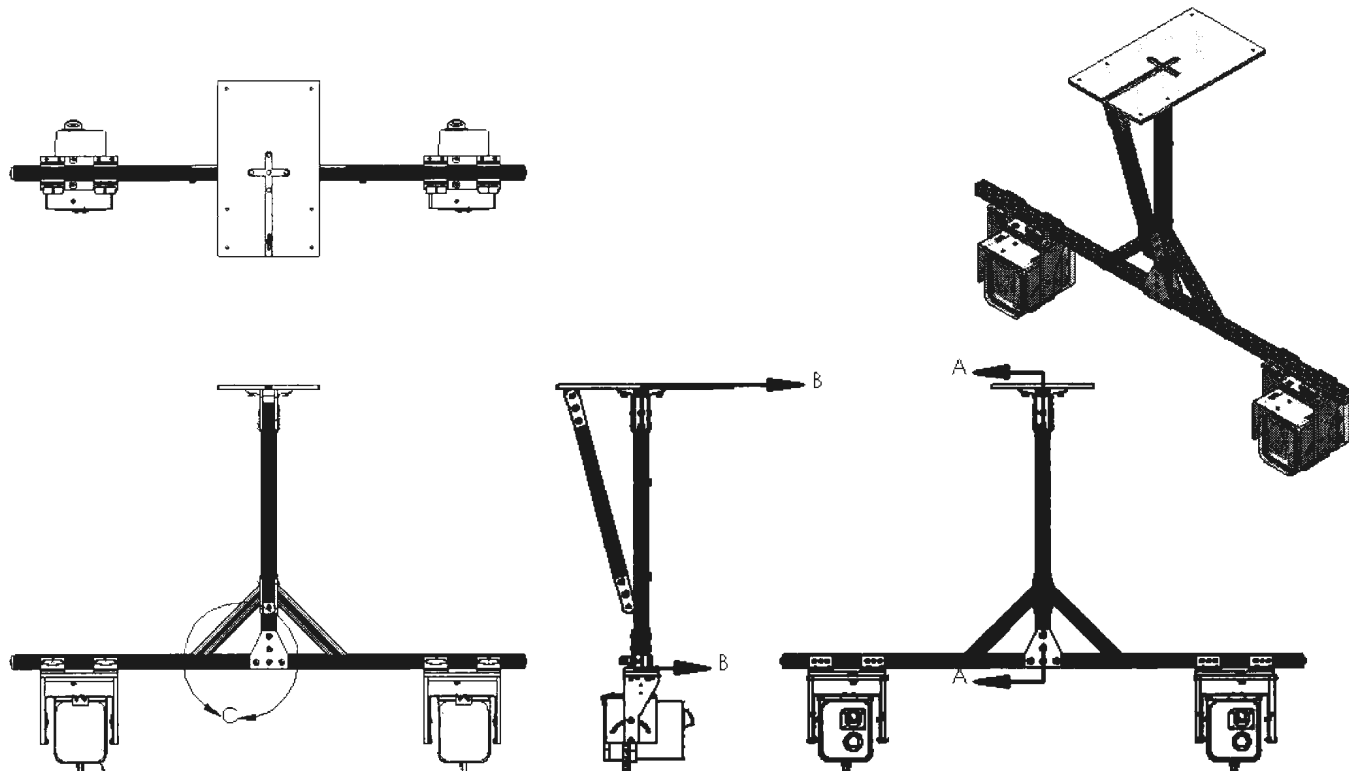
REV

6

SCALE: 1:4 WEIGHT:

SHEET 1 OF 1

Figure 44 - Camera Box Support Technical Drawing



PROPRIETARY AND CONFIDENTIAL
 THE INFORMATION CONTAINED IN THIS
 DRAWING IS THE SOLE PROPERTY OF
 MEMORIAL UNIVERSITY. ANY
 REPRODUCTION IN PART OR AS A WHOLE
 WITHOUT THE WRITTEN PERMISSION OF
 MEMORIAL UNIVERSITY IS
 PROHIBITED.

QUANTITY:	1
SECTION/DETAIL	SHEET NO.
SECTION A	ASSEM00, SHEET 2
SECTION B	ASSEM00, SHEET 2
DETAIL C	ASSEM00, SHEET 2

UNLESS OTHERWISE SPECIFIED:
 DIMENSIONS ARE IN INCHES
 TOLERANCES:
 FRACTIONAL ± 1/4
 ANGULAR: MAX CH ± 0.1° BEND ± 1°
 ONE PLACE DECIMAL ± 0.1
 TWO PLACE DECIMAL ± 0.01
 THREE PLACE DECIMAL ± 0.002
 INTERPRET GEOMETRIC
 TOLERANCING PER:
 MATERIAL
 FINISH

DRAWN DK 24/04/12
 CHECKED
 ENG APPR.
 MFG APPR.
 Q.A.
 COMMENTS:

MI FLUME TANK CAMERAS
 TITLE:
CAMERA SYSTEM
 SIZE DWG. NO. REV
A ASSEM00 2
 SCALE: 1:16 WEIGHT: SHEET 1 OF 3

Figure 45 - Camera Support Frame Technical Drawing



